ASSOCIATION OF CALCIUM BUFFERING CAPACITY AND LOCAL INFLAMMATORY REACTIONS IN INJURY OF MOTOR NEURONS

Ph.D. Thesis

Melinda Paizs

2010

ASSOCIATION OF CALCIUM BUFFERING CAPACITY AND LOCAL INFLAMMATORY REACTIONS IN INJURY OF MOTOR NEURONS

Ph.D. Thesis

Written by: Melinda Paizs

Supervised by: László Siklós D.Sc.

Laboratory of Molecular Neurobiology

Institute of Biophysics

Biological Research Center

2010

Manuscripts providing the basis of the thesis:

I.

Melinda Paizs, József I. Engelhardt, László Siklós:
Quantitative assessment of relative changes of immunohistochemical staining by light microscopy in specified anatomical regions.
Journal of Microscopy, **234:**103-12(2009)

II.

Melinda Paizs, József I. Engelhardt, Zója Katarova, László Siklós:
Hypoglossal motor neurons display a reduced calcium increase after axotomy in mice with upregulated parvalbumin.
Journal of Comparative Neurology, **518:**1946-1961(2010)

TABLE OF CONTENTS

INTRODUCTION

General context of the study

Our study is aimed at understanding the mechanisms underlying the selectivity of degeneration of motor neurons during amyotrophic lateral sclerosis (ALS): why do certain groups of motor neurons succumb to the disease while others are spared. Our hypothesis is that the impaired calcium homeostasis (i.e. increased calcium level) plays a pivotal role in the degeneration of motor neurons (Appel et al, 2001), and by its stabilization an increased resistance could be provided (Siklós and Appel, 2005). Accordingly, factors affecting the maintenance of the intracellular calcium equilibrium, such as the calcium buffering capacity, having the potential to reduce overshoots in calcium signaling, might be a significant feature contributing to the selective resistance of these cells.

Indeed, the increased level of intracellular calcium in the affected motor neurons was documented in ALS patients (Siklós et al, 1996), which study was paralleled by the demonstration of a correlation between the resistance of such cells against injury and their calcium binding protein (CaBP) content (Alexianu et al, 1994; Elliot and Snider, 1995). This observation was subsequently confirmed by a series of *in vitro* (Ho et al, 1996), *ex vivo* (Lips and Keller, 1998; Mosier et al, 2000; Palecek et al, 1999; Vanselow and Keller, 2000; recently reviewed by von Lewinski and Keller, 2005) and *in vivo* (Obál et al, 2006; Siklós et al, 1998) experiments.

With the advent of the transgenic technology, providing gold standards for the research of motor neuron disease (Nagai et al, 2006; Tovar-y-Romo et al, 2009), a direct method became available to test whether an increased calcium buffering capacity provides protection in ALS-like conditions by breeding transgenic animals simultaneously possessing increased calcium buffering capacity and presenting ALS-specific pathological mechanisms. Regarding the documented universal role of an increased level of calcium in cell destruction (Berridge et al, 1998), and the crucial role of calcium increase in a positive feedback loop of the detrimental processes (Appel et al, 2001), the calcium binding protein parvalbumin (PV)-upregulated mice exhibited only an unexpectedly mild protection in a transgenic model of ALS (Beers et al, 2001). These results reduced our confidence in the neuroprotection strategy based on the increased calcium buffering capacity.

To rule out the possibility that our basic proposal (stabilization of the calcium homeostasis) is not relevant at all in rescuing injured motor neurons, experiments were planned to characterize motor neuron populations in PV-upregulated transgenic mice after a sublethal injury, and tested whether a naturally vulnerable cell type could be indeed transformed to a resistant phenotype in these animals. A positive answer to this question may suggest that while the strategy of neuroprotection built on the improved stability of the calcium homeostasis may be correct, a method based on the increased buffering capacity alone, may not be sufficient. In this case, a more efficient approach should be sought.

Brief overview of amyotrophic lateral sclerosis

Clinical features

Amyotrophic lateral sclerosis (also known as Lou Gehrig's disease), the most common adult motor neuron disease (Cleveland and Rothstein, 2001), is a progressive, lethal disorder characterized by degeneration of both upper and lower motor neurons with clinical signs in four areas (brainstem, cervical-, thoracic- and lumbosacral regions) of the central nervous system. Anatomically, the axons of the upper motor neurons (Betz cells, located predominantly in layer V of the motor cortex) connect with the lower motor neurons positioned in the motor nuclei of the brainstem and the anterior horn of the spinal cord. Lower motor neurons project mainly to skeletal muscles. As the disease advances, there are progressive manifestations of combined dysfunctions of lower motor neurons (atrophy, cramps and fasciculations) and upper motor neurons (spasticity and pathological reflexes) in the absence of sensory symptoms (Mulder, 1982). According to the El Escorial- and the revised Airlie House criteria, the diagnosis of clinically definite ALS requires the presence and progression of both upper- and lower motor neuron signs in at least three body regions (Swash, 2000). Clinical, laboratory and neuropathological criteria have also been established for less definitive categories (Cwik, 2006). The relentless progression of muscle atrophy and weakness culminates in respiratory death within 5 years in the majority of the patients (Rowland and Shneider, 2001).

Pathological findings

Until the last two decades, the main pathological findings in postmortem tissue of ALS patients were loss of motor neurons, commonly accompanied by astrocytosis, in the precentral

gyrus, brainstem and spinal cord. Surviving motor neurons showed features of degeneration such as atrophy of the cell body with large number of lipofuscin granules. Secondary changes involved the degeneration of the pyramidal tract, loss of nerve fibers and neurogenic abnormalities in the muscles. However, none of these changes are exclusive for ALS (Hays, 2006). ALS-specific pathological alterations were identified during the past 15-20 years by recognition of intracytoplasmic inclusions in standard pathological (hematoxylin and eosin stained) sections such as Bunina bodies, with an occurrence in the ALS tissue of 65-95% (Hays, 2006). More importantly, after the introduction of immunohistochemical (IHC) analysis into the pathological practice, ubiquitinated inclusions with nearly 100% occurrence and high specificity for ALS were discovered (Kato, 2008). Furthermore, the protein composition of such inclusions, identified also by IHC provided suggestions for the pathobiology of ALS, as well (Strong et al, 2005).

Epidemiology

The incidence of sporadic ALS is reported to be between 1.5 and 2.7 per 100,000 population / year, which corresponds (in agreement with an average of 2-5 years survival) to a point prevalence of 2.7 to 7.4 (Wijesekera and Leigh, 2009). There are conflicting data on gender (Strong, 2003), however, it seems, that the small male preponderance (1.5 male to female ratio) is diminishing with age, suggesting an estrogen-dependence in the pathomechanism (Chio et al, 2009). Although most cases are classed as sporadic ALS (sALS), 5-10% of the patients have a family history (familial ALS; fALS) with often Mendelian inheritance and high penetrance (Wijesekera and Leigh, 2009). Twenty percent of cases with autosomal dominant fALS (and 2% of sALS patients) possess mutations in the Cu/Zn superoxide dismutase (SOD1) gene. Other genes causing familial form of the disease include alsin, senataxin (STX), vesicle associated membrane protein (VAPB), angiogenin, fused in sarcoma/translated in liposarcoma (FUS/TLS) and gene encoding the TAR-DNA binding protein TDP-43 (Valdmanis et al, 2009).

Identified basic mechanisms of degeneration in ALS

According to the contemporary view, ALS is considered as a non cell autonomous (Ilieva et al, 2009) and multifactorial disease (Eisen, 2009). Even though its cause is basically unknown (except for the inherited cases constituting the absolute minority of the patients) several

mechanisms have been identified, which either alone, but rather in a concerted action contribute to the degeneration of motor neurons (Boillée et al, 2006). These include: glutamate excitotoxicity, oxidative damage, mitochondrial dysfunction, protein misfolding and aggregation, defects in axonal transport, immune-inflammatory dysfunction, impairment of the blood-brain/spinal cord barrier and calcium-mediated toxicity.

Glutamate excitotoxicity

This well recognized mechanism of neuronal death resulting from repetitive cell firing (Choi, 1988) has been implicated in the pathogenesis of ALS for a long time, furthermore, Riluzole, an anti-glutamatergic drug, is currently the only one medicine approved to treat ALS (Rattray and Bendotti, 2006). Several experimental studies and clinical observations document that the toxicity exerted on the motor neurons is mediated by an excess level of extracellular glutamate, due to impairment of the astrocytic glutamate transporter EAAT2 (excitatory amino acid transporter 2), which support a non cell autonomous pathological mechanism in ALS (Rothstein, 2009).

In ALS, the 2-amino-3-(3-hydroxy-5-methylisoxazol-4-yl) propionic acid (AMPA) subtype of glutamate receptors is of particular importance. AMPA receptors, assembled from 4 subunits, are normally impermeable to calcium. However, if the GluR2 subunit is missing, the receptors become highly permeable to this ion (Buckingham et al, 2008). Low expression of the GluR2 protein subunit (Shaw et al, 1999) and decreased levels of the mRNS for GluR2 (Williams et al, 1997) are detected in motor neurons of ALS patients.

Oxidative damage

Oxidative stress develops in a system if the balance between the production and neutralization of reactive oxygen species (ROS) is shifted towards production, or the capacity of the repair mechanisms is overwhelmed. The main source of cellular ROS is the leakage of electrons from the mitochondrial respiratory chain which results in production of superoxide anions ($O_2^{\bullet-}$) and hydrogen peroxide (H_2O_2) (Halliwell and Gutteridge, 1999), but other cellular oxidative enzymes in the cytoplasm and the endoplasmic reticulum contribute, as well. The mildly reactive $O_2^{\bullet-}$ and H_2O_2 are further transformed to peroxynitrite ($ONOO^-$) and hydroxyl radicals ($^{\bullet}OH$), which cause nitration of tyrosine residues of accessible proteins, lipid-

peroxidation and oxidative damage of DNA (Barber and Shaw, 2010), which have been documented in ALS patients (Beal et al, 1997).

The role of oxidative mechanisms in the pathobiology of ALS gained an outstanding attention after identification of missense mutations of the SOD1 gene in a population of the patients (Rosen et al, 1993). A novel (gain of) function of the mutated enzyme has been proposed, which exaggerates the oxidative burden of the affected cells (Julien, 2001). An interesting aspect of the malfunction of the mutant SOD1 has been recently discovered: the mutant enzyme, after association with Rac1, a small GTPase that controls the activation of NADPH oxidase (nicotinamid adenosine dinucleotide phosphate, a multiprotein membrane-associated complex whose catalytic subunit is Nox2), locks Nox2 in its active, superoxide-producing form (Harraz et al, 2008). Thus, instead of removing intracellular superoxide, mutant SOD1 is responsible for overproduction of extracellular $O_2^{\bullet-}$ of microglial (phagocytic cell) origin, providing additional evidence for the non cell autonomous pathology underlying ALS (Boillée et al, 2008).

Mitochondrial dysfunction

This is a common feature of many neurodegenerative diseases (Chaturvedi and Beal, 2008). Despite of the documented mitochondrial alterations in patients' biopsy material (Siklós et al, 1996) and in some transgenic models of the disease (Siklós et al, 1998), there is no uniform view how mitochondrial function is actually affected in ALS. Several lines of evidence support that mitochondrial calcium handing mechanism might be altered (see e.g. Damiano et al, 2006), which is fully compatible with the above described excitotoxic mechanisms, thus may be central to the neuronal damage (Boillée et al, 2006). The documented damage evoked by the deposition of mutant SOD1 on the cytoplasmic face of the outer mitochondrial membrane (Vande Velde et al, 2008) together with the notion of an impaired mitochondrial function of astrocytes bearing the mutant enzyme, which promotes the degeneration of motor neurons (Cassina et al, 2008), provide further clue to the cooperative role of different cell types in the disease mechanism.

Protein misfolding and aggregation

Another common feature of neurodegenerative disorders that protein aggregates develop, which may be characteristic for the disease and the degenerating neuronal population, such as senile plaques (amyloid beta aggregation) and neurofibrillary tangles (phosphorylated tau

aggregation) in Alzeimer's disease, Lewy bodies (α-synuclein aggregation) in Parkinson's disease, prion plaques (aggregation of the scrapie isoform of the prion protein) in Creutzfeld-Jacob disease, inclusions (Huntingtin aggregates) in Huntington's disease, etc. (Chaudhuri and Paul, 2006). Since the hypothesis of the mode of action of the mutant SOD1, based on the reduced scavenging activity (Beckman et al, 1993), after the first description of mutant SOD1 enzyme in ALS tissue failed, by now it has been replaced with an idea that the mutant protein misfolds, tends to aggregate which confer toxicity to motor neurons. Besides mutant SOD1, other cytoskeletal proteins, various kinases, heat shock proteins and proteins of the endoplasmic reticulum also contribute to the ubiquin-immunopositive, detergent-insoluble material constituting the cytoplasmic inclusions in ALS (Basso et al, 2009). However, recent observations accentuate the role of SOD1 in the pathomechanism documenting that the wild type enzyme may acquire similar toxic properties as the mutant form possesses through oxidative damage (Ezzi et al, 2007), which may offer a convergence point where the mechanisms underlying fALS and sALS merge. Furthermore, misfolded proteins could also be secreted (Urushitani, 2006), which interact with microglial cells, and by triggering the release of noxious substances provides a molecular clue for an intercellular mechanism how does mutant SOD1 exert its toxic effect on motor neurons (Zhao et al, 2009).

Defects in axonal transport

Aberrant organization and especially misaccumulation of neurofilaments in spheroids in the cell body and proximal axons of motor neurons is a hallmark of both sALS and fALS. These spheroids may physically compromise the axonal transport mechanism, which has been detected in several transgenic models of ALS (Rao and Nixon, 2003). The mechanisms by which the impaired axonal transport contribute to the degeneration of motor neurons is not clear, but could include inadequate delivery and removal of distal mitochondria, and slow the retrograde transport of trophic factors from the periphery (De Vos et al, 2008). Interestingly, overexpression of the neurofilament heavy (NF-H) gene in a transgenic mouse model of ALS provided neuroprotection by a mechanism assumed to be based on attenuating calcium increases at the perikaryal region of motor neurons through calcium binding by the multiple calcium binding sites of NF-H proteins (Coulliard-Després et al, 1998).

Immune-inflammatory dysfunction

The immune privilege of central nervous system (CNS) has been considered as experimentally well defined, however, recent data radically altered this viewpoint: peripheral immune cells can cross the intact blood-brain barrier (BBB), neurons and CNS glial cells actively regulate macrophage and lymphocyte response, and there are immunocompetent cells in the CNS, such as microglial cells (Carson et al, 2006). Although it is still controversial to what extent the role of the adaptive and innate immunity is destructive or protective, their participation in the disease mechanism is undoubted (Appel et al, 2010).

Impairment of the blood-brain/spinal cord barrier

The involvement of the blood vessels in the pathomechanism of ALS has already been suggested by the observation that the deletion of the hypoxia-response element in the (angiogenic) vascular endothelial growth factor (VEGF) results in an ALS-like phenotype in mice (Oosthuyse et al, 2001). Furthermore, the participation of the BBB or blood-spinal cord barrier (BSCB) in the pathogenesis of ALS is supported by the recent results from biochemical (Zhong et al, 2008) and morphological studies (Garbuzova-Davis et al, 2007a, b), obtained with the transgenic mouse model of ALS, showing that disruption of the BBB and BSCB might precede motor neuron degeneration in the spinal cord. Although impairment of the BBB is not a prerequisite to initiate autoimmune responses in the CNS, the accompanying increased exposure of the CNS parenchyma to blood-borne products, particularly to humoral components of the immune response, and the decreased efficacy of the efflux transporters to remove potentially toxic molecules (e.g. excitatory transmitters) may augment the degenerative processes (Carson et al, 2006). In this aspect, the documented presence of immunoglobulin G (IgG) in spinal cord and motor cortex of ALS patients (Engelhardt and Appel, 1990), and the ability of this purified IgG to interact with voltage-gated calcium channels and increase calcium influx might be of primary importance (Engelhardt et al, 1995; Pullen and Humphreys, 2000).

Calcium-mediated toxicity

In excitable cells, like neurons, ionic calcium plays an universal second messenger role, converting electrochemical signal to physiological responses, thus its concentration and intracellular distribution require tight regulation (Brini and Carafoli, 2000). A concentration gradient of Ca^{2+}, spanning four orders of magnitude across the plasma membrane of neurons presents a huge diving force, thus guarantees fast signal transduction in physiological

condition, but could easily lead to large increases in $[Ca^{2+}]_i$ and cellular malfunction, if the control mechanisms are compromised (Nicotera and Orrenius, 1998; Sattler and Tymianski, 2000). Impaired Ca^{2+} homeostasis evoked by injury or alterations of Ca^{2+}-regulating proteins may launch several mechanisms some of them may lead directly to neuronal death (Mattson, 2007). These processes include activation of cystein proteases, calpains resulting in downregulation of Na^+/Ca^{2+} exchanger and impairing Ca^{2+} extrusion (Celsi et al, 2009), activation of caspases that degrade a variety of cytoskeletal proteins, membrane receptors and metabolic enzymes (Chan and Mattson, 1999) and activation/induction of pro-apoptotic proteins such as Bax, Par-4, p53 (Culmsee and Mattson, 2005). Besides these processes, numerous indirect mechanisms are launched, as well, leading to apoptotic or necrotic cell death (Marambaud et al, 2009).

In ALS, the relevance of the altered calcium level and the impaired calcium homeostasis have been documented in motor axon terminals from patients' muscle biopsies (Siklós et al, 1996), as well as in *in vitro* (Colom et al, 1997) and *in vivo* models of ALS-like injury of motor neurons (Siklós et al, 1998).

A synthesis of the basic mechanisms to a putative pathomechanism underlying ALS

Although its etiology is unknown, several mechanisms have been proposed, briefly described above, which most likely through their synergistic action, impair the function and destroy the structure of motor neurons. For the sake of argumentation disregarding the (unknown) initial cause, we demonstrate below, that the individual destructive processes are interconnected in such a way that they mutually augment each other with a positive feedback, thus constitute a complex pathomechanism in which calcium ions play a pivotal role.

Calcium is at centerstage in degeneration

A strong relationship exists between excessive Ca^{2+} influx and glutamate-triggered neuronal injury (Arundine and Tymiansky, 2003), first proposed in ALS twenty years ago (Rothstein et al, 1990). As a consequence of overstimulation, increased amount of calcium enters motor neurons through AMPA receptors, permeable to Ca^{2+} probably due to lack of astrocytic control to upregulate the GluR2 subunit (Van Damme et al, 2007). Elevated calcium, through activation of enzymes like phospholipase A_2, calpain, xantin-oxidase, increase the production of free radicals (Mitsumoto et al, 1997) directly or indirectly after the uptake of Ca^{2+} by

mitochondria (Carriedo et al, 2000). An important consequence of the oxidative stress on membrane proteins (ion pumps and exchangers) is an increased calcium influx, thus the process amplifies itself (Ermak and Davies, 2001). Nevertheless, other proteins such as SOD1, providing the main intracellular antioxidant defense may suffer oxidative damage, as well. Thus, since oxidative stress may equally develop either due to the presence of a mutant SOD1, or to wild type enzyme underwent oxidative damage gaining similar toxic properties as the mutant form (Kabashi et al, 2007), the calcium-mediated amplification cascade persists regardless of the initial trigger.

Another feedback loop of destructive processes with converging effect on motor neurons is associated with glial cells, particularly with astrocytes (Julien, 2007). Although the exact mechanisms are still debated, how do these cells contribute to the degeneration of motor neurons (Foran and Trotti, 2009), certain components of this cascade have already been identified. First, it has been demonstrated that glial glutamate transporter EAAT2 is prone to oxidative injury provided by ROS produced in motor neurons (Rao et al, 2003; Rao and Weiss, 2004), with a consequence of reduced capacity of astrocytes to maintain glutamate level at the synaptic cleft, which as discussed above leads to calcium-mediated toxicity. Another aspect of the interplay between astrocytes and microglial cells is associated with their known activation and proliferation in response to injury. Microglia even in minor pathological events start to proliferate (Kreutzberg, 1996), and reactive microglia are equipped to produce both components (oxygen radicals and NO) of highly toxic $ONOO^-$, which may induce membrane perturbations, and capable to inhibit the function of membrane proteins, like glutamate transporters (Trotti et al, 1996), contributing to elevated glutamate levels and excitotoxicity. Microglial NO production – in physiological conditions – is under the negative feedback control of astrocytes by the release of transforming growth factor β (TGF-β) (Vincent et al, 1997). However, astrocytes maintain this inhibitory control only as long as they remain in their differentiated state. If they are forced to undergo pathological activation, astrocytes may aggravate oxidative neuronal damage by the activation of their own inducible NO-synthase (Schubert et al, 2001). Furthermore, non-differentiated proliferative astrocytes lack of inward rectifying chloride channels, responsible for maintaining their intact membrane potential (Ferroni et al, 1995). Thus, pathologically activated astroglial cells, reverting to their primitive state (Aschner, 1998), may loose their ability to regulate potassium homeostasis

(and also to buffer glutamate), thus, through increased depolarization of excitable cells directly contribute to excitotoxicity. Thus, considerable degree of degeneration may result from the local glial reaction next to the injured motor neurons which converts oxidative stress to calcium-mediated excitotoxic lesion (Barger et al, 2007).

Finally, an important aspect of the impairment of the BBB and BSBB is emphasized, which may lead to an increased concentration of immunoglobulins, at least locally at the lesion sites. The phenomenon possess significance in the pathomechanism of ALS, since the presence of ALS IgG indeed could be demonstrated in the brain and spinal cord of ALS patients (Engelhardt and Appel, 1990) and also in a transgenic rat model of ALS (Nicaise et al, 2009). Purified IgG from the sera of ALS patients is directed against L-type voltage gated Ca^{2+}-channels (Smith el al, 1992). Further experiments have also documented that ALS IgG can interact and alter the function of neuronal N-/ P-/ Q-channels, as well (Llinas et al, 1993). The interaction of ALS IgG with these calcium channels enhances inward calcium current (Mosier et al, 1995) and increases intracellular calcium (Colom et al, 1997) as was demonstrated in a motor neuron cell line.

Expectations from increased calcium buffering capacity

Although several approaches may be feasible how to stabilize intracellular calcium homeostasis, clinical observations and harmonizing experimental data pointed to the possibility that by means of increasing the intracellular buffering capacity through overexpressing calcium binding proteins this goal could be achieved.

Historically, first, a correlation could be established, based on clinical and pathological data, that certain population of motor neurons, possessing higher level of calcium binding proteins calbindin-D_{28k} (CB) and parvalbumin (PV), such as those innervating voluntary sphincter- and external oculomotor muscles do not degenerate during the disease (Ince et al, 1993; Alexianu et al, 1994). These observations culminated in a statement that "*Parvalbumin is a marker of ALS-resistant motor neurons*" (Elliot and Snider, 1995). On this basis, motor neuron pools were selected with relatively easy experimental manipulation possibilities, considered as "prototypes" of vulnerable- and resistant cell, like hypoglossal- and oculomotor neurons, respectively, which were further characterized with electrophysiological methods. In these studies, the correlation between the CaBP content and the ability of the motor neurons

to resist calcium-mediated injury was confirmed (Lips and Keller, 1998; Vanselow and Keller, 2000).

Next, exploiting the discovered potency of the ALS IgG to induce calcium influx, its ability to kill motor neurons was directly tested and proved *in vitro*, using a motor neuron cell line (Smith et al, 1994). This (VSC 4.1) cell line provided the possibility of direct testing their resistance against ALS IgG-mediated toxicity in differentiation and transfection experiments. Undifferentiated VSC 4.1 motor neurons, while they contained calbindin-D_{28K} and parvalbumin, remained resistant to the effects of IgG. Yet, after their differentiation, once they had lost these proteins, the same IgG resulted in calcium influx and caused cell death (Ho et al, 1996). If these cells were transfected with calbindin-D_{28K} cDNA, the level of this calcium-binding protein remained high, even in differentiated cells and the cell remained viable when treated with ALS IgG (Ho et al, 1996).

Finally, the ability of CaBPs to lend resistance in ALS-like conditions was directly tested *in vivo*, as well, in the G93A mutant SOD1 model. Indeed, qualitatively, with a combined light microscopic immunocytochemical and electron microscopic characterizations of oculomotor- and spinal motor neurons, a correlation could be established between the resistance and PV content of motor neurons, which was paralleled with an inverse correlation between the resistance and the intracellular calcium level (Siklós et al, 1998).

Thus, it seemed a reasonable goal to provide resistance of “oculomotor type” to vulnerable neurons by means of an artificial upregulation of parvalbumin expression, at least in suitably designed transgenic animal strains.

Proof of concept experiment: protection by calcium binding in ALS

The acid test of the protective role of calcium buffering capacity concept in ALS is the production and characterization of a model, in which ALS-like stress and increased CaBP level simultaneously exist. In an effort along this line, double transgenic mice possessing mSOD1 transgene, and concurrently exhibiting increased PV levels have been developed. Although these animals exhibited improved parameters with regard to morphological- and physiological characteristics, ultimately could not be cured, furthermore, the gain in the survival data was just above the level, to be accepted as significant (Beers et al, 2001). This

unexpected low efficacy of protection by means of upregulated calcium buffering capacity, in view of the pivotal role of calcium in cell destruction was surprising.

Obviously, next, the reason(s) of the unexpectedly low benefit of this intervention was decided to be investigated, with the hope of finding ways to improve neuroprotection on the same principles, i.e. to stabilize the intracellular calcium homeostasis, if feasible. Along this line, our primary aim was to rule out possible methodological pitfalls, since some of the previous results were based on either morphological or physiological examinations of different groups of cells, and sometimes have been only partially quantified. Thus, our aims in this direction were: setup of a lesion → detection assay based on a uniform intervention (e.g. surgery, like axotomy), and a standardized characterization (e.g. on a morphological basis) of the intracellular calcium changes of the same group of cells, as well as, knowing their involvement in the injury, setup of an assay to quantify the degree of the participation of the non-motoneuronal cells in the injury.

Previous experiments relevant to the present study

Most importantly, an acute injury, i.e. axotomy/target deprivation experimental paradigm has been established, to quantify motoneuronal calcium increase in pools of motor neurons (oculomotor-, hypoglossal motor neurons) with documented different vulnerability to injury in ALS. These experiments, using electron microscopic histochemical methods and light microscopic immunohistochemistry, quantitatively documented a correlation between the resistance of motor neurons against injury and their CaBP level contrasted by an enduring increase in intracellular calcium content in CaBP-low cell types (Obál et al, 2006). Next, more importantly, these experiments provided a reference for comparisons whether an artificial increase is CaBPs could alter the profile of calcium response in these cells.

Problems to be addressed by further experiments

With the above experiment, besides establishing a reproducible experimental paradigm, we could provide additional experimental proof of the protective role of CaBPs in injury. However, since the experiment were performed using wild type animals and different pools of neurons, the question remained: whether the cellular resistance in these cells was provided by means of their increased CaBP level or local environmental factors had a decisive influence. To resolve this dilemma, the same cells with altered CaBPs have to be challenged in their

original environment, and, preferably the environmental change of the injured neurons has to be assayed, at the same time.

AIMS OF THE STUDY

- To demonstrate, whether the scale/profile of intracellular calcium increase after injury in a naturally vulnerably cell type (motor neurons in the hypoglossal nucleus) could be transformed to that of resistant motor neurons (oculomotor neurons) by PV upregulation
- To develop methods to quantify perineuronal (micro)glial reaction after injury
- To analyze the consequence of the reduced motoneuronal calcium increase on the local glial reaction after injury in PV upregulated mice

MATERIALS AND METHODS

Experimental animals

Maintenance of the transgenic colony

The description of the generation of the PV overexpressing (PV+/+) mice used in this study has been given elsewhere (Beers et al, 2001). Parental breeding between transgenic CaMKII-parvalbumin mice #4031x4034, 4035 obtained from Dr. S. H. Appel (The Methodist Hospital Neurological Institute, Houston, TX) was set up at the conventional animal facility of the Institute of Experimental Medicine, Budapest. All transgenic mice used in this study were derived from the original parental cross between transgenic male #4031 mated to 4034 and #4045 females of line Tg (parv 14-4). All litters obtained from this cross (mice #12-21) and subsequent sibling/sibling matings as well as the parents were homozygous for the transgene as proved by testcrosses to wild-type mice. To prove the presence of the transgene, DNA was isolated from tail biopsies and prepared according to a standard protocol published online on the Jackson Laboratory website http://www.jax.org/imr/tail_phenol.html). In general, 0.1 μg of genomic tail DNA was used to amplify the transgene using two different primer pairs: (A): primers derived from the 3d and 4th exon of the endogenous CaMKII gene as: forward 5'-CTGCAGACTCCTTCGACCAC-3' and reverse 5'-GCCATCAGCGTCTTTGTTTC-3'. The

sizes of the products were 200 bp (transgene) and 1400 bp (endogenous CamKII gene). (B) primers were: forward primer 5'-GCGAGCGAGTCGAGTGGTTGTCTG-3' and reverse primer 5'-TTAGCTTTCGGCCACCAGAGTGGAGAATTC-3' (Beers et al, 2001), size of the product 1200 bp. Amplification was as follows: denaturation at 94 ^{o}C for 4', followed by 30 cycles of 30" at 94 ^{o}C, 45" at 57 ^{o}C and 45" at 72 ^{o}C, final extension 7' at 72 ^{o}C. DNA was run on EtBr- containing agarose gels and photographed under UV light.

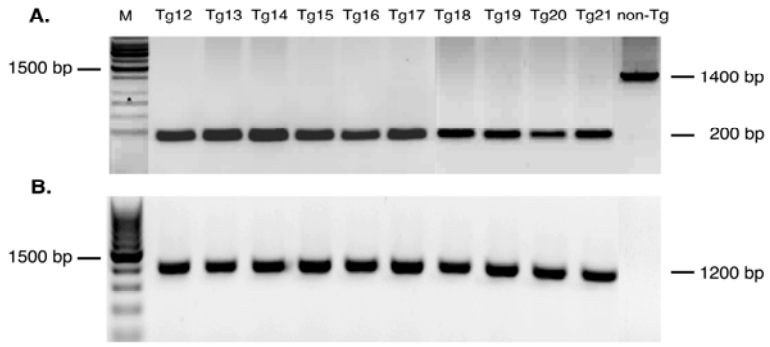

Fig.1. Polymerase chain reaction (PCR)-based genotyping of CamKII-parvalbumin transgenic mice. Transgenic litter from a homozygous cross between mice #4031x#4034, #4045 of line PV 14-4 (#12-21) were tailed-clipped, DNA from tail biopsies was purified and subjected to 30 rounds of PCR with two different primer pairs as detailed below. (A): primers resulting in a transgene-specific 200 bp and 1400 bp (endogenous CamKII gene) were used. This band is missing in the lanes of transgenic DNA because of highly preferential amplification of the transgene. (B): primer pair B was used resulting in a 1200 bp, transgene-specific band. All mice from this cross (Tg12-Tg21) were positive for the transgene.

Characterization of the motoneuron pools in PV+/+ mice

Beside the demonstration of the presence of the transgene in the PV+/+ animals by PCR, hypoglossal- and spinal motor neurons, which are devoid of parvalbumin in the wild type mice were checked for the presence of the PV by light microscopic immunocytochemistry.

In the hypoglossal nucleus, PV was demonstrated using the avidin biotin technique. In these sections, PV-positive motor neurons were identified according to their shape, size and distribution (Fig. 2). PV immunostaining was performed on the 30-µm thickness cryostat sections. Endogenous peroxidase activity was first blocked with H_2O_2, and then sections were immersed in Triton X-100 to enhance antibody penetration. Sections were pretreated with normal rabbit serum for one hour, followed by overnight incubation at 4^0C with 1:60 000

dilution of polyclonal rabbit anti parvalbumin antibody (PV 28, Swant). After washing, 1:200 dilution of biotinylated goat anti rabbit secondary antibody (BA 9200, Vector) was placed on the samples and incubated for one hour. The antibodies were detected with Vectasatin Elite ABC Kit (PK-6100, Vector) and visualized by incubation in diaminobenzidine (DAB, 5% in PBS, Sigma).

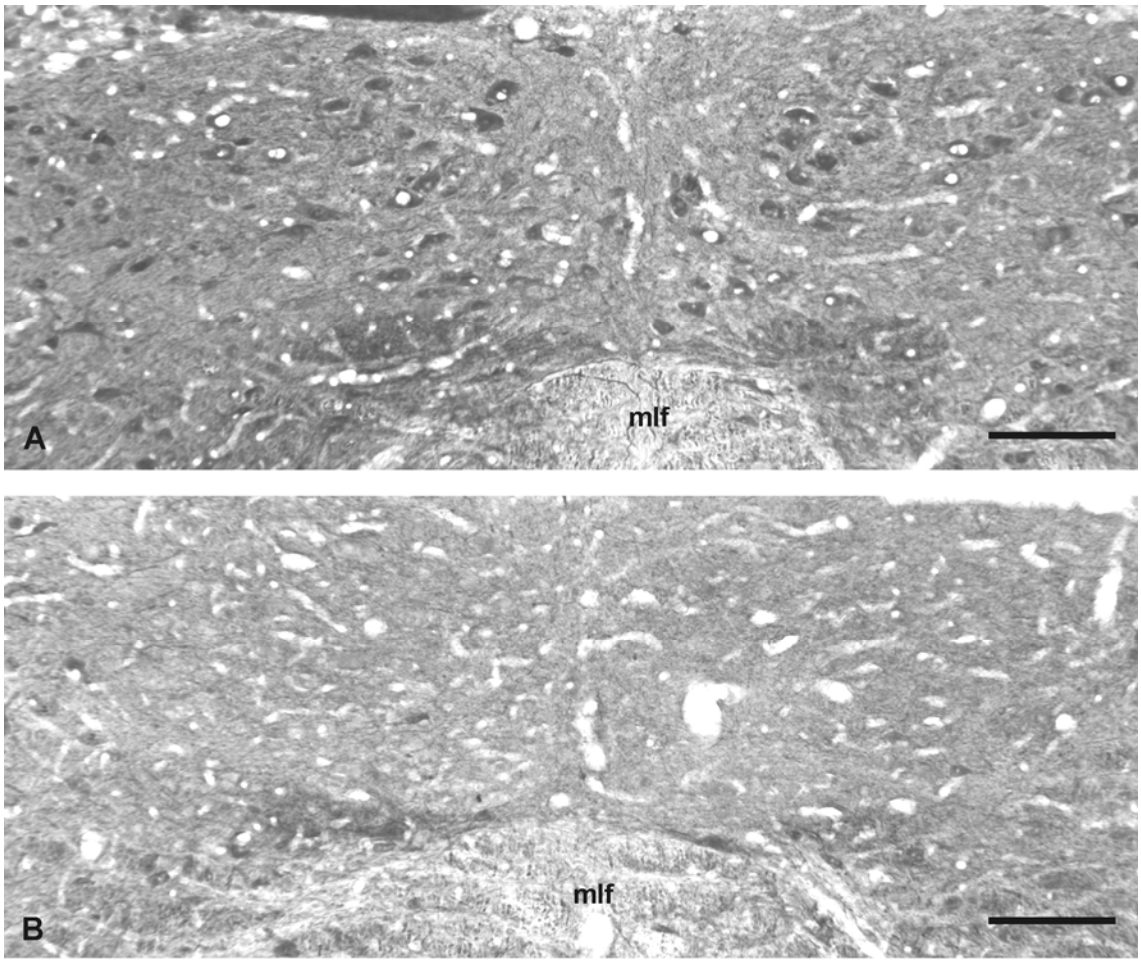

Fig.2. Parvalbumin staining of the hypoglossal of PV+/+ (A) and B6/SJL (B) mice. In the hypoglossal nucleus of the PV+/+ animals, numerous stained cellular profiles are visible which cells, according to their size, shape and distribution can be considered as motor neurons (A). In the hypoglossal nucleus of the B6/SJL mice only background staining can be seen (B). Some stained cellular profiles at the ventro-medial and lateral border of the hypoglossal nucleus in both figures may belong to the nucleus of Roller and the intercalated nucleus of medulla, respectively. mlf: medial longitudinal fasciculus. Bar: 100 μm.

In the spinal cord of PV+/+ mice, double immunostaining, for cholinacetyltransferase (ChAT) and PV was performed, also using 30-μm thick cryostat sections. Endogenous peroxidase

activity was first blocked with H_2O_2, then sections were pretreated with normal donkey serum for one hour, followed by overnight incubation at 4 ^{0}C with a primary antibody cocktail, containing the same polyclonal primary antibody against PV as above (1:60 000) and a polyclonal goat anti ChAT antibody (Chemicon, AB1582; 1:250). After washing, a cocktail of Alexa Fluor 546 (anti rabbit) and Alexa Fluor 488 (anti goat) fluorescent secondary antibodies were placed (1:200) and incubated for one hour at room temperature. Sections were washed in PBS, mounted on silane-coated glass slides, covered with Gel/Mount (Biomeda) and visualized under a laser confocal microscope (Olympus FV1000) (Fig. 3).

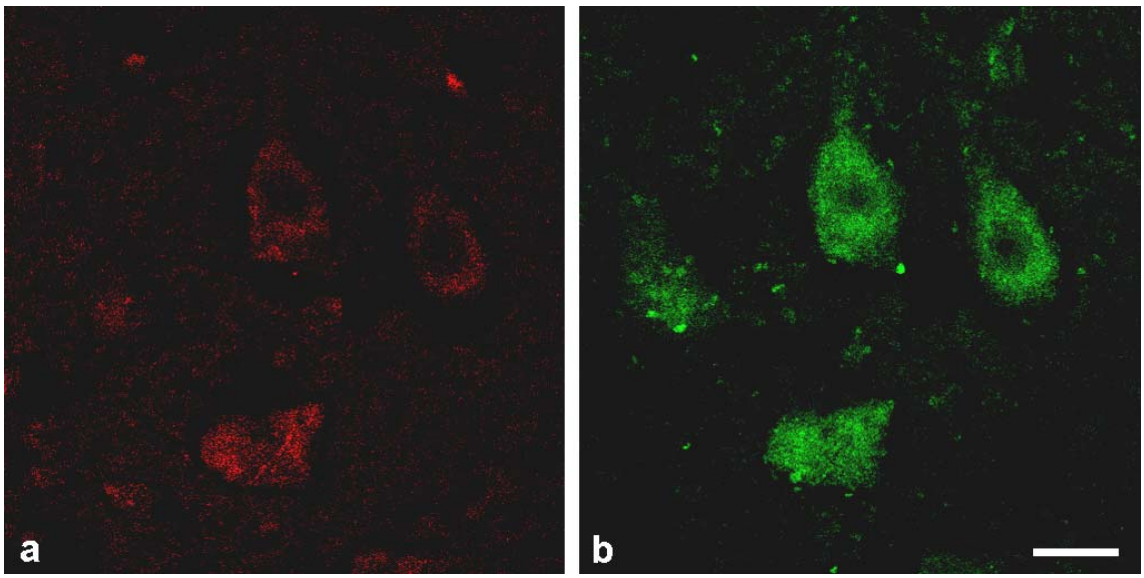

Fig.3. PV-positive motor neurons at the ventro-lateral region of the spinal cord in PV+/+ mice were identified according to a colocalized staining with PV (a) and ChAT (b). Bar: 30 μm.

Axotomy/target deprivation of hypoglossal and oculomotor neurons

Twelve weeks old male B6/SJL mice (BRC, Szeged, Hungary), with breeding pairs originally obtained from Charles River Laboratories (Budapest, Hungary), and PV+/+ mice (IEM, Budapest; BRC, Szeged) were selected for the study. To avoid multiple survival surgery, animals were assigned either for hypoglossal or oculomotor nerve cut experiments. A total of 60 mice were used either for hypoglossal axotomy (n=40) or for oculomotor surgery (n=20). Four animals were euthanized at 5 time points for both types of surgery and were processed for electron microscopic calcium histochemistry study. Surgical procedures were performed under deep anesthesia with Avertin (tribromoethanol; Fluka; 240 mg/kg body weight in a 0.3

ml volume) administered intraperitoneally. The hypoglossal nerve was transected lateral to the hyoid bone and a piece of 3-5 mm nerve segment was removed to prevent regeneration. For transection of left oculomotor nerve, animals were enucleated and the orbits were cleared of the remaining extraocular muscles and nerve segments.

Axotomy of the sciatic nerve

Twelve weeks old male B6/SJL, Balb/C mice (BRC, Szeged) and PV+/+ mice were selected for the study. Animals were assigned either for electron microscopic calcium detection study, or to light microscopic immunocytochemistry, or functional assay study. Surgical procedures were performed under deep anesthesia, as described above. The sciatic nerve was transected at the mid-thigh, and a small piece (3-5 mm) was removed to prevent reinnervation (Fig. 4). In these and in the above experiments the non-operated side served as an internal control. Following surgery animals were housed in a temperature controlled room with a 12 h light/dark cycle, with access to water and food *ad libitum*, and were allowed to survive for 1, 4, 7, 14 and 21 postoperative days. All the experiments were performed in accordance with the institutional guidelines for the use and care of experimental animals and the appropriate governmental laws for animal protection (protocol No. 72-45/b/2001 and No. 03876/0014/2006).

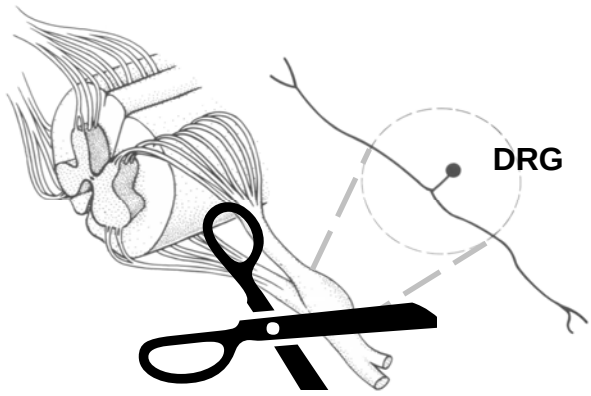

Fig.4. Sciatic lesion model in mice (modified after Kandel et al, 1991; Fig 20-3).

Electron microscopic detection of calcium

Specimen preparation

Mice anesthetized irreversibly with methoxyflurane were perfused transcardially, first with 90 mM potassium oxalate (Sigma) and then with 3% glutaraldehyde (Polysciences) containing 90 mM potassium oxalate (pH 7.4) (Borgers et al, 1977, 1981). Tissue blocks containing either the nuclei of cranial nerves III or XII, or the lumbar segment of the spinal cord were dissected and fixed overnight in the same fixative (4 ^{0}C). Specimens were rinsed in 7.5%

sucrose in 90 mM potassium oxalate (pH 7.4), and then postfixed for 2 h (4 ^{0}C) in 2% potassium pyroantimonate (Merck) and 1% osmic acid (Sigma), adjusted to pH 7.4 with acetic acid (Molar). Following postfixation, specimens were rinsed in distilled water (pH adjusted to 10 with KOH) for 10 minutes, dehydrated in graded series of ethanol, processed through propylene oxide (Sigma) and embedded in plastic (Durcupan ACM, Fluka). Blocks were polymerized for 2 days at 56 ^{0}C.

Semithin (0.3-μm) sections were cut from the blocks on an Ultracut UCT ultramicrotome (Leica), etched (Maxwell, 1978), stained (Richardson et al, 1960) and screened under the light microscope (Olympus Vanox-T) to identify the borders of nuclei III, XII and lamina IX in the spinal motor neurons. After trimming, 50-nm ultrathin sections were obtained, mounted on formvar-coated single-hole copper grids, contrasted with uranyl acetate and lead citrate and analyzed in the electron microscope (Zeiss CEM 902). The procedure resulted in electron-dense deposits (EDDs) due to the precipitation of tissue calcium by the fixative, which was easily recognized by conventional transmission electron microscopy.

Specificity control of the histochemical reaction for calcium

Time-to-time, the specificity of the fixation procedure for calcium was checked by electron spectroscopic imaging (ESI) (Bauer, 1988; Reimer et al, 1988). For such analysis, 15-25-nm sections were prepared, mounted on uncoated 700-mesh copper grids and without contrasting, examined under the electron microscope in ESI mode at Δe=250 eV, which setting was used for structural imaging, as well (Körtje and Körtje, 1992). Such images, resembling "dark-field" images, were then inverted for easier comparison. The analytical image displaying the net calcium distribution was obtained by subtracting the background image (Δe=310 eV) from the "edge" image (Δe=355 eV). The non-significant signal below the [mean + 2.5 × s.d.] level was deleted in the analytical image, and then, for easier comparison of the co-distribution of the EDDs with the true calcium, the significant calcium signal was false-colored according to the significance level in the [mean + 2.5 × s.d.] to [mean + 6 × s.d.] interval. This final image, representing the distribution of the precipitated calcium in the tissue, was compared visually with micrographs obtained by structural imaging of the same area, displaying the arrangement of the EDDs (Fig 5).

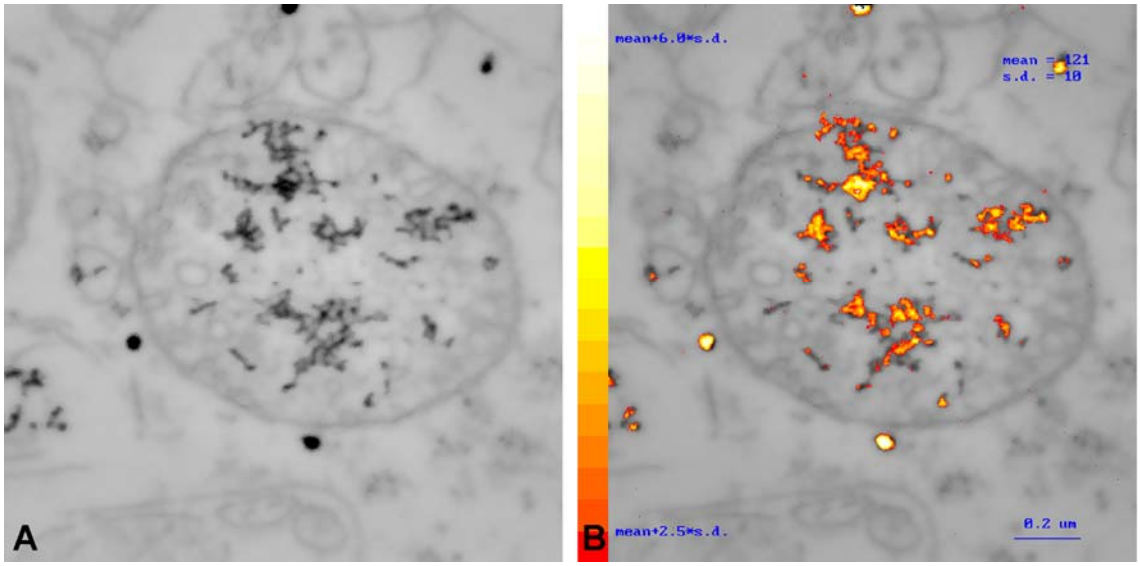

Fig.5. Electron spectroscopic imaging (ESI) of electron-dense deposits (EDDs) of the histochemical reaction. A: Fine structural image of a typical intra-mitochondrial cluster of EDDs. B: The same area was also analyzed by ESI set to produce the net distribution of calcium at the significance level of <background + 2.5 s.d.>. The comparison of (A) with (B) demonstrates a good correlation of the EDDs with the tissue calcium.

Semiquantitative evaluation of the intracellular amount of EDDs

Ultrathin sections were screened under the electron microscope at low magnification (3 000 ×) to identify motor neurons, which were selected randomly for measurements. One region from each cell body, also selected at random, was photographed at a magnification of 12 000 ×, printed at 2.7 × enlargement, until 12-15 samples had been collected from both the operated and the non-operated sides in each animal. The amounts of calcium were determined by measuring the relative volume of the EDDs with respect to selected reference volumes. Three types of reference spaces were selected: either the whole perikaryal volume, or the mitochondrial, or the extra-mitochondrial compartments of the perikaryal space. The three-dimensional parameters were determined with a point counting technique (Mayhew, 1992). After random superimposition of a tessellation of sampling points on the prints, grid points overlying either the EDDs [$P_{EDD(cyt)}$, or $P_{EDD(mit)}$] or the corresponding reference area [$P_{(cyt)}$, or $P_{(mit)}$] were counted. The scores obtained on individual micrographs were pooled according to the operated and non-operated sides and the corresponding ratios expressing the "histochemical concentration of calcium" in the mitochondrial and cytoplasmic compartments were calculated for both sides [$\Sigma P_{EDD(cyt)}/\Sigma P_{(cyt)}$ and $\Sigma P_{EDD(mit)}/\Sigma P_{(mit)}$]. Finally, the

corresponding values obtained on the operated side were divided by those obtained on the non-operated side to express the changes (fold increase) induced by the axotomy in the mitochondrial and cytoplasmic calcium contents for each animal. The fold increases in calcium in the hypoglossal and oculomotor nuclei of the PV+/+ animals and in the hypoglossal nucleus of the B6/SJL mice were compared on postoperative days 1, 4, 7, 14 and 21 statistically (two-way ANOVA with Duncan *post-hoc* comparison; StatSoft Statistica). In the spinal cord, after sciatic axotomy, the fold-increase of calcium was determined only at postoperative day 7, when the glial reaction was at its maximum. The difference between the strains was compared statistically (one-way ANOVA with Duncan *post-hoc* comparison; StatSoft Statistica).

Immunohistochemical characterization of inflammatory markers in the spinal cord

CD11b staining

Microglial acticvation after axotomy was followed by CD11b-staining using light microscopic immuncytochemistry. Mice under irreversible anesthesia were transcardially perfused with 10 mM PBS, followed by 3% paraformaldehyde in 10 mM PBS. The spinal cords were removed and immersed in the same fixative for 24 h (4 ^{0}C). To prevent the formation of freezing artifacts, tissue samples were placed in sucrose (30% in 10 mM PBS, pH 7.4) for at least 2 days at 4 ^{0}C. Sections with a nominal thickness of 30 μm were then cut on a cryostat at -18 ^{0}C, and collected in 10 mM PBS. To detect microglial cells with an IHC procedure, free-floating sections were stained according to the avidin-biotin technique (Cuello, 1993). Sections were rinsed first with 3 changes in PBS, which was followed by a 30-minute blockade of endogenous peroxidase activity with 0.3% hydrogen peroxide in 10 mM PBS containing 0.2% Triton X-100 (Sigma) (TPBS). Then, after washing (3 changes in PBS), to reduce the nonspecific staining, sections were incubated in 2% normal goat serum (Vector) in TPBS for 1 h. Microglial cells were labeled with anti-CD11b antibody (1:500 in TPBS; rat-anti-mouse antibody, Serotec) during incubation at 4^{0}C overnight. After washing in PBS (3 changes), sections were incubated in biotin-labeled secondary antibody for 1 h (1:800 in TPBS, goat-anti-rat IgG, Vector), followed by washing in PBS (3 changes), and incubation in the avidin-biotin complex (1:1600 in PBS, Vector) for 1 h, at room temperature. Finally, after washing in PBS, the reaction was visualized by incubation in DAB (5% in PBS; Sigma)

for 15 min. Stained sections were thoroughly rinsed in PBS, mounted on silane-coated glass slides, dehydrated in graded series of ethanol, processed through xylane (Molar) and coverslipped with Entellan (Merck).

MCP1 staining

The immunostaining to detect the chemokine MCP-1 (monocyte chemotactic protein-1) was performed similarly, as above on free-floating 30-µm thickness cryostat sections, using the avidin-biotin method adapted to the primary antibody: polyclonal rabbit anti-murine JE antibody (PeproTech, 1:1000).

Evaluation of the functional recovery after sciatic nerve cut

Additional, twelve week old, male PV+/+, B6/SJL and Balb/C mice (4 animals in each group) were allocated for the study. Following sciatic nerve cut, animals were housed in a temperature controlled room with a 12h light/dark cycle, and had access to water and food *ad libitum.* The function of the operated hindlimb of animals was characterized daily at the same time. An arbitrary, but systematically applied scale was used to asses the recovery of the hindlimb function (Table 1).

Table 1. Assay of recovery of the hindlimb function after sciatic nerve cut

Grade	Definition
1	Practically no function on the operated side, the animal does not rear
2	Drags paralyzed hindlimb, the overall behavior, mobility is sluggish
3	Occasionally uses operated limb, increased mobility, cannot climb on the grid
4	Walks actively using both hindlimbs, still cannot bend fingers on the operated side
5	Tries to bend fingers during walking, but cannot grasp grid during climbing
6	Time-to-time bends fingers during walking but still cannot do that during rearing
7	Walks normally but easily tired, still cannot grasp grid with the fingers
8	Normal walking, increased ability to grasp the grid with the fingers
9	Normal walking, only occasional problems during rearing and grasping the grid
10	Full recovery

The subjectivity in grading the hindlimb function was tried to be reduced by evaluating the animals in the different groups in a single session in each day by pinpointing even slight relative differences in the behavior. Furthermore, all the evaluation processes as well as the daily animal care during the 28-day course of the study was performed by the same person.

RESULTS

Calcium increase is reduced after injury in hypoglossal motor neurons of PV+/+ mice

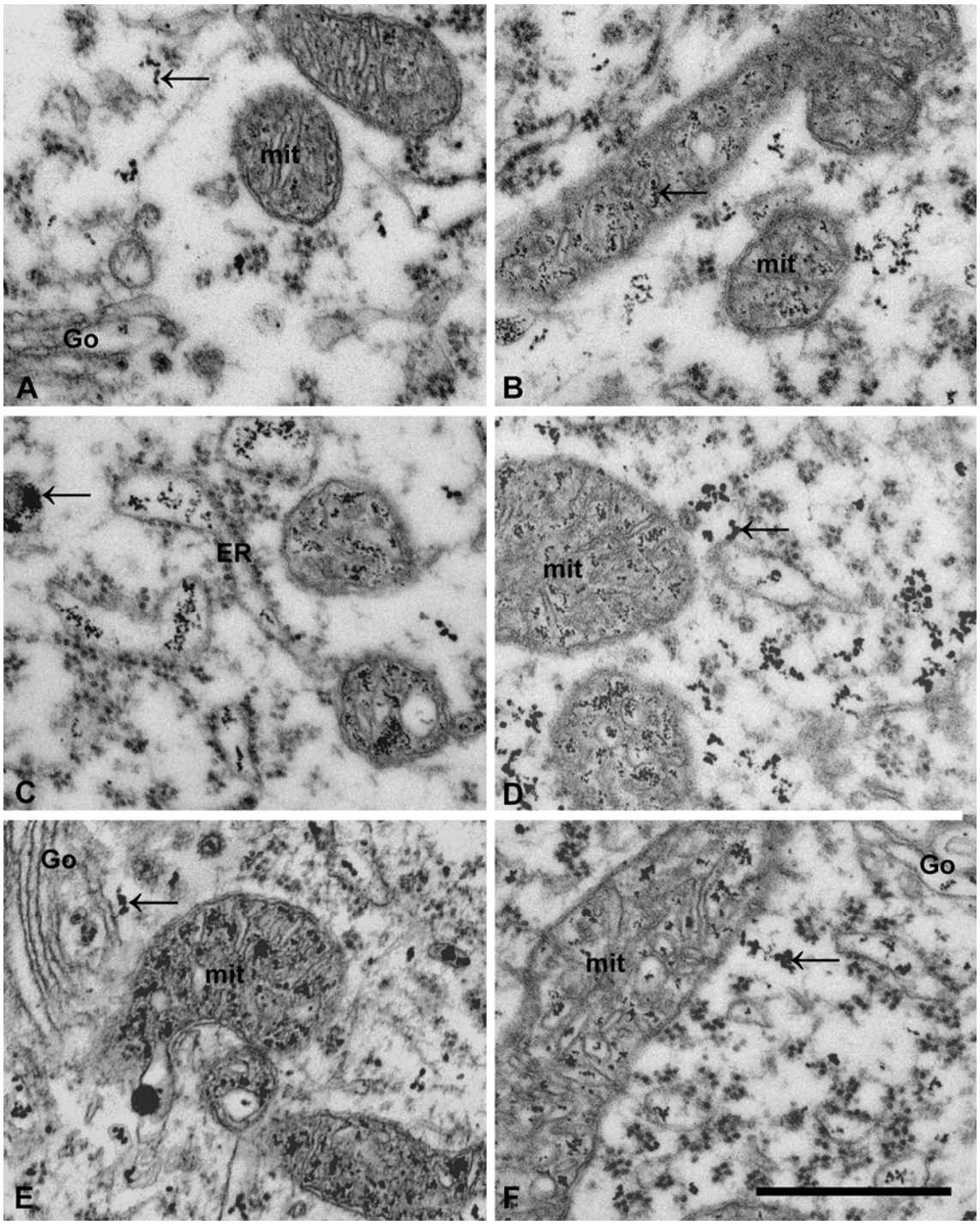

Fig.6. Calcium in the hypoglossal motor neurons of B6/SJL mice. A: non-operated side, B-F: operated side at postoperative day 1, 4, 7, 14 and 21. Go: Golgi apparatus, mit: mitochondrion, arrow: EDD. Bar: 1 μm.

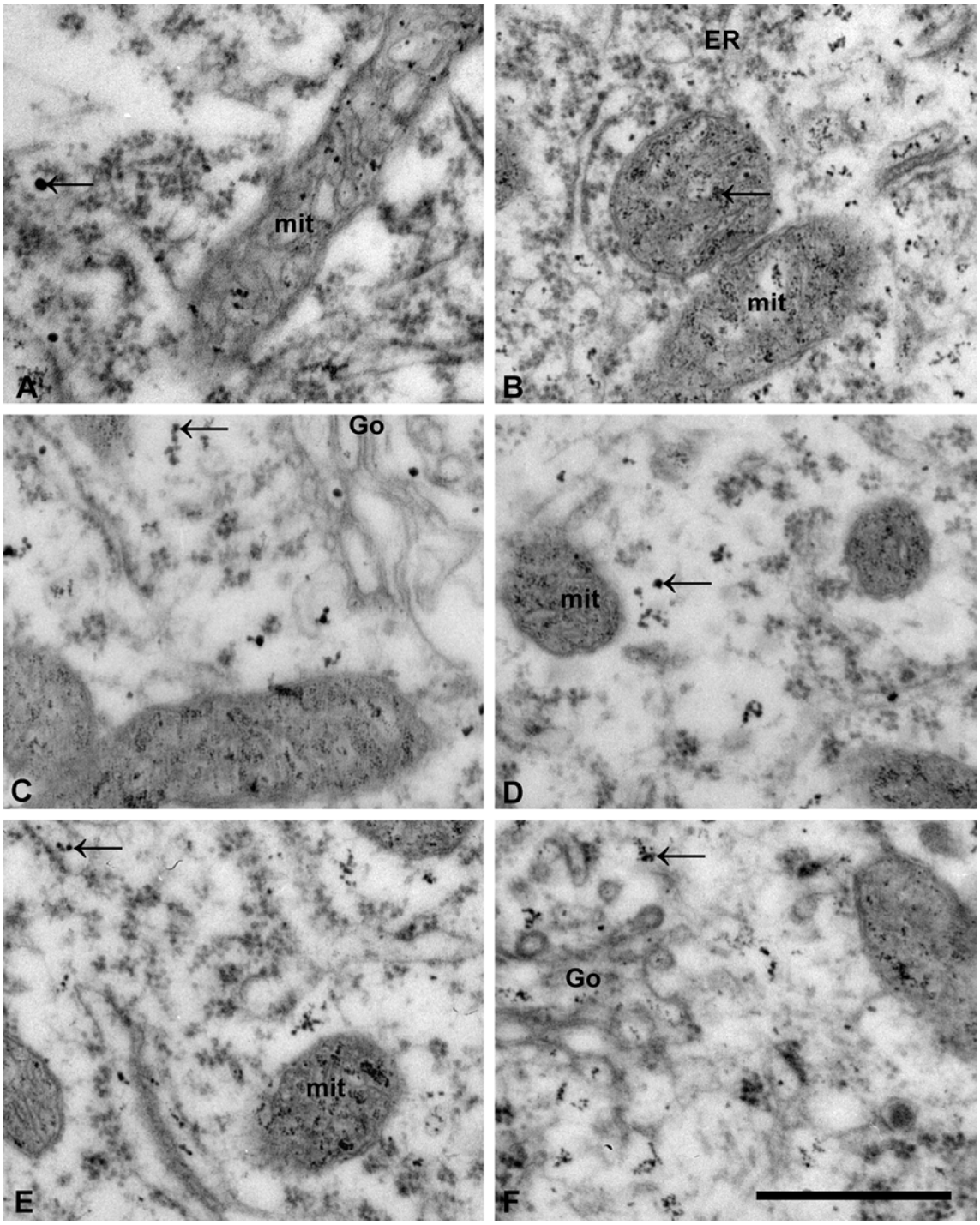

Fig.7. Reduced calcium increase after axotomy in the hypoglossal motor neurons of PV+/+ mice compared to theB6/SJL strain. A: non-operated side, B-F: operated side at postoperative day 1, 4, 7, 14 and 21, respectively. Go: Golgi apparatus, mit: mitochondrion, arrow: EDD. Bar: 1 μm.

Qualitatively a gradual elevation of the intracellular calcium content in the axotomized hypoglossal motor neurons of the B6/SJL mice was seen with increasing postoperative time relative to the non-operated side, with a tendency to return to the control level by postoperative day 21 (Fig. 6). In the hypoglossal neurons of the PV+/+ animals, however, except for a slight increase in the mitochondrial calcium content on postoperative day 1, the calcium content was observed not to be elevated relative to the control side on any postoperative day (Fig. 7). In the oculomotor neurons of the PV+/+ mice, similarly as in the hypoglossal neurons in these animals, no calcium increase was detected in the injured neurons as compared with the intact cells at any time point after the surgery (not shown).

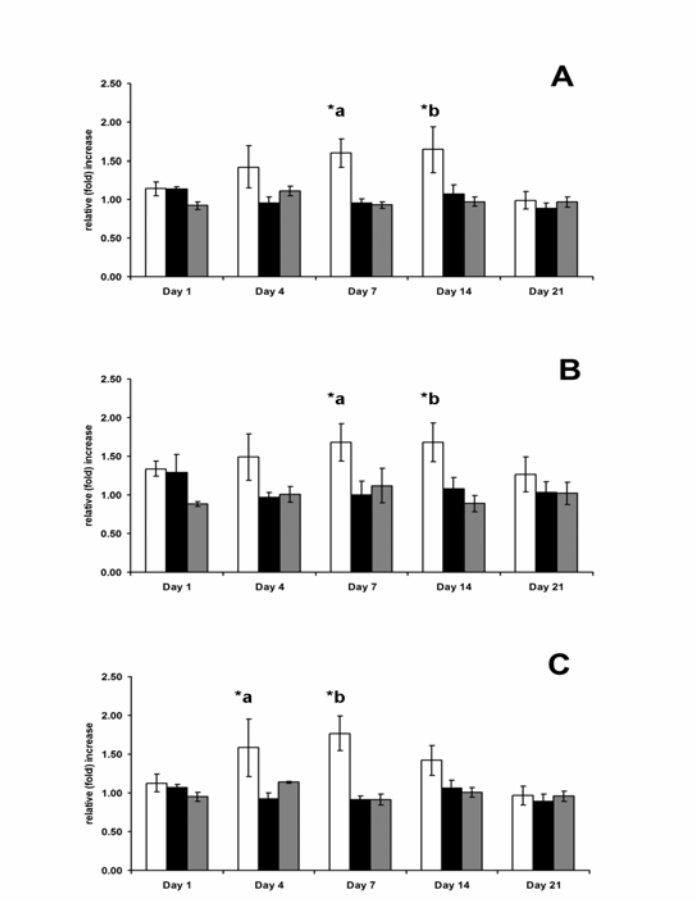

In both motor nuclei, the volume fraction of the EDDs, characterizing the distribution of calcium in the tissue, was expressed quantitatively. Statistically, the time dependences of the calcium levels in the two nuclei in the PV+/+ strain did not differ, regardless of whether the total calcium ($p=0.21$), or the cytoplasmic ($p=0.43$) and mitochondrial ($p=0.20$) calcium levels separately were compared (Fig. 8). However, the postoperative calcium increase in the motor neurons from the B6/SJL mice was significantly different from that of the PV+/+ animals ($p=0.001$).

Fig.8. Quantification of the amount of EDDs in the perikaryal volume (A), in the mitochondria (B) and in the cytoplasm (C) of the hypoglossal motor neurons of B6/SJL (white bars) and PV+/+ mice (black bars) and of the oculomotor neurons of PV+/+ animals (gray bars). Data are expressed as the fold increases relative to the non-operated side on days 1, 4, 7, 14 and 21 postoperatively. The overall calcium increase in the motor neurons from the B6/SJL mice was significantly different from that for the PV+/+ animals ($p=0.001$, two-way ANOVA) with slight differences at day 4, 7 and 14 postoperative times in the different cellular compartments.

These data provide evidence for that – with regard to the calcium handling after injury – an increased calcium buffer may confer an "oculomotor-like resistant phenotype" to the naturally vulnerable hypoglossal motor neurons against injury. For more details see Paizs et al. (2010a).

Inflammatory reaction can be quantified by systematic sampling and background corrected segmentation using immunohistochemistry

Inflammatory responses in the CNS are commonly assayed by the reaction of the immuno-competent microglial cells in the CNS, characterized by IHC. Obtaining reliable conclusions on the basis of IHC staining is hindered by the regular need of subjective judgments, due inconsistencies of the staining intensity from section-to-section or in repeated experiments. Our method, utilizing digital image analysis, is based on the use of an internal reference area on the analyzed sections, which makes the relative changes of IHC staining in different experiments comparable, independent of the examiner (Fig. 9). Another source of variability of staining could be attributed to the internal heterogeneity of the object to be characterized, which means that identical fields could never be analyzed. To compensate also for this variability, a systematic random sampling paradigm was designed, which provides data, expressed in single numbers, describing the dimension and strength of IHC staining in the entire volume to be characterized (Fig. 10). In this integrated approach, the figures are derived by pooling relative IHC staining intensities from all of the sections of the series from a particular animal. The procedure (1) eliminates the problem due to the personal assessment of the significance of IHC staining intensity, (2) does not depend on the precise dissection of the tissue on a gross scale, i.e. considerably reduces the consequences of a limited, arbitrary sampling of the region of interest, and finally (3) arrives at quantitative data characterizing the extent of inflammation in the animal. The procedure has been validated in a well documented experimental paradigm, selected to be analogous to our intended experimental plan. Thus, as a positive test, inflammatory reactions in the spinal cord, measured as microglial activation, were followed by IHC after axotomy of the sciatic nerve in mice, and, then, the effect of a known anti-inflammatory compound (minocycline) has been tested. These measurements proved that our quantification procedure is capable to measure inflammatory reactions light microscopically and sensitive enough to demonstrate the efficacy of anti-inflammatory interventions (Table 2). For more details see Paizs et al. (2009).

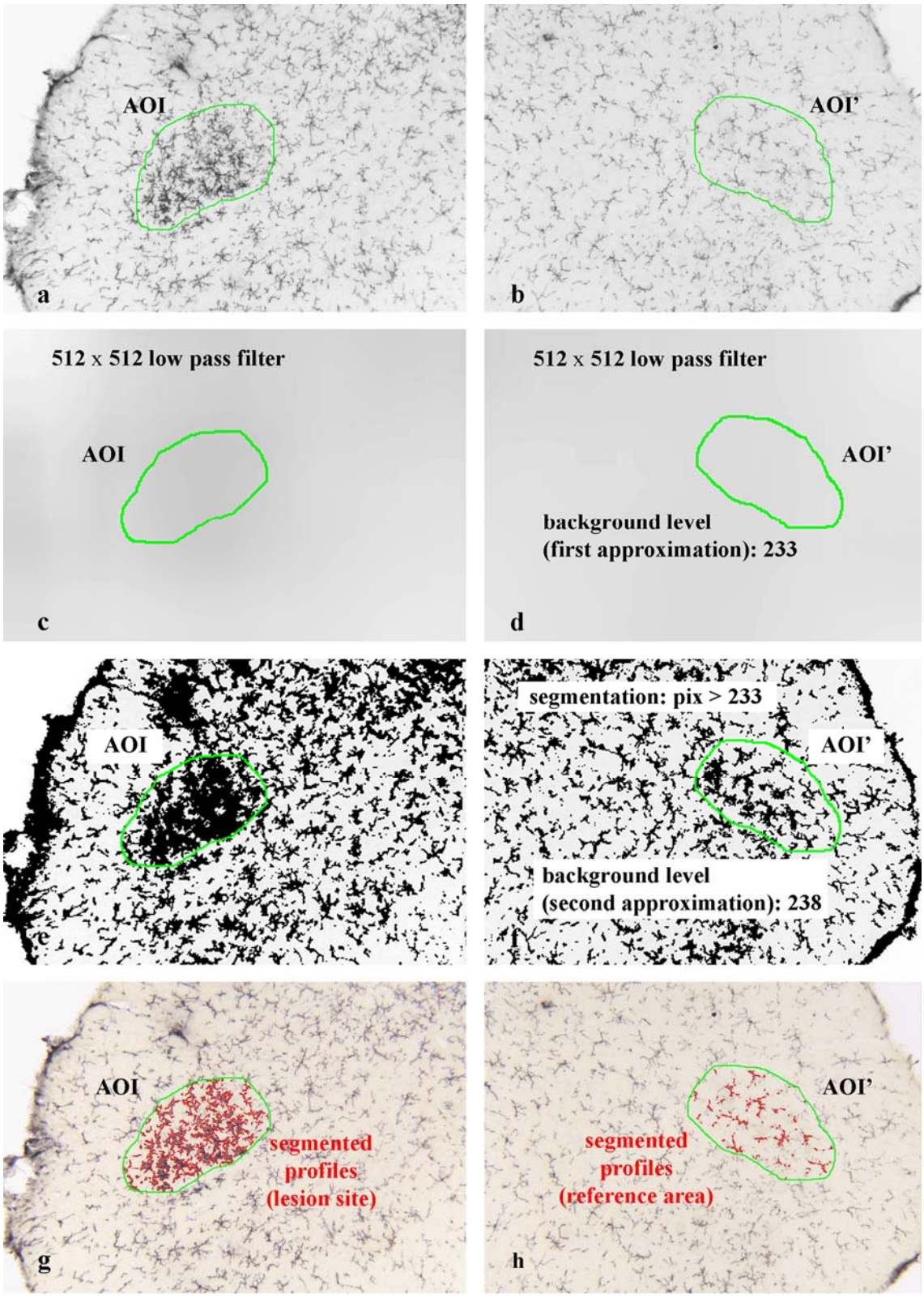

*Fig.9. Approximate area of the expected reaction is marked on the spinal cord sections (**a**: AOI), then mirrored to the non-operated (unaffected) side (**b:** AOI'), The background intensity has been determined using the unaffected side as reference (**c-f**), then the significant signal has been segmented automatically (**g, h**).*

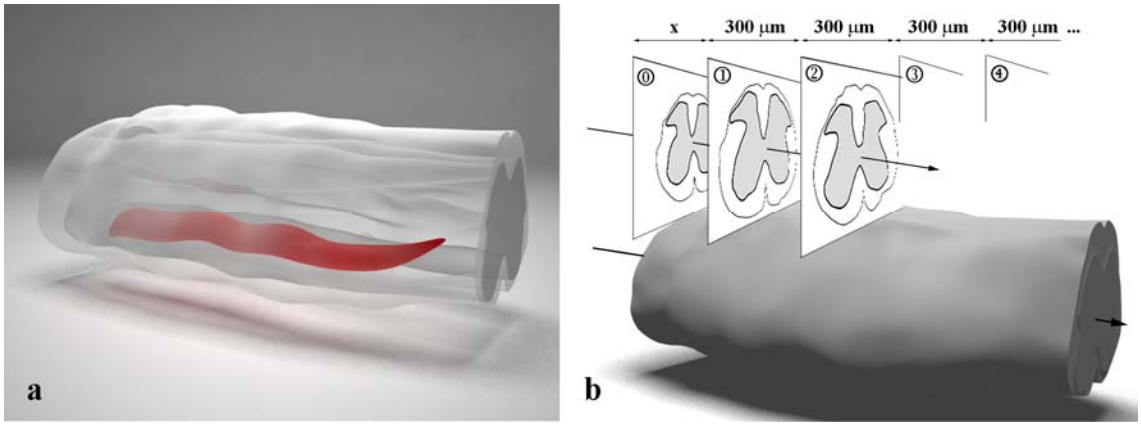

Fig.10. Expected dimension of the microglial reaction in the spinal cord after the lesion of the sciatic nerve (a: red shaded volume), which is assayed by systematic sectioning (at 300 µm) started at a random (x) position (b).

With this integrated sampling/calculation procedure the anti-inflammatory effect of minocycline could be demonstrated (Table 2; $p < 0.05$). Similar significant results could be obtained either by measuring the pooled relative staining intensity or the pooled relative area density covered by the stained cells (Table 2).

Table 2. Effect of minocycline treatment on CD11b IHC staining after sciatic nerve cut

animals	operated only		operated + minocycline	
	poled relative stained area [%]	pooled intensities [–ln(I(op)/I(co))]	pooled relative stained area [%]	pooled intensities [–ln(I(op)/I(co))]
#1	374.28	1.67	375.79	1.47
#2	394.03	1.83	425.09	1.97
#3	549.73	2.38	417.56	1.92
#4	642.55	3.19	365.81	1.72
#5	541.82	2.47	--	--
#6	657.43	3.24	--	--
mean	526.64	2.46	396.06	1.77
S.E.M.	49.01	0.66	14.81	0.23

Increased motoneuronal calcium buffer reduces local inflammation after acute lesion

The relationship between the increased calcium buffering capacity of motor neurons and the altered local inflammatory reaction has been examined in the spinal cord of PV+/+ and control (B6/SJL and Balb/c) mice after the lesion of the sciatic nerve. The temporal change of the inflammatory markers has been followed in 21 days after the operation with IHC (total of 30 mice; 2 in each group) supplemented with the characterization of the recovery of the

hindlimb function (4 mice in each group). Calcium level of the motor neurons was determined at day 7, when the inflammatory reaction peaked (6 mice in each group).

Resting microglial cells (Fig. 11a) surrounding motor neurons, after the injury of these cells become activated, change their morphology: withdraw their processes, which, as well as their cell bodies turn to be hypertrophic (Fig. 11c). At the same time, the injured motor neurons release factors, such as MCP1 (Fig. 11b), attracting microglia to the site of injury.

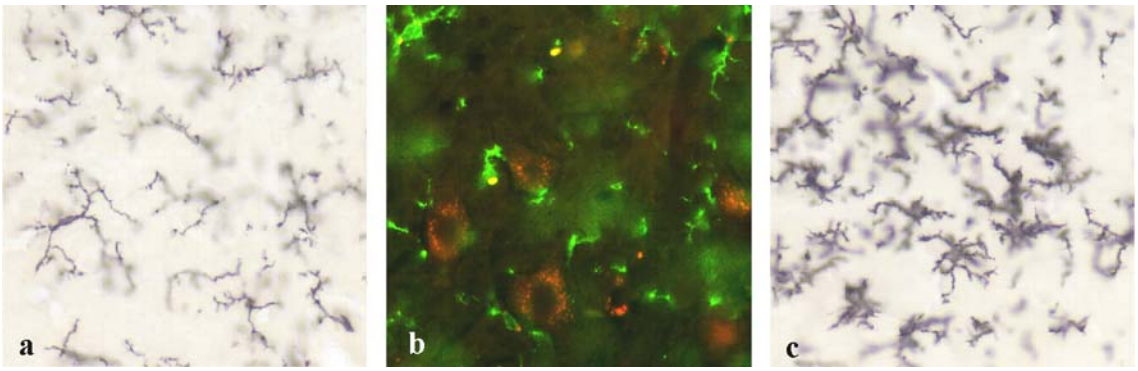

Fig.11. Resting microglial cells (a) become activated (c; b: green color) around motor neurons after injury; motor neurons release chemokine MCP1 (b; red color) serving as a chemotactic signal.

Indeed, by regular inspection of the whole cross sections of the spinal cords of the operated animals it could be documented, that both the microglial activation/reaction (except for the input region of the sensory fibers; c.f. Fig. 4) and the MCP1 release was restricted to, and around the ventro-lateral pool of motor neurons (Fig. 12).

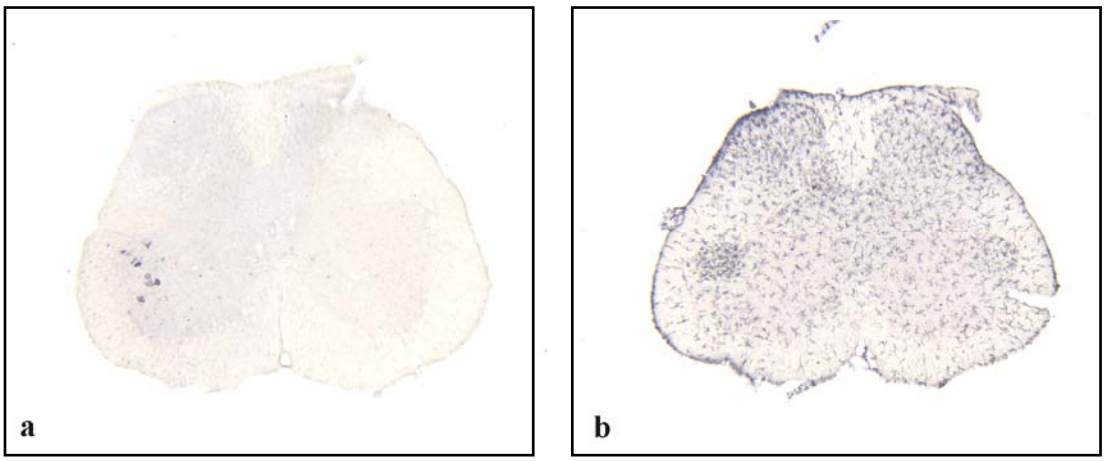

Fig.12. MCP1 staining (a) and increased CD11b staining (b) is confined to the area occupied by the injured motor neurons. Microglial activation at the input of the sensory fibers has not been evaluated in this study.

The inflammatory reaction commenced as early as day 1 after operation in the spinal cord, either the MCP1 chemotactic signal, or the altered CD11b expression is considered. These reactions lasted at least 3 weeks long, however with a different decay time: the decrease of the release of the MCP1 by the injured motor neurons preceded the attenuation of the microglial reaction at their vicinity (Fig. 13). Nevertheless, the decrease of both of these inflammatory markers was significantly faster in the PV+/+ mice compared to the control strains (Fig. 13).

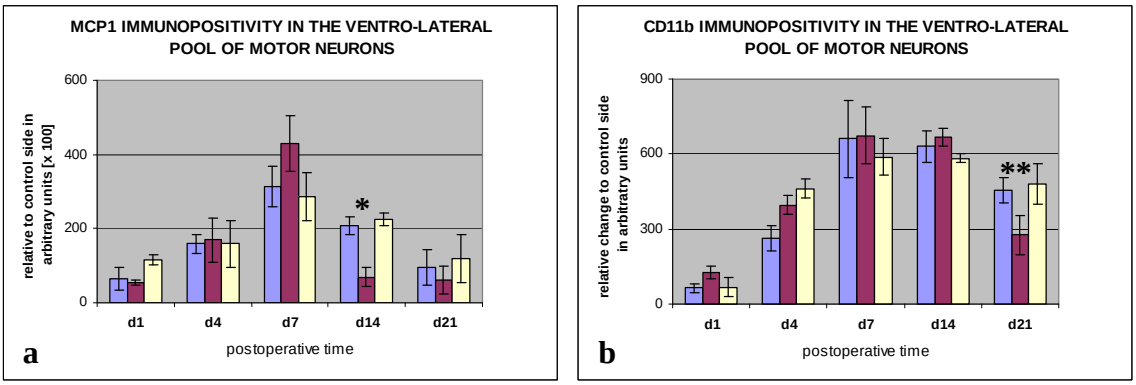

Fig.13. A difference has been demonstrated between the decay of the expression of the chemotactic signal, MCP1 (a), released by the injured motor neurons, and the CD11b (b) staining, characterizing the microglial reaction after axotomy. Most importantly the MCP1 release of the motor neurons from the PV+/+ mice (claret colored bars) returned to close to the baseline at day 14 after operation, significantly (: p<0.008) faster than in the control mouse lines (blue: B6/SJL; yellow: Balb/c), followed by a similarly faster decrease of the microglial reaction, demonstrated at day 21 after the operation (**: p<0.04).*

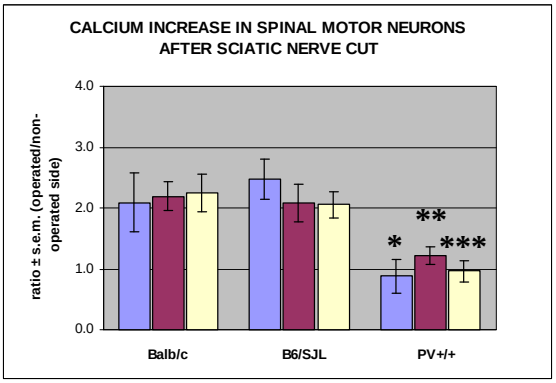

Fig.14. Cytoplasmic- (blue), mitochondrial- (claret) and total calcium (yellow) increase is smaller in the cytoplasm (: p<0.05), in mitochondria (**: p<0.03) and in the perikaryal space (***: p<0.005) in the PV+/+ mice than in the controls.*

An important result of the present experiments is – similar to the hypoglossal motor neurons of the PV+/+ mice – that the PV upregulation attenuated the increase of the intracellular calcium after axotomy in the spinal motor neurons, as well. The calcium measurements have been performed at postoperative day 7, at the time when the calcium increase in the wild type hypoglossal neurons was significantly higher than in those of the PV+/+ mice. Thus, without performing a complete time series

analysis, it can be assumed, that the PV upregulation lends the same “oculomotor-type” resistance to the spinal motor neurons as to the hypoglossal neurons, which is most likely paralleled with a reduction of the calcium mediated injury. In accord with this assumption, the expression of the distress signal, represented by the chemokine MCP1, disappears in the PV+/+ motor neurons faster than in the control strains, followed by a similarly faster elimination of the microglial activation at the vicinity of these cells (Fig. 13). Thus, the reduction of calcium increase in motor neurons is indeed capable of reducing local inflammation, furthermore, according to the observed rate of improvement of the hindlimb function in these animals in the same period, leads to a faster functional recovery (Fig. 15).

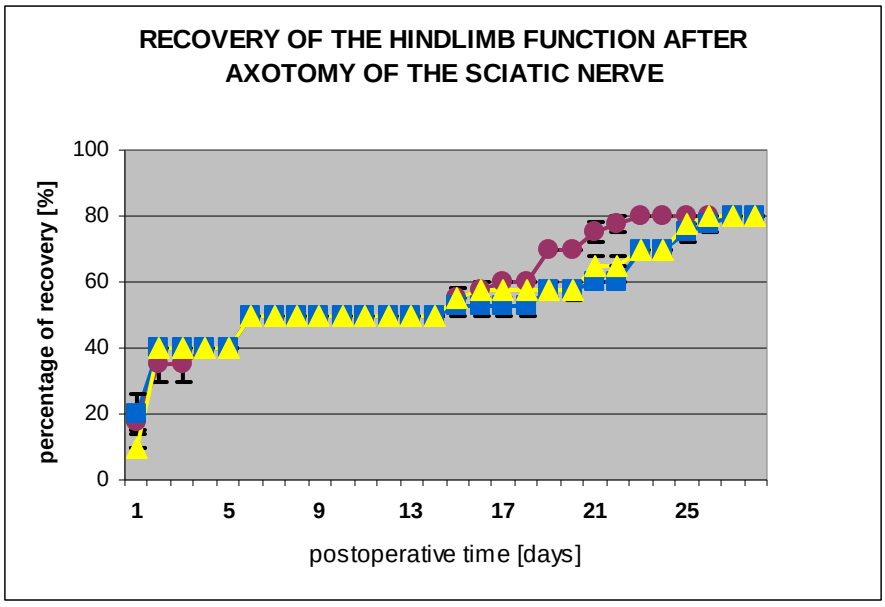

Fig.15. Recovery of the function of the operated hindlimb of PV+/+ (claret color), B6/SJL (blue) and Balb/c (yellow) mice. The recovery was estimated on a 1-10 (10-100%) scale, as described in Table 1. Data are expressed as mean ± s.e.m.

With regard to the rate of recovery, two further comments can be made: (1) even in an extended period of observation after the surgery (4 weeks) no full recovery could be noticed in either strains, (2) although no daily data are available about the microglial activation, the increase in the rate of recovery in the PV+/+ mice was in the same timeframe as the significant decrease of microglial activation compared to the control strains (cf. Fig. 15 and Fig. 13).

DISCUSSION

The role of calcium and CaBPs in neuronal degeneration

It is well documented, that abnormal and sustained increases in intracellular calcium induce a series of calcium-dependent enzymatic processes – not only in motor neurons – which participate in cellular destruction. Certainly, several catabolic enzymes, including protein kinase C, calpains, phospholipase A_2, nitric oxide synthase and endonucleases are directly involved (see e.g. Berridge, 1998; Berridge et al, 1998). Furthermore, excess calcium ions facilitate other destructive processes as well (se e.g. Marambaud et al, 2009). However, it has been debated for a long time whether the calcium buffering capacity plays a role in modifying the outcome of these processes.

CaBPs within the cells are commonly located at critical positions: in the vicinity of plasmalemmal calcium pumps and channels, around the mitochondria and endoplasmic reticulum, organelles known to play key roles in Ca^{2+} signaling and buffering (Brini, 2003). Thus, these proteins may slow down the diffusion of calcium ions away from the influx regions, or facilitate their recycling into internal stores, and thereby reduce the amplitude of calcium concentration changes in the cytosol (Müller et al, 2007; Vanselow and Keller, 2000; von Lewinski and Keller, 2005). The concept that CaBPs may exert a general neuroprotective effect was proposed on the basis of data acquired from a wide range of *in vitro* (Clementi et al, 1996; Mattson et al, 1991; McMahon et al, 1998) and *in vivo* experiments (Beck et al, 1994; Rami et al, 1992; Tortosa and Ferrer, 1993). The idea has received additional support from a variety of clinical observations, e.g. the age-dependent loss of CB from the cholinergic neurons of the basal forebrain in humans displayed a similar pattern to that of the loss of these cells in Alzheimer's disease (Geula et al, 2003), while in Huntington's disease those striatal neuronal groups which contained high levels of CB proved to have a decreased vulnerability (Mitchell and Griffiths, 2003). In Parkinson's disease, the CB-positive dopaminergic neurons in the substantia nigra are relatively spared. Finally, in ALS, the most susceptible motor neurons are comparatively deficient in CB and/or PV (Alexianu et al, 1994; Ince et al, 1993).

However, not all studies lend support to the protective role of the CaBPs during injury. The reports range from documentation of the inability of a high CaBP content to confer resistance on the (Purkinje) cells in the cerebellum (Slemmer et al, 2005), through the lack of a

correlation between the CB and/or PV content and the neuronal vulnerability in the hippocampus (Freund et al, 1990), to the finding that PV actually enhances NMDA-mediated toxicity (Hartley et al, 1996), or to the notion that not an excess, but rather a deficiency in CB might be protective (Klapstein et al, 1998). The diversity of these results, however, might be attributed to the fact that the actual impact of the CaBPs on survival is affected by the local cellular environment, and influenced by the neuronal network properties of the injured cells. In an effort to eliminate such perturbations of the results, in the present study, we decided to assay the changes in calcium level after injury in motor neurons with an artificially elevated PV content, and to compare the results obtained from the same population of neurons with a naturally low PV content in wild-type animals.

Lesion induced by axotomy

Axonal transection is an experimental method for the study of neuronal responses to injury leading to degeneration, or resulting in plastic changes and recovery (Price et al, 1992), some of which resemble those seen in ALS (Price et al, 1994). Factors known to influence the outcome of axotomy-induced injury are the type of lesion (crush, cut, target deprivation or avulsion), the location of the trauma relative to the perikaryon, differences in species, type of the motor neurons and, most importantly, age of the animals (Koliatsos and Price, 1996). For example, approximately 70% of adult hypoglossal motor neurons survive target deprivation in rats, but only 40% survive if the surgery is made during the first postnatal week (Snider and Thanedar, 1989). Similarly, in the spinal cord of newborn animals, while avulsion or crush of the sciatic nerve produces a 73-80% loss of lumbar motor neurons (Koliatsos and Price, 1996), axotomy of the same nerve in adult animals generates no visible loss of motor neurons (Schmalbruch, 1984). Thus, in this study, to evoke sublethal injury, we performed the surgical interventions in animals 12 weeks of age, when the adult response was already present.

Calcium level changes induced by axotomy

The lesion of the hypoglossal nerve of the B6/SJL animals was followed by a transient increase in the intracellular calcium in the corresponding motor neurons, with a peak increase of approximately 1.5-fold around day 7-14. In the same hypoglossal motor neurons of the PV+/+ animals, apart from a slight, insignificant increase in the mitochondrial calcium on day 1 after surgery, no increase was detected relative to the calcium level in the motor neurons on the non-operated side at any time point postoperatively. Likewise, no calcium increase was

seen in the motor neurons of the oculomotor nuclei of the PV+/+ mice after axotomy, and no significant difference could be discerned statistically between the two examined motor nuclei of the PV+/+ animals. Based on these results, in the spinal cord, only one time point, postoperative day 7 was selected to check the calcium increase, when the maximum change in the calcium level could be expected in the motor neurons of the wild type animals. In spinal motor neurons of the PV+/+ mice, similarly to the hypoglossal neurons, no significant calcium increase could be demonstrated, while in the same motor neurons from both control strains a 1.5-2-fold calcium increase, comparable to that of the wild type hypoglossal motor neurons could be demonstrated.

In our earlier study, to compare the calcium response in the hypoglossal and oculomotor neurons of wild type animals, the Balb/c mouse strain was used, and an increased resistance of the oculomotor neurons was documented (Obál et al, 2006). Those experiments left open the question whether the differences in the cellular environment could have contributed to the different resistance. Since, in the present study, we could document a similarity between the responses to axotomy of the same (spinal) motor neurons from two control strains (Balb/c mice and the B6/SJL parental mice to the PV+/+ animals), as well as a similarity between the responses to axotomy of different (hypoglossal- and spinal) motor neurons from the same (PV+/+) strain, we may assume, that neither the diversity in the strains, nor the difference between the cellular environment, but the changed calcium buffering capacity is indeed responsible for the contrasting resistance of these cells, at least in acute lesion paradigms.

The role of inflammatory factors in injury of motor neurons

Microglial activation and proliferation is a nearly stereotypical response to any insult to neuronal tissue. Resting microglial cells normally sense neuronal damage, readily transform into an activated state (undergo morphologic changes of process retraction and cell body enlargement as well as functional changes of increased expression of immune/inflammatory markers) and respond to remove damaged cells by phagocytosis (Kreutzberg, 1996). Microglia may exert both positive and negative effects in the context of neuronal lesion (Kempermann and Neumann, 2003). The positive aspect, besides the removal of the potentially damaging debris left behind following neuronal death (i.e., macrophage function) may involve the production of certain growth factors. However, activated microglia can also

cause neuronal damage, even cell death, through release of a number of cytotoxic mediators, including cytokines, free (oxygen) radicals, nitric oxide etc.

In the present experiments we documented that increasing the calcium buffering capacity in motor neurons reduces the increase of intracellular calcium level after acute injury (Fig. 14), and anticipated that such a way the calcium mediated injurious processes could be attenuated, as well. In agreement with this assumption, the duration of the expression of the chemokine MCP1 by the motor neurons (considered as a distress signal) has been considerably and significantly reduced: it was confined to 14 days after operation, while at two weeks this signal in the control mouse strain was still significantly high (Fig. 13). Following the shorter emission of MCP1 in the PV+/+ mice, the microgial activation started to turn to the baseline also significantly earlier than in the control mouse strains (Fig. 13). In addition to the reduced inflammatory reaction of PV+/+ mice, a further support for the protective role of PV-upregulation in motor neurons was provided by the faster functional recovery data in these mice (Fig. 15). These results together provide evidence for the protective role of PV in acute injury and suggest that the inflammatory reaction might be graded after injury, determined by the magnitude (and/or duration) of the primary lesion.

Quantification of the inflammatory markers by light microscopic IHC

As a byproduct of (or necessity of our experiments) was the development of a reproducible, quantitative light microscopic procedure to assay the magnitude of inflammatory reaction after the neuronal lesion. The procedure practically eliminates the subjectivity of the operator in assessment of the significance (degree of positivity) of the immune-staining, and compensates for a frequently neglected effect of the so-called "random sampling" as illustrated in Fig. 16. Clearly, even using internal standards in the section, the calculated intensity (characterizing microglial activation) strongly depends on the position of the sampling, which cannot be easily reproduced. Our method,

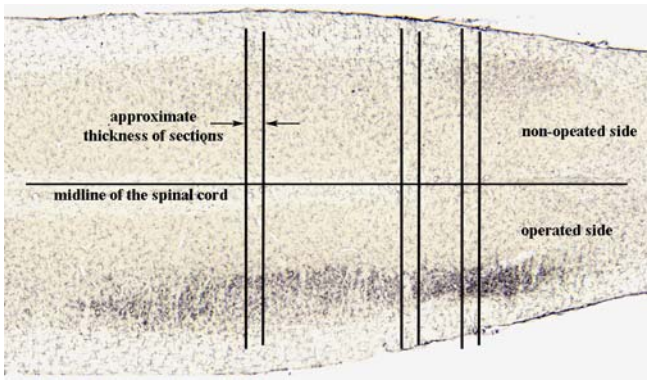

Fig.16. Dorsal view of a spinal cord segment, displaying the distribution of the microglial cells after cutting the sciatic nerve. Note the irregular distribution of the activated cells along the rostro-caudal axis.

bracketing the whole spinal cord with the expected region for analysis, and sampling it systematically, integrates the numbers obtained from the individual sections, thus considerably reduces the variability of the results. As a consequence, we could achieve a precision high enough for our conclusions using only two animals at each time point to record the temporal dependence of the inflammatory reaction.

Relevance of the results in relation to the mechanisms of ALS

The suggestion that CaBPs may protect motor neurons in ALS was based on the parallelism observed between the relatively spared motor functions in patients, such as the eye movement and voluntary sphincter functions. The most widely used model of ALS suitable for *in vivo* research is a variety of transgenic mice developed on the basis of mutations of the enzyme SOD1 detected in a subpopulation of ALS patients (Deng et al, 1993; Gurney et al, 1994; Rosen et al, 1993). Using transgenic animals based on the G93A mutation of SOD1, we earlier demonstrated not only that changes in the intracellular calcium level paralleled the degeneration of the motor neurons, but also that the survival of the motor neurons was associated with higher levels of CB and/or PV (Siklós et al, 1998). Since those experiments still involved the comparison of different motor neurons, (spinal versus oculomotor neurons), it was decided to develop a mouse line with an elevated PV content, suitable for measurement the protective effect of CaBPs in the same neuronal population *in vivo* (Beers et al, 2001). When PV+/+ transgenic mice were bred to the mutant SOD1 animals, a significantly increased preservation of the spinal motor neurons and a delayed onset of the disease was noted as compared with the mice containing only the SOD1 transgene. Although the survival of the double transgenic mice was also improved, the animals could not be ultimately rescued.

To test directly whether an elevated PV level attenuates the calcium increases in the motor neurons, in the present study, PV+/+ mice were subjected to axotomy, which is accepted as a standard model for the induction of an acute sublethal injury in adult-type neurons (Koliatsos and Price, 1996). As expected, a non-significant calcium level increase was demonstrated in the hypoglossal and spinal motor neurons of PV+/+ mice, which was similar to that measured in the oculomotor neurons. Thus, the lack of success in preventing the death of mutant SOD1 animals by the upregulation of PV in the motor neurons could be a consequence of the CaBPs acting solely as calcium buffers, which could be saturated if the stress signal endures (Siklós and Appel, 2005). This is in accord with the observation that the sphincter functions are also

impaired in the patients, just only at the late phase of the disease (Bergmann et al, 1995). On the basis of this concept, with increasing the calcium buffering capacity, the maximum goal would be a delay of the injury of the vulnerable motor neurons and a provision of a neuroprotection similar to that present in the relatively resistant motor neurons.

Alternatively, we may assume that the neighboring cells contribute to the damage of the motor neurons (Boillée et al, 2006; Julien, 2007; Obál et al, 2001). In the present study we demonstrated that however, at least in acute injury, the magnitude of the primary lesion of the motor neurons is that which determines the extent/duration of the inflammatory reaction, thus it seems still a reasonable aim to concentrate the protection mostly on motor neurons, but more effectively than the improved calcium buffering capacity can afford. In this respect our current experiments are aimed at characterizing the effect on the calcium level and survival of motor neurons of antagonists of calcium channels (AMPA receptors), which are relevant in the pathomechanism of ALS in the G93A transgenic model of ALS, i.e. during chronic stress (Paizs et al, 2010b).

Finally, we wish to think that our results about the disturbed calcium levels in the motor neurons of ALS patients and in the motor neurons of certain ALS models contributed significantly to the determination of starting a clinical trial with Talampanel, an AMPA-receptor antagonist (Pascuzzi et al, 2009).

SUMMARY

- In hypoglossal motor neurons of B6/SJL mice (parental line of the PV+/+ animals), as large as 1.7-fold calcium increase after axotomy was demonstrated, compared to the non-operated conditions, which was significantly different from the calcium increase in the oculomotor neurons of the same animals.
- In the PV+/+ mice there was no calcium increase either in the hypoglossal- or oculomotor neurons, providing evidence for that PV upregulation lends an "oculomotor-like" resistance .
- In the spinal motor neurons of PV+/+ mice a similarly reduced calcium level was demonstrated after injury as in the hypoglossal motor neurons, suggesting that independent of the local neuronal environment, PV upregulation indeed contributes to the resistance against calcium increase.
- In the spinal cord of the PV+/+ mice a reduced and a faster resolving inflammatory reaction could be demonstrated after acute injury compared to the B6/SJL mice. These observations, together with the reduced calcium increase in PV+/+ spinal motor neurons suggest that the magnitude of the primary lesion in the motor neurons determines the surrounding microclial activation, and stabilization of the calcium homeostasis in motor neurons may be indeed protective.
- With regard to the inflammatory reactions, a computerized method has been developed, based on light microscopic IHC and image analysis, which is able to reproducibly quantify the expression of certain inflammatory markers with high precision. The method has a general applicability.

The results confirm that elevated intracellular calcium buffer could attenuate both the *intracellular calcium increase (thus calcium-mediated degenerative processes)* and the *local inflammatory reactions* after acute injury, but leaves open the possibility that such a buffer may exhaust if the stress endures. Under chronic stress conditions, such as in animals with pathogenic mutations, which start working as early as *in utero*, an alternative way of reducing calcium levels, based e.g. on special ion channel blockers, is suggested.

REFERENCES

Alexianu ME, Ho BK, Mohamed AH, La Bella V, Smith RG, Appel SH: The role of calcium binding proteins in selective motoneuron vulnerability in amyotrophic lateral sclerosis. *Ann Neurol,* **36:**846-858(1994)

Appel SH, Beers DR, Henkel JS: T cell-microglial dialogue in Parkinson's disease and amyotrophic lateral sclerosis: are we listening? *Trends Immunol,* **31:**7-17(2010)

Appel SH, Beers D, Siklós L, Engelhardt JI, Mosier DR: Calcium: the Darth Vader of ALS. *Amyotroph Lateral Scler Other Motor Neuron Disord,* **1:**S47-54(2001)

Arundine M, Tymiansky M: Molecular mechanisms of calcium-dependent neurodegeneration in excitotoxicity. *Cell Calcium,* **34:**325-337(2003)

Aschner M: Astrocytes as mediators of immune and inflammatory responses in the CNS. *Neurotoxicol,* **19:**269-289(1998)

Barber SC, Shaw PJ: Oxidative stress in ALS: key role in motor neuron injury and therapeutic target. *Free Rad Biol Med,* **48:**629-641(2010)

Barger SW, Goodwin ME, Porter MM, Beggs ML: Glutamate release from activated microglia requires oxidative burst and lipid peroxidation. *J Neurochem,* **101:**1205-1213(2007)

Basso M, Samengo G, Nardo G, Massignan T, D'Alessandro G, Tartari S et al: Characterization of detergent-insoluble proteins in ALS indicates a causal link between nitrative stress and aggregation in pathogenesis. *Plos One,* **4:**e8130(2009)

Bauer R: Electron spectroscopic imaging: An advanced technique for imaging and analysis in transmission electron microscopy. *Meth Microbiol,* **20:**113-146(1988)

Beal MF, Ferrante RJ, Browne SE, Matthews RT, Kowall NW, Brown RH Jr: Increased 3-nitrotyrosine in both sporadic and familial amyotrophic lateral sclerosis. *Ann Neurol,* **42:**644-654(1997)

Beck KD, Hefti F, Widmer HR: Deafferentation removes calretinin immunopositive terminals, but does not induce degeneration of calbindin D-28k and parvalbumin expressing neurons in the hippocampus of adult rats. *J Neurosci Res,* **39:**298-304(1994)

Beckman JS, Carson M, Smith CD, Koppenol WH: ALS, SOD and peroxynitrite. *Nature,* **364:**584(1993)

Beers DR, Ho BK, Siklós L, Alexianu ME, Mosier DR, Mohamed AH et al: Parvalbumin overexpression alters immune-mediated increases in intracellular calcium, and delays disease onset in a transgenic model of familial amyotrophic lateral sclerosis. *J Neurochem,* **79:**499-509(2001)

Bergmann M, Volpel M, Kuchelmeister K: Onuf's nucleus is frequently involved in motor neuron disease/amyotrophic lateral sclerosis. *J Neurol Sci,* **129:**141-146(1995)

Berridge MJ: Neuronal calcium signaling. *Neuron,* **21:**13-26(1998)

Berridge MJ, Bootman MD, Lipp P: Calcium – a life and death signal. *Nature,* **395:**645-648(1998)

Boillée S, Cleveland DW: Revisiting oxidative damage in ALS: microglia, Nox, and mutant SOD1. *J Clin Invest,* **118:**474-478(2008)

Boillée S, Vande Velde C, Cleveland DW: ALS: a disease of motor neurons and their nonneuronal neighbors. *Neuron,* **52:**39-59(2006)

Borgers M, De Brabander DM, Van Reempts DJ, Awouters F, Jacob WA: Intranuclear microtubules in lung mast cells of guinea pigs in anaphylactic shock. *Lab Invest,*. **37:**1-8(1977)

Borgers M, Thoné F, van Neuten JM: The subcellular distribution of calcium and the effects of calcium-antagonists as evaluated with a combined oxalate- pyroantimonate technique. *Acta Histochem,* **24S:**327-332(1981)

Brini M: Ca^{2+} signaling in mitochondria: Mechanism and role in physiology and pathology. *Cell Calcium,* **34:**399-405(2003)

Brini M, Carafoli E: Calcium signaling: a historical account, recent developments and future perspectives. *Cell Mol Life Sci,* **57:**354-370(2000)

Buckingham SD, Kwak S, Jones AK, Blackshaw SE, Sattelle DB: Edited GluR2, a gatekeeper for motor neuron survival? *BioEssays,* **30:**1185-1192(2008)

Carriedo SG, Sensi SL, Yin HZ, Weiss JH: AMPA exposures induce mitochondrial Ca^{2+} overload and ROS generation is spinal motor neurons *in vitro*. *J Neurosci,* **20:**240-250(2000)

Carson MJ, Doose JM, Melchio B, Schmid CD, Ploix CC: CNS immune privilege: hiding in plain sight. *Immunol Rev,* **213:**48-65(2006)

Cassina P, Cassina A, Pehar M, Castellanos R, Gandelman M, de León A et al: Mitochondrial dysfunction in $SOD1^{G93}$-bearing astrocytes promotes motor neuron degeneration: prevention by mitochondrial-targeted antioxidants. *J Neurosci,* **28:**4115-4122(2008)

Celsi F, Pizzo P, Brini M, Leo S, Fotino C, Pinton P, Rizzuto R: Mitochondria, calcium and cell death: a deadly triad in neurodegeneration. *Biochim Biophys Acta,* **1787:**335-344(2009)

Chan SL, Mattson MP: Caspase and calpain substrates: roles in synaptic plasticity and death. *J Neurosci Res,* **58:**167-190(1999)

Chaturvedi RK, Beal MF: Mitochondrial approaches for neuroprotection. *Ann N Y Acad Sci,* **1147:**395-412(2008)

Chaudhuri TK, Paul S: Protein-misfolding diseases and chaperone-based therapeutic approaches. *FEBS J,* **273:**1331-1349(2006)

Chio A, Logroscino G, Hardiman O, Swingler R, Mitchell D, Beghi E, Traynor BG: Prognostic factors in ALS: A critical review. *Amyotr Lat Scl,* **10:**310-323(2009)

Choi DW: Glutamate neurotoxicity and diseases of the nervous system. *Neuron* **1:**623-34(1988)

Clementi E, Racchetti G, Melino G, Meldolesi J: Cytosolic Ca^{2+} buffering, a cell property that in some neurons markedly decreases during aging, has a protective effect against NMDA/nitric oxide-induced excitotoxicity. *Life Sci,* **59:**389-397(1996)

Cleveland DW, Rothstein JD: From Charcot to Lou Gehrig. Deciphering selective motor neuron death in ALS. *Nat Rev Neurosci,* **2:**806-819(2001)

Colom LV, Alexianu ME, Mosier DR, Smith RG, Appel SH: Amyotrophic lateral sclerosis immunoglobulins increase intracellular calcium in a motoneuron cell line. *Exp Neurol,* **146:**354-360(1997)

Couillard-Després S, Zhu Q, Wong PC, Price DL, Cleveland DW, Julien JP: Protective effect of neurofilament heavy gene overexpression in motor neuron disease induced by mutant superoxide dismutase. *Proc Natl Acad Sci USA,* **95:**9626-9630(1998)

Cuello AC: Immunohistochemistry II. John Wiley & Sons, Chichester, New York, Brisbane, Toronto, Singapore, 1993

Culmsee C, Mattson MP: p53 in neuronal apoptosis. *Biochem Biophys Res Commun,* **331:**761-777(2005)

Cwik VA: ALS clinical motor signs and symptoms. In: *Amyotrophic Lateral Sclerosis.* (eds: Mitsumoto H, Przedborski S, Gordon PH). Taylor & Francis Group, New York, London, pp. 99-115, 2006

Damiani M, Starkov AA, Petri S, Kipiani K, Kiaei M, Mattiazzi M et al: Neural mitochondrial Ca^{2+} capacity impairment precedes the onset of motor symptoms in G93A Cu/Zn-superoxide dismutase mutant mice. *J Neurochem,* **96:**1349-1361(2006)

Deng HX, Hentati A, Tainer JA, Iqbal Z, Cayabyab A, Hung WY et al: Amyotrophic lateral sclerosis and structural defects in Cu,Zn superoxide dismutase. *Science,* **261:**1047-1051(1993)

De Vos KJ, Grierson AJ, Ackerley S, Miller CCJ: Role of axonal transport in neurodegenerative diseases. *Ann Rev Neurosci,* **31:**151-173(2008)

Eisen A: Amyotrophic lateral sclerosis: A 40-year personal perspective. *J Clin Neurosci,* **16:**505-512(2009)

Elliott JL, Snider WD: Parvalbumin is a marker of ALS-resistant motor neurons. *NeuroReport,* **6:**449-452(1995)

Engelhardt JI, Appel SH: IgG reactivity in the spinal cord and motor cortex in amyotrophic lateral sclerosis. *Arch Neurol,* **47:**1210-1216(1990)

Engelhardt JI, Siklós L, Kőműves L, Smith RG, Appel SH: Antibodies to calcium channels from ALS patients passively transferred to mice selectively increase intracellular calcium and induce ultrastructural changes in motor neurons. *Synapse,* 20:185-199(1995)

Ermak G, Davies KJA: Calcium and oxidative stress: from cell signaling to cell death. *Mol Immunol,* **38:**713-721(2001)

Ezzi SA, Urushitani M, Julien JP: Wild type superoxide dismutase acquires binding and toxic properties of ALS-linked mutant forms through oxidation. *J Neurochem,* **102:**170-178(2007)

Ferroni S, Marchini C, Schubert P, Rapisarda C: Two distinct inward rectifying conductances are expressed in cultured rat cortical astrocytes after long term dibutyryl-cyclic-AMP treatment. *FEBS Lett,* **267:**319-325(1995)

Foran E, Trotti D: Glutamate transporters and the excitotoxic path to motor neuron degeneration in amyotrophic lateral sclerosis. *Antiox Redox Signaling*, **11:**1587-1602(2009)

Freund TF, Buzsáki G, Leon A, Baimbridge KG, Somogyi P: Relationship of neuronal vulnerability and calcium binding protein immunoreactivity in ischemia. *Exp Brain Res,* **83:**55-66(1990)

Garbuzova-Davis S, Haller E, Saporta S, Kolomey I, Nicosia SV, Sanberg PR: Ultrastructure of blood-brain barrier and blood-spinal cord barrier in SOD1 mice modeling ALS. *Brain Res,* **1157:**126-137(2007a)

Garbuzova-Davies S, Saporta S, Haller E, Kolomey I, Benett SP, Potter H, Sanberg PR: Evidence of compromised blood-spinal cord barrier in early and late symptomatic SOD1 mice modeling ALS. *PLoS One,* **2:**e1205(2007b)

Geula C, Bu J, Nagykery N, Scinto LFM, Chan J, Joseph J et al: Loss of calbindin-D_{28K} from aging human cholinergic basal forebrain: relation to neuronal loss. *J Comp Neurol,* **455:**249-259(2003)

Gurney ME, Pu H, Chiu AY, Dal Canto MC, Polchow CY, Alexander DD et al: Motor neuron degeneration in mice that express a human Cu,Zn superoxide dismutase mutation. *Science,* **264:**1772-1775(1994)

Hartley DM, Neve RL, Bryan J, Ullrey DB, Bak S-Y, Lang P, Geller AI: Expression of the calcium-binding protein, parvalbumin, in cultured cortical neurons using a HSV-1 vector system enhances NMDA neurotoxicity. *Mol Brain Res,* **40:**285-296(1996)

Hays AP: The pathology of amyotrophic lateral sclerosis. In: *Amyotrophic Lateral Sclerosis.* (eds: Mitsumoto H, Przedborski S, Gordon PH). Taylor & Francis Group, New York, London, pp. 43-80, 2006

Halliwell B, Gutteridge JMC: Free radicals in biology and medicine. 3rd ed, Oxford Univ Press, Oxford, 1999

Harraz MM, Marden JJ, Zhou W, Zhang Y, Williams A, Sharov VS et al: SOD1 mutations disrupt redox-sensitive Rac regulation of NADPH oxidase in a familial ALS model. *J Clin Invest,* **118:**659-670(2008)

Ho B-K, Alexianu ME, Colom LV, Mohamed AH, Serrano F, Appel SH: Expression of calbindind-D_{28K} in motoneuron hybrid cells after retroviral infection with calbindin-D_{28K} cDNA prevents amyotrophic lateral sclerosis IgG-mediated cytotoxicity. *Proc Natl Acad Sci,* **93:**6796-6801(1996)

Ilieva H, Polymenidou M, Cleveland DW: Non-cell autonomous toxicity in neurodegenerative disorders: ALS and beyond. *J Cell Biol,* **187:**761-772(2009)

Ince P, Stout N, Shaw P, Slade J, Hunziker W, Heizmann CW, Baimbridge KG: Parvalbumin and calbindin D-28k in the human motor system and in motor neuron disease. *Neuropathol Appl Neurobiol,* **19:**291-299(1993)

Julien JP: Amyotrophic lateral sclerosis: unfolding the toxicity of the misfolded. *Cell,* **104:**581-591(2001)

Julien JP: ALS: astrocytes move in as deadly neighbors. *Nature Neurosci,* **10:**535-537(2007)

Kabashi E, Valdmanis PN, Dion P, Rouleau GA: Oxidized/misfolded superoxide dismutase-1: the cause of all amyotrophic lateral sclerosis? *Ann Neurol,* **62:**553-559(2007)

Kandel ER, Schwartz JH, Jessell TM: Principles of neural science. Third edition; Elsevier; New York, Amsterdam, London, Tokyo, 1991

Kato S: Amyotrophic lateral sclerosis models and human neuropathology: similarities and differences. *Acta Neuropathol,* **115:**97-114(2008)

Kempermann G, Neumann H: Microglia: the enemy within? *Science,* **302:**1689-1690(2003)

Klapstein GJ, Vietla S, Lieberman DN, Gray PA, Airaksinen MS, Thoenen H et al: Calbindin-D_{28k} fails to protect hippocampal neurons against ischemia in spite of its cytoplasmic calcium buffering properties: Evidence from calbindin-D28k knockout mice. *Neurosci,* **85:**361-373(1998)

Koliatsos VE, Price DL: Axotomy as an experimental model of neuronal injury and cell death. *Brain Pathol,* **6:**447-465(1996)

Körtje KH, Körtje D:The application of electron spectroscopic imaging for quantification of the area fractions of calcium-containing precipitates in nervous tissue. *J Microsc,* **166:**343-358(1992)

Kreutzberg GW: Microglia: a sensor for pathological events in the CNS. *Trends Neurosci,* **19:**312-318(1996)

Lips MB, Keller BU: Endogenous calcium buffering in motoneurones of the nucleus hypoglossus from mouse. *J Physiol,* **511:**105-117(1998)

Llinás R, Sugimori M, Cherksey BD, Smith RG, Delbono O, Stefani E, Appel S: IgG from amyotrophic lateral sclerosis patients increases current through P-type calcium channels in

mammalian cerebellar Purkinje cells and in isolated channel protein in lipid bilayer. *Proc Natl Acad Sci USA*, **90:**11743-11747(1993)

Marambaud P, Dreses-Werringloer U, Vingtdeux V: Calcium signaling in neurodegeneration. *Mol Neurodeg,* **4:**20-35(2009)

Mattson MP: Calcium and neurodegeneration. *Aging Cell,* **6:**337-350(2007)

Mattson MP, Rychlik B, Chu C, Christakos S: Evidence for calcium-reducing and excito-protective roles for the calcium-binding protein calbindin-D_{28k} in cultured hippocampal neurons. *Neuron,* **6:**41-51(1991)

McMahon A, Wong BS, Iacopino AM, Ng MC, Chi S, German DC: Calbindin-D_{28k} buffers intracellular calcium and promotes resistance to degeneration in PC12 cells. *Mol Brain Res,* **54:**56-63(1998)

Maxwell MH: Short technical note: Two rapid and simple methods used for the removal of resins from 1.0 μm thick epoxy sections. *J Microsc,* **112:**253-255(1978)

Mayhew TM: A review of recent advances in stereology for quantifying neural structure. *J Neurocytol,* **21:**313-328(1992)

Mosier DR, Baldelli P, Delbono O, Smith RG, Alexianu ME, Appel SH, Stefani E: Amyotrophic lateral sclerosis immunoglobulins increase Ca^{2+} currents in a motoneuron cell line. *Ann Neurol,* **37:**102-109(1995)

Mosier DR, Siklós L, Appel SH: Resistance of extraocular motoneuron terminals to effects of amyotrophic lateral sclerosis sera. *Neurology,* **54:**252-255(2000)

Mitchell IJ, Griffiths MR: The differential susceptibility of specific neuronal populations: insights from Huntington's disease. *IUBMB Life,* **55:**293-298(2003)

Mitsumoto H, Chad DA, Pioro EP: Excitotoxicity and oxidative damage in ALS pathogenesis. In: *Amyotrophic lateral sclerosis,* FA Davis Company, Philadelphia, pp. 197-225, 1997

Mulder DW: Clinical limits of amyotrophic lateral sclerosis. *Adv Neurol,* **36:**15-22(1982)

Müller M, Felmy F, Schwaller B, Schneggenburger R: Parvalbumin is a mobile presynaptic Ca^{2+} buffer in the calyx of held that accelerates the decay of Ca^{2+} and short-term facilitation. *J Neurosci,* **27:**2261-2271(2007)

Nagai M, Kikuchi H, Przedborski S: Experimental models of motor neuron disease. In: *Amyotrophic lateral sclerosis.* (eds: Mitsumoto H, Przedborski S, Gordon PH). Taylor & Francis Group, New York, London, pp. 525-549, 2006

Nicaise C, Mitrecic D, Demetter P, De Decker R, Authelet M, Boom A, Pochet R: Impaired blood-brain and blood-spinal cord barriers in mutant SOD1-linked rats. *Brain Res,* **1301:**152-162(2009)

Nicotera P, Orrenius S: The role of calcium in apoptosis. *Cell Calcium,* **23:**173-80(1998)

Obál I, Engelhardt JI, Siklós L: Axotomy induces contrasting changes in calcium and calcium binding protein content in oculomotor and hypoglossal nuclei of Balb/c mice. *J Comp Neurol,* **499:**17-32(2006)

Obál I, Soós J, Jakab K, Siklós L, Engelhardt JI: Recruitment of activated microglia cells in the spinal cord of mice by ALS IgG. *NeuroReport,* **12:**2449-2452(2001)

Oosthuyse B, Moons L, Storkebaum E, Beck H, Nuyens D, Brusselmans K et al: Deletion of the hypoxia-response element in the vascular endothelial growth factor promoter causes motor neuron degeneration. *Nat Genet,* **28:**131-138(2001)

Paizs M, Engelhardt JI, Katarova Z, Siklós L: Hypoglossal motor neurons display a reduced calcium increase after axotomy in mice with upregulated parvalbumin. *J Comp Neurol,* **518:**1946-1961(2010a)

Paizs M, Engelhardt JI, Siklós L: Quantitative assessment of relative changes of immuno-histochemical staining by light microscopy in specified anatomical regions. *J Microscopy,* **234:**103-12(2009)

Paizs M, Tortarolo M, Bendotti C, Siklós L: Effect of an AMPA receptor antagonist, Talampanel, on the calcium level of the spinal motor neurons of G93A SOD1 mutant mice. IBRO International Workshop, January 21-23, Pécs, 2010b

Palecek J, Lips MB, Keller BU: Calcium dynamics and buffering in motoneurons of the mouse spinal cord. *J Physiol,* **520:**485-502(1999)

Pascuzzi RM, Shefner J, Chappell AS, Bjerke JS, Tamura R, Chaudhry V et al: A phase II trial of talampanel in subjects with amyotrophic lateral sclerosis. *Amyotr Lat Scl,* **Early Online:**1-6(2009)

Price DL, Cleveland DW, Koliatsos VE: Motor neuron disease and animal models. *Neurobiol Dis,* **1:**3-11(1994)

Price DL, Martin LJ, Clatterbuck RE, Koliatsos VE, Sisodia SS, Walker LC, Cork LC: Neuronal degeneration in human diseases and animal models. *J Neurobiol,* **23:**1277-1294(1992)

Pullen AH, Humphreys P: Ultrastructural analysis of spinal motoneurons from mice treated with IgG from ALS patients, healthy individuals, or disease controls. *J Neurol Sci,* **180:**35-45(2000)

Rami A, Rabié A, Thomasset M, Krieglstein J: Calbindin-D_{28k} and ischemic damage of pyramidal cells in rat hippocampus. *J Neurosci Res,* **31:**89-95(1992)

Rao MV, Nixon RA: Defective neurofilament transport in mouse models of amyotrophic lateral sclerosis. A review. *Neurochem Res,* **28:**1041-1047(2003)

Rao SD, Weiss JH: Excitotoxic and oxidative cross-talk between motor neurons and glia in ALS pathogenesis. *Trends Neurosci*. **27:**17-23(2004)

Rao SD, Yin HZ, Weiss JH: Disruption of glial glutamate transport by reactive oxygen species produced in motor neurons. *J Neurosci,* **23:**2627-2633(2003)

Rattray M, Bendotti C: Does excitotoxic cell death of motor neurons in ALS arise form glutamate transporter and glutamate receptor abnormalities? *Exp Neurol,* **201:**15-23(2006)

Reimer L, Fromm I, Rennekamp R: Operation modes of electron spectroscopic imaging and electron energy-loss spectroscopy in a transmission electron microscope. *Ultramicroscopy,* **24:**339-254(1988)

Richardson KC, Jarett L, Finke EH: Embedding in epoxy resins for ultrathin sectioning in electron microscopy. *Stain Technol,* **35:**313-323(1960)

Rosen DR, SiddiqueT, Patterson D, Figlewich DA, Sapp P, Hentati A et al: Mutation in Cu/Zn superoxide dismutase gene are associated with familial amyotrophic lateral sclerosis. *Nature,* **362:**59-62(1993)

Rothstein JD: Current hypotheses for the underlying biology of amyotrophic lateral sclerosis. *Ann Neurol,* **65:**S3-S9(2009)

Rothstein JD, Tsai G, Kuncl RW, Claewson L, Cornblath DR, Drachman DB et al: Abnormal excitatory amino acid metabolism in amyotrophic lateral sclerosis. *Ann Neurol,* **28:**18-25(1990)

Rowland LP, Shneider NA: Amyotrophic lateral sclerosis. *N Eng J Med,* **344:**1688-1700(2001)

Sattler R, Tymianski M: Molecular mechanisms of calcium-dependent excitotoxicity. *J Mol Med,* **78:**3-13(2000)

Schmalbruch H: Motoneuron death after nerve section in newborn rats. *J Comp Neurol,* **224:**252-258(1984)

Schubert P, Ogata T, Marchini C, Ferroni S: Glia-related pathomechanisms in Alzheimer's disease: a therapeutic target? *Mech Aging Developm,* **123:**47-57(2001)

Shaw PJ, Slade JY,Williams TL, Eggett CJ, Ince PG: Low expression of GluR2 AMPA receptor subunit by human motor neurons. *Neuroreport,* **10:**261-265(1999)

Siklós L, Appel SH: Calcium binding proteins in selective vulnerability of motor neurons. In: *Neurodegenerative Disease.* (eds: Beal MF, Lang AE) Cambridge University Press, pp. 65-79, 2005

Siklós L, Engelhardt JI, Alexianu ME, Gurney ME, Siddique T, Appel SH: Intracellular calcium parallels motoneuron degeneration in SOD-1 mutant mice. *J Neuropathol Exp Neurol,* **57:**571-87(1998)

Siklós L, Engelhardt JI, Harati Y, Smith RG, Joó F, Appel SH: Ultrastructural evidence for altered calcium in motor nerve terminals in amyotrophic lateral sclerosis. *Ann Neurol,* **39:**203-216(1996)

Slemmer JE, De Zeeuw CI, Weber JT: Don't get too excited: mechanisms of glutamate-mediated Purkinje cell death. *Prog Brain Res,* **148:**367-390(2005)

Smith RG, Alexianu ME, Crawford G, Nyormoi O, Stefani E, Appel SH: Cytotoxicity of immunoglobulins from amyotrophic lateral sclerosis patients on a hybrid motoneuron cell line. *Proc Natl Acad Sci US.A,* 91:3393-3397(1994)

Smith RG, Hamilton S, Hofmann F, Schneider T, Nastainczyk W, Birnbaumer L et al: Serum antibodies to L-type calcium channels in patients with amyotrophic lateral sclerosis. *New Eng J Med,* **327:**1721-1728(1992)

Snider WD, Thanedar S: Target dependence of hypoglossal motor neurons during development and in maturity. *J Comp Neurol,* **279:**489-498(1989)

Strong MJ: The basic aspects of therapeutics in amyotrophic lateral sclerosis. *Pharmacol Therapeut,* **98:**379-414(2003)

Strong MJ, Kesavapany S, Pant HC: The pathobiology of amyotrophic lateral sclerosis: A proteinopathy? *J Neuropathol Exp Neurol,* **64:**649-664(2005)

Swash M: Clinical features and diagnosis of amyotrophic lateral sclerosis. In: Amyotrophic Lateral Sclerosis. (eds: Brown RH Jr, Meininger V, Swash M) Martin Dunitz, pp.3-30, 2000

Tortosa A, Ferrer I: Parvalbumin immunoreactivity in the hippocampus of the gerbil after transient forebrain ischaemia: A qualitative and quantitative sequential study. *Neurosci,* **55:**33-43(1993)

Tovar-y-Romo LB, Santa-Cruz LD, Tapia R: Experimental models for the study of neurodegeneration in amyotrophic lateral sclerosis. *Mol Neurodegeneration,* **4:**31-43(2009)

Trotti D, Rossi D, Gjesdal O, Levi LM, Racagni G, Danbolt NC, Volterra A: Peroxinitrite inhibits glutamate transporter subtypes. *J Biol Chem,* **271:**5976-5979(1996)

Urushitani M, Sik A, Sakurai T, Nukina N, Takahashi R, Julien JP: Chomogranin-mediated secretion of mutant superoxide dismutase proteins linked to amyotrophic lateral sclerosis. *Nat Neurosci,* **9:**108-118(2006)

Van Damme P, Bogaert E, Dewil M, Hersmus N, Kiraly D, Scheveneels W et al: Astrocytes regulate GluR2 expression in motor neurons and their vulnerability to excitotoxicity. *Proc Natl Acad Sci,* **104:**14825-14830(2007)

Vande Velde C, Miller TM, Cashman NR, Cleveland DW: Selective association of misfolded ALS-linked mutant SOD1 with the cytoplasmic face of mitochondria. *Proc Natl Acad Sci USA,* **105:**4022-4027(2008)

Vanselow BK, Keller BU: Calcium dynamics and buffering in oculomotor neurones from mouse that are particularly resistant during amyotrophic lateral sclerosis (ALS)-related motoneurone disease. *J Physiol,* **525:**433-445(2000)

Valdmanis PN, Daoud H, Dion PA, Rouleau GA: Recent advances in the genetics of amyotrophic lateral sclerosis. *Curr Neurol Neurosci Rep,* **9:**198-205(2009)

Vincent VAM, Tilders FJH, van Dam AM: Inhibition of endotoxin-induced oxide synthase production in microglial cells by the presence of astroglial cells: a role of transforming growth factor β. *Glia,* **19:**190-198(1997)

von Lewinski F, Keller BU: Ca^{2+}, mitochondria and selective motoneuron vulnerability: implications for ALS. *Trends Neurosci,* **28:**494-500(2005)

Wijesekera LC, Leigh PN: Amyotrophic lateral sclerosis. *Orphanet J Rare Dis,* **4:**3-24(2009)

Williams TL, Day NC, Ince PG, Kamboj RK, Shaw PJ: Calcium permeable alpha-amino-3-hydroxy-5-methyl-4-isoxazole propionic acid receptors: a molecular determinant of selective vulnerability in amyotrophic lateral sclerosis. *Ann Neurol,* **42:**200-207(1997)

Zhao W, Beers DR, Henkel JS, Zhang W, Urushitani M, Julien JP, Appel SH: Extracellular mutant SOD1 induces microglial mediated motoneuron injury. *Glia,* **58:**231-243(2009)

Zhong Z, Deane R, Ali Z, Parisi M, Shapovalov Y, O'Banion MK et al: ALS-causing SOD1 mutants generate vascular changes prior to motor degeneration. *Nature Neurosci,* **11:**420-422(2008)

ACKNOWLEDGEMENTS

All the experiments provided the basis of the this thesis have been performed in the Laboratory of Molecular Neurobiology, Institute of Biophysics, Biological Research Center of the Hungarian Academy of Sciences.

I would like to express my gratitude to my supervisor, László Siklós, Ph.D., Head of Laboratory of Molecular Neurobiology, who introduced me to the field of neurobiology, supported me in all aspects of the laboratory work, and guided me through the difficulties of designing and performing the experiments.

I am thankful for the technical assistance of Erika Rácz, János Szeles and Szabolcs Ábrahám.

Special thanks go to my family, especially to my fiancé for their support and love, and to friends who were with me during this period.

These studies have been performed within the framework of the "Neuroscience Program" of the "Theoretical Medical Sciences" Ph.D. school of the University of Szeged, headed by Prof. Dr. Gábor Jancsó, and have been supported by the following grants: OTKA-T 048718, GVOP-3.2.1. 2004-04-0052/3.0, TÁMOP-4.2.2/08/1/2008-0002 and TéT, IT 27/2007.

APPENDIX

Reprints of the publications providing the basis of the thesis

I.

Melinda Paizs, József I. Engelhardt, László Siklós:
Quantitative assessment of relative changes of immunohistochemical staining by light microscopy in specified anatomical regions.
Journal of Microscopy, **234:**103-12(2009)

II.

Melinda Paizs, József I. Engelhardt, Zója Katarova, László Siklós:
Hypoglossal motor neurons display a reduced calcium increase after axotomy in mice with upregulated parvalbumin.
Journal of Comparative Neurology, **518:**1946-1961(2010)

Journal of Microscopy, Vol. 234, Pt 1 2009, pp. 103–112
Received 2 September 2008; accepted 1 December 2008

Quantitative assessment of relative changes of immunohistochemical staining by light microscopy in specified anatomical regions

M. PAIZS*, J.I. ENGELHARDT† & L. SIKLÓS*
**Institute of Biophysics, Biological Research Center, Szeged, Hungary*
†*Department of Neurology, University of Szeged, Szeged, Hungary*

Key words. Enzyme-based method, image analysis, immunohistochemistry, light microscopy, quantification, sampling paradigm.

Summary

Despite the advent of ever newer microscopic techniques for the study of the distribution of macromolecules in biological tissues, the enzyme-based immunohistochemical (IHC) methods are still used widely and routinely. However, the acquisition of reliable conclusions from the pattern of the reaction products of IHC procedures is hindered by the regular need for subjective judgments, in view of frequent inconsistencies in staining intensity from section to section or in repeated experiments. Consequently, when numerical comparisons are required, light microscopic morphological descriptions are commonly supplemented with analytical data (e.g. from Western blot analyses); however, these cannot be directly associated with accurate structural information and can easily be contaminated with data from outside the region of interest. Alternatively, to eliminate the more or less subjective evaluation of the results of IHC staining, procedures should be developed that correct for the variability of staining through the use of objective criteria. This paper describes a simple procedure, based on digital image analysis methods and the use of an internal reference area on the analyzed sections, that reduces the operator input and hence subjectivity, and makes the relative changes in IHC staining intensity in different experiments comparable. The reference area is situated at a position of the section that is not affected by the experimental treatment, or a disease condition, and that can therefore be used to specify the baseline of the IHC staining. Another source of staining variability is the internal heterogeneity of the object to be characterized, which means that identical fields can never be analyzed. To compensate for this variability, details are given of a systematic random sampling paradigm, which provides simple numerical data describing the extent and strength of IHC staining throughout the entire volume to be characterized. In this integrated approach, the figures are derived by pooling relative IHC staining intensities from all sections of the series from a particular animal. The procedure (1) eliminates the problem arising from the personal assessment of the significance of the IHC staining intensity, (2) does not depend on the precise dissection of the tissue on a gross scale and (3) considerably reduces the consequences of limited, arbitrary sampling of the region of interest for IHC analysis. The quantification procedure is illustrated by data from an experiment in which inflammatory reactions in the murine spinal cord, measured as microglial activation, were followed by IHC after the lesion of the sciatic nerve.

Correspondence to: László Siklós. Tel: + 36-62-599 611; fax: +36-62-433 133; e-mail: siklos@brc.hu

Introduction

There is a continuous need for accurate comparisons of the distributions of macromolecules in experimental biology or in medical diagnostics, and recurrent attempts are made to achieve the objective light microscopic characterization of the intensity and distribution of reaction products in immunohistochemically (IHC) stained sections. The primary obstacle during the quantification of staining is the frequent non-reproducibility of the pattern, strength and contrast of staining in repetitive investigations. This can originate from variations in the recording conditions (e.g. from uncontrolled, illumination-induced fading in fluorescent microscopy [Kirkeby & Thomsen, 2005], or from differences in the alignment and aperture setting in transmitted light microscopy), which can be at least partially corrected or compensated. However, even with identical microscopic conditions, certain variations still arise from unavoidable differences in the replication of the staining protocols in repeated experiments. Although this manuscript focuses on the problems associated with enzyme-based techniques,

some of the difficulties are common in both enzyme- and fluorescence-based methods. To overcome the difficulties of quantification, individualized classification criteria are often introduced. The methods applied may involve an entirely subjective approach, based on the observer's estimation of staining intensity, stained cell density and cell morphology (Colburn *et al*, 1997; He *et al.*, 1997). Alternatively, a semi-quantitative analysis may be applied, with the measurement of greyscale intensity, an operator-dependent thresholding method being used for determination of the percentage of the total area covered by stained cells (Blackbeard *et al.*, 2007). Automated analysis of corrected immunoreactive areas in selected sections from the region of interest is also possible, likewise based on a subjective, visual selection of the threshold for image segmentation (Stuesse *et al.*, 2000).

The other major cause of problems during quantification is the biological variability. The main source of such experimental error is the interindividual variability, which is responsible for about 70% of the observed experimental variance (Howard & Reed, 1998). Further variance stems from the hierarchical nature of microscopic investigations, that is, from the frequently neglected differences between blocks and sections: in other words, from the way the object is sampled. The contribution of this factor to the overall variance is in the range of 20–25% (Howard & Reed, 1998). Generally speaking, such statistical variability may be decreased by increasing the number of observations (Gundersen & Østerby, 1981). The first problem, however, is associated at least in part, with observer subjectivity. This type of error (bias) does not affect the precision of the measurements, but since the real values sought experimentally are normally not known, the systematic deviations from these values cannot be estimated (see e.g. West, 1999).

The present manuscript provides an integrated procedure that attempts to correct for both types of variability. The method consists of two modules: compensation for the changes in staining intensity at the section level, and the application of systematic sampling at the object level. The irregularity of staining in repeated experiments is taken into account by determining the staining intensity in reference regions in each section that are presumed to be unaffected by the experimental treatment. The density of IHC staining (or the percentage area covered by stained profiles) in the area of interest (AOI) will be related to that in the reference area (AOI′) in the same section. To determine the positivity (significance) of the immune reaction, objective criteria are used: the standard deviation (SD) and the background level of the staining intensity are determined for the AOI′ and a segmentation threshold (background + 2 × SD) is then applied to the whole section. Regions with staining intensity exceeding this limit are accepted as significantly stained profiles. To compensate for the non-homogeneous spatial distribution of the stained structures within the volume to be characterized, a robust systematic random sampling is applied (Gundersen & Jensen, 1987). A specimen containing the entire region of interest is dissected and sectioned equidistantly, with a starting position set at random. The parameters characterizing the IHC staining in each section, related to the AOI′, are then pooled to arrive at simple numerical data expressing the IHC staining of the object of interest.

To illustrate the procedure step by step, an experimental model of nerve injury is used. Nerve transection (axotomy), which is a well-established model of neuronal injury (Koliatsos & Price, 1996), leads to the activation of microglial cells at the site of injury in the central nervous system (Kreutzberg, 1996; Obál *et al.*, 2001). This type of cellular response can be attenuated by treatment with minocycline, a member of the tetracycline class of antibiotics (Zemke & Majid, 2004). In our example, the microglial response in the ventrolateral horn of the murine spinal cord to axotomy of the sciatic nerve is compared with that after minocycline treatment. An enzyme-based IHC method is used to detect the microglia, and the proposed integrated evaluation/sampling procedure is applied to demonstrate the effect of treatment.

Material and methods

Animals

B6/SJL hybrid mice were bred in the Biological Research Center (Szeged, Hungary) from breeding pairs originally obtained from Charles River Laboratories (Budapest, Hungary). Twelve-week-old male mice were used for this study. All animal experiments were performed in accordance with the institutional guidelines for the use and care of animals and with Hungarian governmental laws relating to animal protection (protocol no. XVI./03876/001/2006). The animals were housed (at most four animals per cage) at room temperature under a 12:12 h light/dark cycle, with free access to food and water.

Surgical procedure and pharmacological treatment

Surgery was performed under Avertin (tribromoethanol; Fluka, Buchs, Switzerland) anaesthesia (240 mg kg^{-1} body weight in a 0.3 mL volume, administered intraperitoneally). The left sciatic nerve was transected in the mid-thigh, and a 3–4-mm portion was removed to prevent regeneration. The incision was then sutured, and the animals were returned to their cages after they had recovered from the narcosis. One group of operated mice were injected intraperitoneally once a day with minocycline (an inhibitor of microglial activation; Sigma, Budapest, Hungary), dissolved in sterile saline solution (40 mg kg^{-1} body weight in a 0.1 mL volume), first applied 1 h prior to the surgery. The animals in both groups (operated + minocycline-treated, or operated only) were sacrificed on day 7 after the sciatic nerve transection.

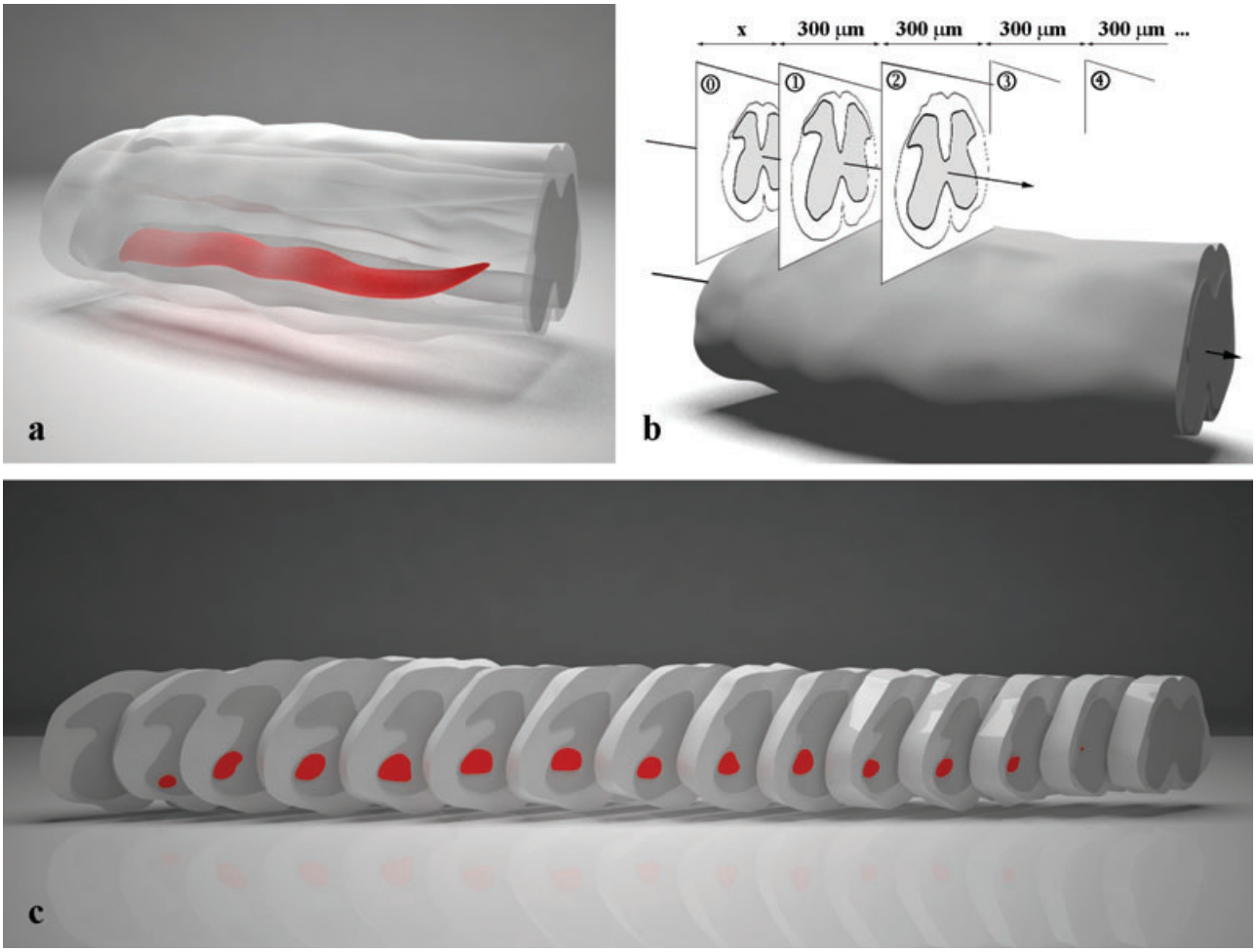

Fig. 1. Dissection and sampling of tissue for immunohistochemical (IHC) characterization. (A) A piece of tissue (with a characteristic length of 10–12 mm) from the lumbar portion of the spinal cord was dissected, post-fixed and embedded for sectioning. The dissection was made according to gross anatomical landmarks in such a way that the specimen encapsulated the entire region with the expected inflammatory reaction (red-shaded area). It is not necessary to know the exact location of the region of interest within the dissected tissue. (B) The dissected piece of the spinal cord was systematically sampled by transverse sectioning along the axis of the spinal cord. The starting position for sampling was randomly selected by determining the first location of the specimen where the entire cross-section of the spinal cord could be recognized (onset point; section no. 0); then, before collection of the sections, a random number of sections (between 1 and 10) with 30-μm thickness were cut and discarded. Thus, the sampling started with section no. 1 located at an arbitrary distance x μm ($1 < x < 300$ μm) from the border of the tissue. Next, a systematic set of sections was cut at 300 μm distances until the whole spinal cord sample was sectioned through. (C) A set of equidistantly spaced sections was prepared from each spinal cord for IHC staining and quantification, which means that each section in the series represented a 300-μm transverse slice of the spinal cord (15 slices in the figure). The region of interest within the sections was determined by means of microscopic landmarks in the sections. Since the size (length) of the dissected tissue was intentionally larger than that of the region with the expected inflammation (red-shaded area), the very first and the very last sections in the series may not display an increased number of microglial cells in the region of interest.

Tissue preparation and sampling

Under terminal anaesthesia, the animals were perfused transcardially with 30-mL phosphate-buffered saline (PBS; 10 mM) followed by 30 mL 3% paraformaldehyde (PFA; Sigma) in 10 mM PBS. The lumbar segments of the spinal cords throughout the entire region involving the expected inflammatory reaction (approximately 10–12 mm in length) were removed and post-fixed overnight in 3% PFA (in 10 mM PBS) at 4°C (Fig. 1(A)). Tissue blocks were then cryoprotected in 30% sucrose (Sigma) in 10 mM PBS for 3 days at 4°C, and embedded in OCT medium (Tissue-Tek, Zoeterwoude, the Netherlands) for transverse sectioning. Transverse sections at a thickness of 30 μm were cut from the spinal cord along its longitudinal axis on a cryostat (Kryostat 1720; Leitz, Wetzlarr, Germany) in such a way that the starting positions were selected at random: the first N sections (N selected at random between 1 and 10) were cut and discarded; then, systematically, each section at a distance of 300 μm was harvested, until the segment of spinal cord had been sectioned

through (Figs 1(B) & (C)). Sections were collected in 10 mM PBS in a 24-well tissue culture plate (one section in each well) and stored at 4°C until processed further.

Immunohistochemical staining of sections

To detect microglial cells with an IHC procedure, free-floating sections were stained according to the avidin–biotin technique (Cuello, 1993). Sections were rinsed first with three changes in PBS, which was followed by a 30-min blockade of endogenous peroxidase activity with 0.3% hydrogen peroxide in 10 mM PBS containing 0.2% Triton X-100 (TPBS; Sigma). Then, after washing (three changes in PBS), to reduce the non-specific staining, sections were incubated in 2% normal goat serum (Vector, Burlingame, CA, USA) in TPBS for 1 h. Microglial cells were labelled with anti-CD11b antibody (1:500 in TPBS; rat-anti-mouse antibody, Serotec, Oxford, UK) during incubation at 4°C overnight. After washing in PBS (three changes), sections were incubated in biotin-labelled secondary antibody for 1 h (1:800 in TPBS, goat anti-rat IgG, Vector), followed by washing in PBS (three changes), and incubation in the avidin–biotin complex (1:1600 in PBS, Vector) for 1 h, at room temperature. Finally, after washing in PBS, the reaction was visualized by incubation in diaminobenzidine (DAB, 5% in PBS; Sigma) for 15 min. Stained sections were thoroughly rinsed in PBS, mounted on silane-coated glass slides, dehydrated in graded series of ethanol, processed through xylane (Molar, Budapest, Hungary) and cover-slipped with Entellan (Merck, Darmstadt, Germany).

Light microscopic image recording

IHC-stained sections were examined in an Olympus Vanox-T AH-2 light microscope (Olympus, Tokyo, Japan). The alignment of the microscope was checked at the beginning of each microscopic session with special attention to the coaxial position of the lenses, the apertures and the recording CCD camera. The same magnification (objective lens) was used to record all images belonging in a particular series. To avoid any slight variability in reproducing aperture settings, both the field limiting and contrast apertures were kept at the fully open position during (digital) photography. Images were recorded with a Spot RT CCD camera (Diagnostic Instruments, Sterling Heights, MI, USA) in colour mode, using full (1600 × 1200 bit) resolution at 8-bit depth for each (RGB) colour component. The automatic exposure option of the camera was used if all the image components of interest in a section could fit into a single field of view. When more than one grabbed image was necessary from a section, the first snapshot was made with automatic camera control, and the following photographs were taken with the same exposure settings as the first. At the beginning of each microscopic session, a flatfield image was taken and used through the session to correct for uneven illumination. The white balance was adjusted for each individual slide. Recorded images were stored in colour mode in uncompressed files with tagged image file format.

Image analytical procedures in single sections

Digital images were analyzed by using the built-in functions of the Image-Pro-Plus image analysis software (Media Cybernetics, Silver Spring, MD, USA) running under the Windows XP operation system on a PC. (Most of the used or equivalent operations are also available in other free or commercial software.)

Although the original colour (digital) pictures were used for easier orientation and to specify the AOI in the sections, all operations were performed on images previously converted to 8-bit greyscale. The evaluation steps included (1) specification of the AOI and AOI′, (2) calculation of the background level and variance of the staining intensity on the 0–255 greyscale, (3) segmentation of the significantly stained pixels and (4) calculation of the percentile area of the significantly stained profiles and/or their average density in the AOI, relative to the similar values in the AOI′. A simplified version of such calculations to estimate relative changes in IHC staining has already been tested in another model of nerve injury (Obál *et al.*, 2006).

Specification of the AOI and the corresponding AOI′. The AOI in a single section could be determined by using characteristic anatomical landmarks, such as, in our case, the border of the grey and white matter, the position of the central channel and the perimeter of the pools of motor neurons (Fig. 2(A)). In complex structures, detailed atlases should be consulted, but in most cases the specific regions can be easily marked. In our study, a general histological stain (cresyl violet, which stains Nissl substance and cell bodies) was used in one set of sections to prove that correct orientation was achieved in the IHC-stained sections with no counterstaining, or without the regular need for reference material (Fig. 2(B)). When the region to be analyzed was successfully identified in a section, it was outlined with the pointer device and marked as an (irregular) AOI. For reference purposes, any indifferent region of the section would be suitable; however, exploiting the symmetric organization of the nervous system, we propose that an identical area on the contralateral side of the section should be used. To define this area, the AOI on the operated side was mirrored about the symmetry axis of the section; then, to correct for occasional slight distortions of the sections, it was manually positioned to the corresponding location on the non-operated side (Fig. 2(B)).

Calculation of the background level and variance of the staining for segmentation. The major anatomical landmarks were first identified in the original colour images of the sections, and the area where an increased immune reaction was expected on the operated side and the reference area on the contralateral side were then marked accordingly (Figs 3(A) & (B)). The colour

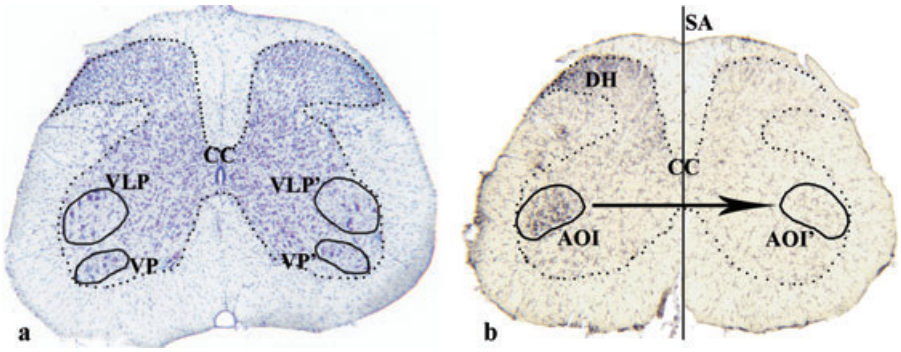

Fig. 2. Specification of the reference area and the area to be analyzed. (A) A section containing the whole cross-sectional area of the spinal cord of a non-operated animal was stained with cresyl violet, which reveals the distribution of neuronal and glial cells. The border of the grey and white matter is readily recognized (dotted line), as are the positions of the central channel (CC) and the pools of symmetrically positioned large motor neurons at ventral (VP and VP') and ventrolateral (VLP and VLP') locations (as outlined, left and right). (B) On individual microglia (CD11b) staining, the major anatomical landmarks in the section remain identifiable (border of the grey and white matter, central channel). The sciatic nerve cut induced microglial activation at the dorsal horn (DH), and in the ventral + ventrolateral pools of motor neurons. The border of the ventro-lateral pool was outlined (area of interest, AOI), the AOI was then mirrored to the symmetry axis (SA) of the section to define the reference area (AOI′). The position of AOI′ was manually corrected, if this was required owing to slight asymmetry of the section.

image was next converted to the greyscale with a range of 0–255 (Figs 3(C) & (D)). To determine the background level, a large format low-pass filter (512 × 512 pixels) was first applied to the greyscale image (Figs 3(E) & (F)), which smoothed out the variability in the image owing to differences in IHC staining by substituting the grey value of each pixel with the average grey value of its neighbourhood with a dimension of 512 × 512 pixels. Although the image obtained approximated the grey level very well at image points outside the stained profiles (cf. Figs 3(D) & (F)), this background distribution is certainly contaminated with the signal from the heavily stained area, which is obvious from a comparison of Figs 3(C) and (E). Next, to correct for this effect, an adjusted (second) background level was calculated. To derive this number, the first background level within the AOI′ was used for thresholding: all the image points darker than this level (which, at this approximation, were regarded as the stained profiles) were excluded from the image, and an average grey value was calculated for the remainder of the pixels within the AOI′ (Figs 3(G) & (H)). This number was accepted as the final value representing the grey level of the background (BCKGND).

The variance of the staining, that is, the variance of the grey level distribution of the images, in addition to the BCKGND value, was used as an aid to determine which image point should be regarded as significantly stained. To calculate the standard deviation (SD) of the distribution of staining intensity, all the image points within the AOI′ of the original greyscale images were taken into account. Finally, those pixels in the AOI and AOI′, whose grey values were lower than BCKGND – 2 × SD (i.e. significantly darker than the background), were dissected and accepted as significantly stained image points. For illustration and for visual control of the results, image areas with dissected pixels were outlined, and these profiles and the perimeters of the AOI and AOI′ were superimposed on the original colour images (Figs 3(I) & (J)).

Calculation of tissue-specific parameters from the relative changes in IHC staining in individual sections. Two types of (non-independent) parameters were derived: (i) the percentile areas of the significantly stained profiles within the AOI and AOI′ and (ii) the intensities of average staining within these areas. The first parameter was readily obtained after segmentation of the greyscale images at the cut-off level, since this operation yields the total area of the AOI (equal to that of AOI′) and the sum of the areas of the segmented profiles in both regions. The numerical difference of these percentile areas results in a relative number describing how much larger the coverage of the cellular staining on the operated site is than that of an unperturbed, control area (Δ(area)).

The attenuation law (Bouguer–Lambert–Beer law) states that

$$I_t = I_0 \times \mathrm{e}^{-M \times T \times C},$$

where I_0 is the incident and I_t is the transmitted light intensity, M denotes the molar absorptivity (extinction coefficient), T is the section thickness and C is the local concentration of the absorbing species. Assuming homogeneous section thickness and similar extinction properties of the absorbing material in the AOI and AOI′, analogous equations can be written for the operated and control sides as:

$$I_{t(\text{operated})} = I_0 \times \mathrm{e}^{-M \times T \times C(\text{operated})}$$
$$I_{t(\text{control})} = I_0 \times \mathrm{e}^{-M \times T \times C(\text{control})}.$$

Hence,

$$-\ln(I_{t(\text{operated})}/I_{t(\text{control})})/M/T = C(\text{operated}) - C(\text{control}),$$

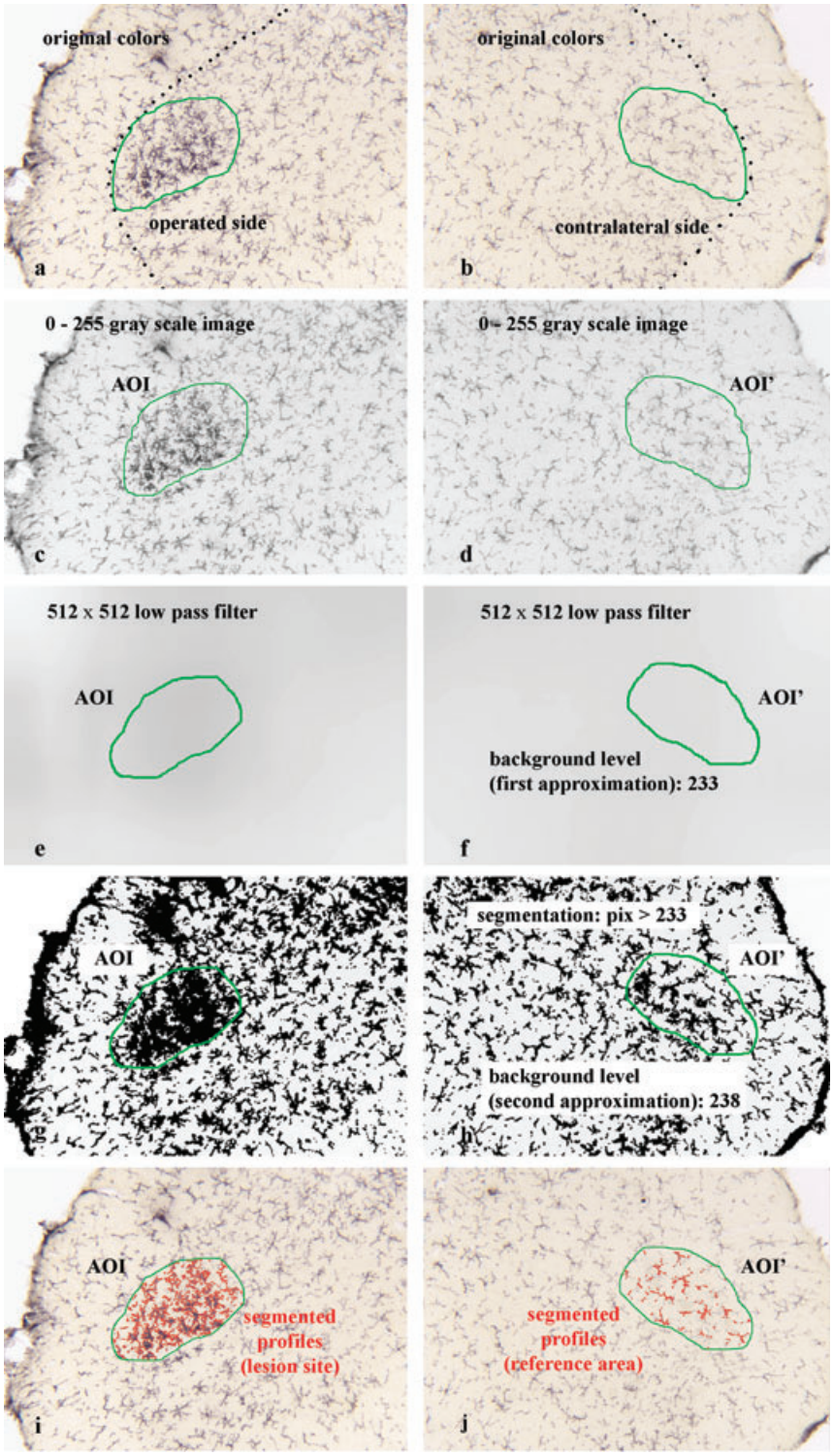

Fig. 3. Step-by-step procedure for the segmentation of significantly stained profiles in IHC-stained sections. (A, B) According to the anatomical landmarks (shape of the section, border of the grey and the white matter [dotted line], etc.), the region where the increased staining is accepted is outlined on the operated side; then, symmetrically, the reference area is specified on colour images of the section (RGB, 8-bit depth). (C, D) The colour pictures are converted to greyscale images with a range of 0–255 (from black to white) and the AOI and AOI′ are next copied as overlay images. (E, F) Application of a large-scale low-pass filter (512 × 512 pixels) to the whole images resulted in approximated background images by smoothing (averaging) the details in the greyscale images. In this particular case, the filtering process resulted in an average greyscale (background) level of 233 in the reference area (AOI′). Comparison of the greyscale distribution within and outside the AOI on the operated side indicates how the recruitment of the stained cells

Fig. 3 continued (Fig. 3E) affects the local grey level of the background. (G, H) When the segmentation threshold was set to the calculated background (a grey value of 233 in the presented case), all the pixels with grey values lower than this limit (black 'holes' in the image) were excluded from the image, and a new average background level (238) was then calculated for the remainder of the pixels within the reference area (AOI′). With this new value for the background (BCKGND), a standard deviation (SD) of the greyscale distribution was calculated for the pixels darker than this level (i.e. grey values lower than this number) within the AOI′ in the greyscale images (Fig. 3D), and a cut-off value for the segmentation of the significantly stained profiles was calculated at BCKGND – 2 × SD. (I, J) With the cut-off value, the segmented profiles within the AOI and the AOI′ were outlined and superimposed on the original colour images for visual control of the results representing the significantly stained profiles.

which means that the logarithm of the ratio of the light intensities (measured on a greyscale in this case) in the AOI and the AOI′ is proportional to the difference in concentration of the absorbing species in these areas, that is, the target of determination (Δ(concentration)).

Obtaining parameters which characterize the entire volume to be analyzed

In each equidistant section cut from the tissue, consistent individual parameters can be derived which are either proportional to the concentration of the IHC reaction products (Δ(concentration)), or to their dimensions (Δ(area)) on the operated side relative to the corresponding data on the control side. Summation of the corresponding data obtained from each section, furnished simple numerical data characterizing the dimension (ΣΔ(area)) or the extent of IHC staining (ΣΔ(concentration)) throughout the whole volume of the region of interest from a given animal (Figs 4(A) & (B)). The process of summation of data situated equidistantly along the third Cartesian axis is equivalent to a certain type of integration, which incorporates the third dimension; thus, the calculated numerical data should be regarded as having dimensions of volume and mass on an arbitrary scale.

Results

Six animals serving as controls underwent sciatic nerve transection, while four other mice received minocycline treatment in addition to the axotomy. The reducing effect of the minocycline treatment on the microglial activation in the spinal cord following axotomy was tested by comparing the levels of CD11b IHC staining in the 'operated only' and 'operated + minocycline' groups of animals with the methods presented earlier. The data in Table 1 reveal that for both the reduction in the volume occupied by the significantly stained cells ($P = 0.022$), and the reduction in the total density of staining ($P = 0.026$) in the ventrolateral pool of motor neurons, the effect of minocycline was significant (Student one-tailed *t*-test).

Discussion

Although snap freezing can reduce the tissue preparation time considerably, which may be critical if tissue bio-banking is associated with a rapid intra-operative diagnosis, perfusion or immersion fixation gives superior tissue preservation (Beltz & Burd, 1989); furthermore, even for diagnostic purposes, most of the tissue is still treated with formalin fixative (Steu *et al.*, 2008). Admitting also that snap-frozen tissue can additionally

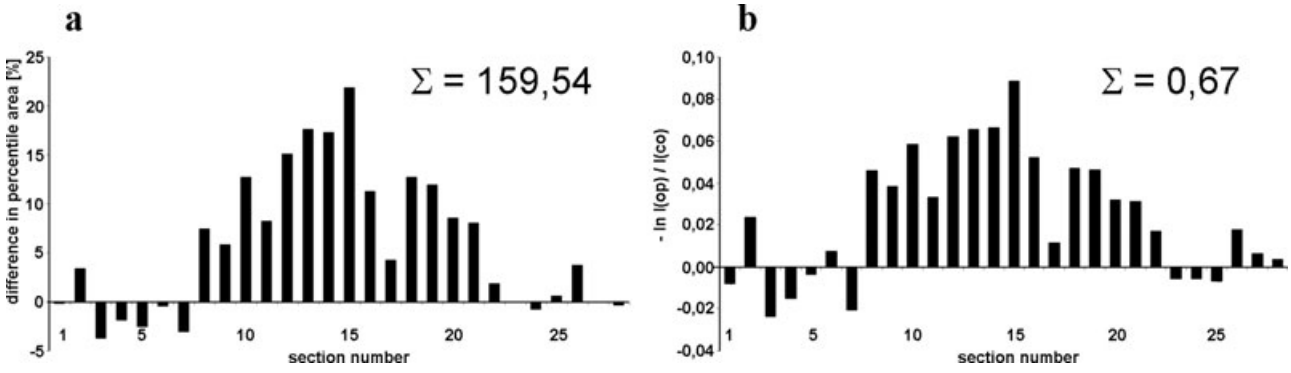

Fig. 4. Charts showing relative area (A) and density (B) data obtained from the analysis of individual sections belonging in the same systematic random series. The category axis gives the serial numbers of consecutive sections. Obviously, the exact location of the starting point of the systematic sampling is indifferent, since the difference between the operated and non-operated sides fluctuates around zero outside the volume affected by the experiment, and is therefore cancelled out on a statistical basis during summation of the data. (A) The percentile area covered by the IHC products in the reference area (AOI′) was subtracted from that in the region of interest (AOI) in each section and plotted. The sum of the data (taking into account their signs) is 159.54, which characterizes the extent of the IHC-stained structures within the volume to be analyzed. (B) The calculated numbers from each section [–ln(*I*(op)/*I*(co))], which are directly proportional to the differences in concentration of the IHC-stained structures, are plotted against the section number. The result of summation (0.67) characterizes the accumulation of IHC-stained material in the volume of interest.

Table 1. Effect of minocycline treatment on CD11b IHC staining after sciatic nerve cut.

	Operated only		Operated + minocycline	
Animals	Sum of relative stained area (%)	Sum of ln(I(op)/I(co))	Sum of relative stained area [%]	Sum of ln(I(op)/I(co))
#1	374.28	1.67	375.79	1.47
#2	394.03	1.83	425.09	1.97
#3	549.73	2.38	417.56	1.92
#4	642.55	3.19	365.81	1.72
#5	541.82	2.47	–	–
#6	657.43	3.24	–	–
Mean	526.64	2.46	396.06	1.77
SEM	49.01	0.66	14.81	0.23

offer exceptional possibility of the combination of stereological, histological and molecular analyses of adjacent sections from the same tissue (Schmitz *et al.*, 2000), the chemical fixation preparation methods for IHC are still more widespread than the physical freezing procedures. For this reason, we followed the traditional perfusion fixation protocol for tissue preparation in the present study.

The commonly experienced difficulties inherent in the interpretation of IHC-stained sections are mainly due to unavoidable variations arising from two main sources: the variability of the staining at the section level and the diversity of the structure at the tissue level. In consequence, subjective input from the operator is necessary at critical points in the evaluation, which influences the results to an incalculable degree. The approach presented here for the evaluation of IHC-stained specimen, exemplified by an experimental application, attempts to reduce these uncertainties.

Procedures at the section level

Operator input. In the presented method, the input of the operator is reduced to one unavoidable step: specification of the boundary of the studied AOI. The use of an identical AOI′ in the same section for control purposes ensures that changes relative to an indifferent area are calculated in each case even if, by chance, the specification of the AOI is not absolutely precise. If the AOI is to some extent smaller than the area delineated by the boundary of the anatomical region to be analyzed, the area will be under-represented, but the calculated relative difference between the AOI and AOI′ will not be considerably affected. If the AOI is somewhat larger than the area to be analyzed, the measured difference from the control region will be only slightly 'diluted' with data from an unaffected area, that is, the method will merely lose some sensitivity. The major landmarks in the sections, however, allow easy and reliable delineation of the area AOI (see Fig. 2). Accordingly, all such inconsistencies would cause relatively minor changes in the results.

Determination of the background staining. In the present experiments, no counterstaining was performed, and there was therefore no need for spectral (colour) aided segmentation of the IHC-stained profiles from the counterstained background, which would have required complex operations (van der Laak *et al.*, 2000; Brey *et al.*, 2003; Pham *et al.*, 2007). Thus, instead of the selection of a specific wavelength (or colour) for analysis, or decoupling of the intensity data from the red–green–blue colour model, all images were converted to greyscale images represented only by 8-bit data at each image point, and the image analysis procedures were performed in a single channel with simplified calculations.

In each section, the intensity of the background staining (determined in an indifferent reference area) is used to identify image points with a level of staining significantly above that of the surroundings both in the AOI′ and within the AOI. Thus, the procedure ensures that the variability of staining in repeated experiments or the heterogeneity of the staining from section to section in a given series will be compensated. The procedure, which automatically calculates the background intensity on the basis of the distribution of the staining intensity without the aid of the operator, consists of two steps. In the first step, an average background image is calculated by applying a large-format low-pass filter to the digital image of the section, which yields a greyscale value at each image point with the average for its 512×512 pixel neighbourhood (Figs 3(E) & (F)). Since the great majority of the image points show no evidence of staining (Figs 3(C) & (D)), the result of this filter approximates closely, though not perfectly to the true background distribution (Figs 3(E) & (F)). After low-pass filtering, an average grey value (approximate background level) can be calculated within the AOI′ (233; Fig. 3(F)). The deviation of this number from the true (unknown) background is obviously greater in those regions where stained profiles is notably accumulate (cf. Figs 3(C), (E) and (D), (F)). To correct for this 'contamination' of the background distribution from the stained cells, as a second approximation, all image points with grey values lower than the calculated first background value (233) are excluded from the calculation, and a new average background value (BCKGND = 238) is determined for the remainder of the pixels within the AOI′. This procedure of successive approximation of the true average background

within the AOI′ should in principle be stopped when the difference between the results of successive iterations is smaller than a specified limit. In the presented experimental example, even in the third step, the change in the calculated average background greyscale value was less than one digit on the 0–255 scale, and accordingly no further iterations were performed.

Segmentation of stained profiles and calculation of parameters characterizing the stained structures. After determination of the BCKGND and the SD values of the greyscale distribution in the AOI′, a cut-off level is determined to segment those image points that are considered significantly stained, that is, pixels with grey values significantly different from that of the background. This seemingly arbitrary decision is supported by statistical principles if the deviation of the cut-off level from the BCKGND value is set in units of SD, which determines the confidence of the results. In biological applications, this offset is normally set to a value in the range 2 × SD to 3 × SD implicating a probability between 67 and 99% for the segmented image to reflect the distribution of the authentic stained profiles. In our application example, the level BCKGND – 2 × SD was consistently applied.

After segmentation, different parameters were derived to characterize the extent and strength of the IHC staining in the AOI relative to the AOI′. The difference between the numbers of pixels segmented in the AOI and the AOI′ (since these areas are identical) reflects the net increase in the stained cellular profiles due to the treatment. For easier comparison of the results obtained from different sections and different animals, these raw data were normalized to the total number of pixels within the AOI or the AOI′, and expressed as the percentile area difference (Δ(area)). The difference in staining intensity between the AOI and the AOI′ was determined directly by using the attenuation (Bouguer–Lambert–Beer) law, applied to the whole area of the AOI and the AOI′. Through measurement of the average (optical) density in these areas, a number corresponding to the difference in the percentile stained area was obtained (Δ(concentration)). The method is analogous to the classical procedures applied successfully in conventional (electron) microscopy to determine the local mass of a specimen by measuring the contrast of the micrographs (Halliday & Quinn, 1960; Zeitler & Bahr, 1965; Edie & Karlsson, 1977).

Procedures at the tissue level

Determination of the boundary of the AOI and the setting-up of the exact anatomical location along the direction perpendicular to the plane of the sections (unlike the same procedure within the plane of the section) is often hindered by the missing characteristic landmarks that can be recognized only in a set of consecutive sections (see Fig. 1). Thus, to overcome the need for serial sectioning in order to determine the exact anatomical location within the tissue, if probing of a tissue by means of microscopic sections is intended, arbitrary (random) sampling is often the choice. The paradigm, however, can lead to misleading results, due to the intra-individual variability of the tissue, an effect which is frequently neglected. However, as illustrated qualitatively in a composite figure assembled from the sections of our application example (Fig. 5), huge differences may be observed in the amount of staining, depending on the actual position of the section within the region to be analyzed. Quantitatively, as depicted in Fig. 4, fluctuations from section to section as large as 50–100% of the derived parameter values can be determined in the region of the tissue containing the expected reaction.

The proposed procedure of systematic sampling is not sensitive to the actual positions of the sections within the tissue, since the intra-individual variations average out during summation of the results obtained on the individual sections. The method is not sensitive to the actual starting point of

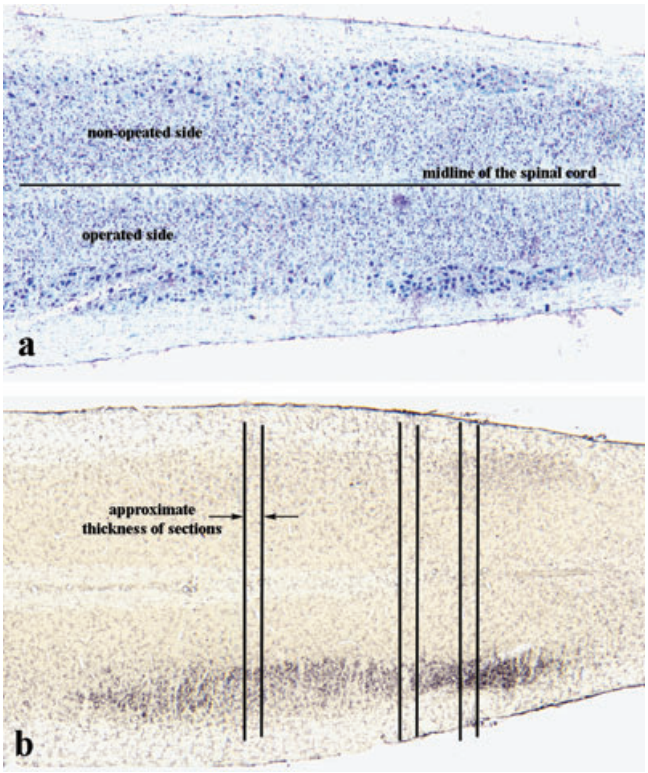

Fig. 5. Composite images from sections of the spinal cord along its axis. View from the back of the animals (upper view). (A) Cresyl violet staining of the sections reveals the major structures within the tissue: the midline of the spinal cord and the large (motor) neurons on the operated and non-operated sides are clearly visible. Heterogeneity of the distribution of the large motor neurons along the axis of the spinal cord on both sides is evident. (B) CD11b IHC staining demonstrates a non-homogeneous distribution of activated microglial cells along the axis of the spinal cord on the operated side, which may correspond to the similar heterogeneous distribution of the injured motor neurons. Clearly, a large variation in the number of stained cells may be expected, depending on the actual positions of the sections within the region of the injury.

the sampling either, as long as the dissected tissue contains the entire region of interest, since the differences neutralize each other during the summation process outside the affected volume, due to the statistical nature of the variations between the operated and the control side (see Fig. 4).

Application of the procedure

In our application example, as a positive control, the effect of an antibiotic (minocycline) on the local microglial reaction on the spinal cord was tested experimentally after lesion of the sciatic nerve. This known anti-inflammatory compound has been shown to improve regeneration and reduce microglial activation in neuronal lesions (Blackbeard *et al.*, 2007; Shankaran *et al.*, 2007; Henry *et al.*, 2008; Mishra & Basu 2008). In accordance with the literature data, our method to quantify the relative staining intensity of IHC-stained microglial cells after axotomy, demonstrated a significant decrease in microglial activation after minocycline treatment (Table 1). The presented procedure is of general applicability when an unbiased estimation of relative changes in IHC staining intensity is required in specified anatomical regions of biological tissue.

Acknowledgements

This work was supported by grants from the Hungarian Scientific Research Fund (OTKA-T 048718) and the Hungarian National Office for Research and Technology (GVOP-3.2.1. 2004–04-0052/3.0 and RET-DNT 08/04). The authors are grateful to Mr. Szabolcs Siklósi for his help with the artwork.

References

Beltz, B.S. & Burd, G.D. (1989) *Immunocytochemical Techniques: Principles and Practice*. Blackwell Scientific Publications, Inc., Cambridge, Oxford, London, Edinburgh, Carlton.

Blackbeard, J., O'Dea, K.P., Wallace, V.C.J., *et al.* (2007) Quantification of the rat spinal microglial response to peripheral nerve injury as revealed by immunohistochemical image analysis and flow cytometry. *J. Neurosci. Methods* **164**, 207–217.

Brey, E.M., Lalani, Z., Johnston, C., Wong, M., McIntire, L.V., Duke, P.J. & Patrick, C.W., Jr. (2003) Automated selection of DAB-labeled tissue from immunohistochemical quantification. *J. Histochem. Cytochem.* **51**, 575–584.

Colburn, R.W., DeLEo, J.A., Rickman, A.J., Yeager, M.P., Kwon, P. & Hickey, W.F. (1997) Dissociation of microglial activation and neuropathic pain behaviors following peripheral nerve injury in the rat. *J. Neuroimmunol.* **79**, 163–175.

Cuello, A.C. (1993) *Immunohistochemistry II*. John Wiley & Sons, Chichester, New York, Brisbane, Toronto, Singapore.

Edie, J.W. & Karlsson, U.L. (1977) Contrast and quantitation in uniform regions of thin sections using transmission electron microscopy. *J. Microsc.* **111**, 179–191.

Gundersen, H.J.G. & Jensen, E.B. (1987) The efficiency of systematic sampling in stereology and its prediction. *J. Microsc.* **147**, 229–263.

Gundersen, H.J.G. & Østerby, R. (1981) Optimizing sampling efficiency of stereological studies in biology: or 'Do more less well!' *J. Microsc.* **121**, 65–73.

Halliday, J.S. & Quinn, T.F.J. (1960) Contrast of electron micrographs. *Br. J. Appl. Phys.* **11**, 486–491.

He, B.P., Tay, S.S.W.H. & Leong, S.K. (1997) Microglial responses in the CNS following sciatic nerve transaction in C57BL/WldS and Balb/v mice. *Exp. Neurol.* **146**, 587–595.

Henry, C.J., Huang, Y., Wynne, A., *et al.* (2008) Minocycline attenuates lipopolysaccharide (LPS)-induced neuroinflammation, sickness behavior, and anhedonia. *J. Neuroinflamm.* **5**, 15–29.

Howard, C.V. & Reed, M.G. (1998) *Unbiased Stereology. Three-Dimensional Measurement in Microscopy*. Bios Scientific Publishers, Oxford.

Kirkeby, S. & Thomsen, C.E. (2005) Quantitative immunohistochemistry of fluorescence labeled probes using low-cost software. *J. Immunol. Methods* **301**, 102–113.

Koliatsos, V.E. & Price, D.L. (1996) Axotomy as an experimental model of neuronal injury and cell death. *Brain Pathol.* **6**, 447–465.

Kreutzberg, G.W. (1996) Microglia: a sensor for pathological events in the CNS. *Trends Neurosci.* **19**, 312–318.

Mishra, M.K. & Basu, A. (2008) Minocycline neuroprotects, reduces microglial activation, inhibits caspase 3 induction, and viral replication following Japanese encephalitis. *J. Neurochem.* **105**, 1582–1595.

Obál, I., Engelhardt, J.I. & Siklós, L. (2006) Axotomy induces contracting changes in calcium and calcium-binding proteins in oculomotor and hypoglossal nuclei of Balb/c mice. *J. Comp. Neurol.* **499**, 17–32.

Obál, I., Soós, J., Jakab, K., Siklós L. & Engelhardt, J.I. (2001) Recruitment of activated microglia cells in the spinal cord of mice by ALS IgG. *NeuroReport* **12**, 2449–2452.

Pham, N.A., Morrison, A., Schwock, J., *et al.* (2007) Quantitative image analysis of immunohistochemical stains using a CMYK color model. *Diag. Pathol.* **2**, 8–18.

Schmitz, C., Dafotakis, M., Heinsen, H., *et al.* (2000) Use of cryostat sections from snap-frozen nervous tissue for combining stereological estimates with histological, cellular, or molecular analyses on adjacent sections. *J. Chem. Neuroanat.* **20**, 21–29.

Shankaran, M., Marino, M.E., Busch, R., *et al.* (2007) Measurement of brain microglial proliferation rates in vivo in response to neuroinflammatory stimuli: application to drug discovery. *J. Neurosci. Res.* **85**, 2374–2384.

Steu, S., Baucamp, M., von Dach, G., *et al.* (2008) A procedure for tissue freezing and processing applicable to both intra-operative frozen section diagnosis and tissue banking in surgical pathology. *Virchows Arch.* **452**, 305–312.

Stuesse, S.L., Cruce, W.L.R., Lovell, J.A., McBurney, D.L. & Crisp, T. (2000) Microglial proliferation in the spinal cord of aged rats with a sciatic nerve injury. *Neurosci. Lett.* **287**, 121–124.

Van Der Laak, J.A.W.M., Pahlplatz, M.M.M., Hanselaar, A.G.J.M. & de Wilde, P.C.M. (2000) Hue-saturation-density (HSD) model for stain recognition in digital images from transmitted light microscopy. *Cytometry* **39**, 275–284.

West, M. (1999) Stereological methods for the estimating the total number of neurons and synapses: issues of precision and bias. *Trends Neurosci.* **22**, 21–61.

Zeitler, E. & Bahr, G.F. (1965) Contrast and mass thickness. *Lab. Invest.* **14**, 142–153.

Zemke, D. & Majid, A. (2004) The potential of minocycline for neuroprotection in human neurologic diseases. *Clin. Neuropharmacol.* **27**, 293–298.

Hypoglossal Motor Neurons Display a Reduced Calcium Increase After Axotomy in Mice with Upregulated Parvalbumin

Melinda Paizs,[1] József I. Engelhardt,[2] Zója Katarova,[3] and László Siklós[1]*

[1]Institute of Biophysics, Biological Research Center, Szeged, H-6701, Hungary
[2]Department of Neurology, University of Szeged, Szeged, H-6701, Hungary
[3]Institute of Experimental Medicine, Budapest, H-1450, Hungary

ABSTRACT

Motor neurons that exhibit differences in vulnerability to degeneration have been identified in motor neuron disease and in its animal models. The oculomotor and hypoglossal neurons are regarded as the prototypes of the resistant and susceptible cell types, respectively. Because an increase in the level of intracellular calcium has been proposed as a feature amplifying degenerative processes, we earlier studied the calcium increase in these motor neurons after axotomy in Balb/c mice and demonstrated a correlation between the susceptibility to degeneration and the intracellular calcium increase, with an inverse relation with the calcium buffering capacity, characterized by the parvalbumin or calbindin-D_{28k} content. Because the differential susceptibility of the cells might also be attributed to their different cellular environments, in the present experiments, with the aim of verifying directly that a higher calcium buffering capacity is indeed responsible for the enhanced resistance, motor neurons were studied in their original milieu in mice with a genetically increased parvalbumin level. The changes in intracellular calcium level of the hypoglossal and oculomotor neurons after axotomy were studied electron microscopically at a 21-day interval after axotomy, during which time no significant calcium increase was detected in the hypoglossal motor neurons, the response being similar to that of the oculomotor neurons. The hypoglossal motor neurons of the parental mice, used as positive controls, exhibited a transient, significant elevation of calcium. These data provide more direct evidence of the protective role of parvalbumin against the degeneration mediated by a calcium increase in the acute injury of motor neurons. J. Comp. Neurol. 518:1946–1961, 2010.

INDEXING TERMS: calcium; calcium buffering; parvalbumin; axotomy; neuroprotection

Motor neuron disease (or amyotrophic lateral sclerosis [ALS]) is a fatal degenerative disorder of the nervous system that affects primarily the upper and lower motor neurons (Rowland and Shneider, 2001). Its etiology is basically unknown, although several mechanisms have been proposed, which probably contribute synergistically to the destruction of the motor neurons (Boillée et al., 2006; Bendotti and Carri, 2009; Rothstein, 2009). The sequence of events during these pathologic processes is mostly known, and some aspects of their reciprocal contribution to the propagation of the injury cascade have been well described (Mattson, 1998).

Our research focuses on the role of the increase in the intracellular calcium level of the motor neurons during degeneration. We hypothesize that the inability of the motor neurons to cope successfully with a nonphysiologic calcium load after or during injury may be one of the key events maintaining the complex destructive machinery through a positive feedback of the elementary steps, and an elevated calcium buffering capacity may attenuate the degree of the lesion during stress conditions (Appel et al., 2001; Siklós and Appel, 2005). Support for this hypothesis has emerged from clinical observations and experimental studies. Patients with ALS present an increased

Grant sponsor: the Hungarian Scientific Research Fund; Grant number: OTKA-T 048718; Grant sponsor: the Hungarian National Office for Research and Technology; Grant number: GVOP-3.2.1. 2004-04-0052/3.0; Grant number: TÁMOP-4.2.2/08/1/2008-0002.

*CORRESPONDENCE TO: László Siklós, Ph.D., Laboratory of Molecular Neurobiology, Institute of Biophysics, Biological Research Center, P.O. Box 521, H-6701 Szeged, Hungary. E-mail: siklos@brc.hu

Received July 3, 2009; Revised November 24, 2009; Accepted November 24, 2009
DOI 10.1002/cne.22312
Published online December 17, 2009 in Wiley InterScience (www.interscience.wiley.com)

level of calcium in the affected motor nerve terminals (Siklós et al., 1996), with a correlation between the preservation of specific motor (external oculomotor and voluntary sphincter) functions and the intracellular levels of certain calcium binding proteins ([CaBPs] calbindin-D_{28k} [CB] and parvalbumin [PV]) in the corresponding motor neurons (Ince et al., 1993; Alexianu et al., 1994).

In accordance with these observations, in transgenic animals containing the G93A mutation of the Cu/Zn superoxide dismutase (SOD1) gene, which serve as a model for the familial form of ALS (Gurney et al., 1994), the viability of the motor neurons paralleled their PV content; in contrast, in accord with our hypothesis, increases are observed in the intracellular calcium, with structural abnormalities in these cells (Siklós et al., 1998). On the basis of in vitro physiology measurements in oculomotor and hypoglossal neurons, the prototypes of motor neurons with high and low CaBP content, respectively, a correlation was proposed between the CaBP content and the ability of the motor neurons to resist calcium-mediated injury (Lips and Keller, 1998; Vanselow and Keller, 2000). Our earlier electron microscopic study following axotomy/target deprivation in these same motor nuclei in vivo provided further support for this concept: a lower increase in calcium level and less significant degeneration were demonstrated in the oculomotor neurons in which the PV content was higher than that in the hypoglossal motor neurons, in which PV and CB could not be detected (Obál et al., 2006).

The results of the above experiments provided indirect evidence of the calcium buffer hypothesis, because different pools of motor neurons were compared in each case. In fact, the embedding of these motor neurons into different neuronal networks and different microenvironments may contribute to their different susceptibilities to degeneration. In order to test the hypothesis of the protective role of CaBPs more directly, the same population of motor neurons, but with different CaBP contents should be challenged experimentally. For this purpose, a transgenic homozygous mouse strain with elevated PV content (PV+/+) has been developed (Beers et al., 2001) and applied in axotomy/target deprivation experiments, similarly as in our earlier study (Obál et al., 2006). The changes in level of the intracellular calcium in the hypoglossal motor neurons were determined in the 21-day period after the lesion, and compared with the corresponding data obtained in wild-type animals. In accordance with our hypothesis, we could not demonstrate either a significant calcium increase in the hypoglossal motor neurons of the PV+/+ animals, or a difference from the oculomotor neurons from the same animals, whereas a transient, but significant calcium elevation was detected in the hypoglossal motor neurons from mice of the parental line.

MATERIALS AND METHODS

Experimental animals

The description of the generation of the PV overexpressing mice used in this study has been given elsewhere (Beers et al., 2001). Parental breeding between transgenic CaMKII-parvalbumin mice #4031 × 4034, 4035 obtained from Dr. S.H. Appel (The Methodist Hospital Neurological Institute, Houston, TX) was set up at the conventional animal facility of the Institute of Experimental Medicine, Hungarian Academy of Sciences, Budapest. All transgenic mice used in this study were derived from the original parental cross between transgenic male #4031 mated to 4034 and #4045 females of line Tg (parv14-4). All litters obtained from this cross (mice #12–21) and subsequent sibling/sibling matings as well as the parents were homozygous for the transgene as proved by test crosses to wild-type mice.

To prove the presence of the transgene, DNA was isolated from tail biopsies and prepared according to a standard protocol published online on the Jackson Laboratory website (http://www.jax.org/imr/tail_phenol.html). In general, 0.1 μg of genomic tail DNA was used to amplify the transgene by using two different primer pairs:

1. Primers derived from the third and fourth exons of the endogenous CaMKII gene as follows: forward: 5′-CTGCAGACTCCTTCGACCAC-3′ and reverse 5′-GCCATCAGCGTCTTTGTTTC-3′. The sizes of the products were 200 bp (transgene) and 1,400 bp (endogenous CamKII gene).
2. Primers were: forward primer 5′-GCGAGCGAGTC GAGTGGTTGTCTG-3′ and reverse primer 5′-TTAGCT TTCGGCCACCAGAGTGGAGAATTC-3′ (Beers et al., 2001), size of the product 1,200 bp.

Amplification was as follows: denaturation at 94°C for 4 minutes, followed by 30 cycles of 30 seconds at 94°C, 45 seconds at 57°C and 45 seconds at 72°C, final extension 7 minutes at 72°C. DNA was run on EtBr-containing agarose gels and photographed under UV light.

Axotomy experiments

Twelve-week-old male B6/SJL mice and PV+/+ mice were selected for the study. To avoid multiple survival surgery, animals were assigned either to hypoglossal or to oculomotor nerve cut experiments. A total of 60 mice were used either for hypoglossal axotomy (n = 40) or for oculomotor surgery (n = 20). Four animals were euthanized at five time points for each type of surgery and were processed for electron microscopic calcium histochemistry study. Surgical procedures were performed under deep anesthesia with Avertin (tribromoethanol,

Fluka, Buchs, Switzerland; 240 mg/kg body weight in a 0.3-ml volume) administered intraperitoneally. The hypoglossal nerve was transected lateral to the hyoid bone and a 3–5-mm nerve segment was removed to prevent regeneration. For transection of the left oculomotor nerve, the animals were enucleated and the orbits were cleared of the remaining extraocular muscles and nerve segments. In both cases, the nonoperated side served as an internal control.

Following surgery, the animals were housed in a temperature-controlled room with a 12-hour light/dark cycle, with access to water and food ad libitum, and were allowed to survive for 1, 4, 7, 14, or 21 postoperative days. All the experiments were performed in accordance with the institutional guidelines for the use and care of experimental animals and the appropriate governmental laws for animal protection (protocols 72-45/b/2001 and 03876/0014/2006).

Immunocytochemical staining procedures

A detailed characterization of the PV+/+ mice has been presented in our earlier research paper (Beers et al., 2001). In addition, in the present study, PV was demonstrated in nerve nuclei III and XII in selected B6/SJL ($n = 2$) and PV+/+ ($n = 2$) mice by means of light microscopic immunocytochemistry using a polyclonal primary antibody against PV and the avidin-biotin detection technique. This antibody, obtained from Swant (Bellinzona, Switzerland; code no. PV-28, lot no. 5.5) as lyophilized antiserum, was produced in rabbits by using rat muscle PV as the antigen. According to the manufacturer's data sheet, the PV-28 antiserum labels a subpopulation of neurons in the normal mouse brain with high efficiency, but does not stain the brain of PV knockout mice. In our titration experiment, a 1:60,000 dilution of the antibody was selected for subsequent regular use.

As a positive control, sections obtained from the brainstem and cerebellum of normal nice were stained and a pattern of immunoreactivity was obtained that was similar to that described as PV immunoreactivity in the literature (Celio, 1990) (data not shown). For immunocytochemical staining, mice under irreversible anesthesia with methoxyflurane were perfused transcardially with phosphate-buffered saline (PBS; 10 mM, pH 7.4), followed by 3% paraformaldehyde in 10 mM PBS (pH 7.4). The brains were removed and immersed in the same fixative for 24 hours (4°C), and tissue blocks containing either the entire hypoglossal or the oculomotor nuclei were then prepared. To prevent the formation of freezing artifacts, tissue samples were placed in sucrose (30% in 10 mM PBS, pH 7.4) for at least 2 days at 4°C. Sections with a nominal thickness of 30 μm were then cut on a cryostat at −18°C (Kriostat 1720; Leitz, Wetzlar, Germany), and collected in PBS.

Immunostaining was performed on free-floating sections. Endogenous peroxidase activity was first blocked with H_2O_2 (Sigma, St. Louis, MO; 0.3% in 10 mM PBS) for 20 minutes, followed by incubation in Triton X-100 (Sigma; 0.2% in 10 mM PBS) for 30 minutes to enhance antibody penetration. Sections were pretreated with normal goat serum (Vector [Burlingame, CA] S-1000; 2% in 10 mM PBS) for 1 hour, followed by an overnight incubation at 4°C with the primary antibody. After washing, sections were incubated in biotinylated goat-anti-rabbit secondary antibody (Vector BA-9200; 1:200) for 1.5 hours at room temperature. The bound antibodies were detected with the Vectastain Elite ABC Kit (Vector PK-6100) and visualized with diaminobenzidine (DAB; Sigma). After washing, sections were finally mounted on silane-coated glass slides, dehydrated, and coverslipped with Entellan (Merck, Darmstadt, Germany). Parvalbumin-positive motor neurons in nerve nuclei III and XII were identified according to their shape, size, and distribution.

Light microscopic evaluation of parvalbumin immunostaining

Stained sections were examined in an Olympus Vanox-T AH-2 light microscope. Images were recorded with a Spot RT CCD camera (Diagnostic Instruments, Sterling Heights, MI) at 1,600 × 1,200 pixel resolution and stored as 8-bit uncompressed grayscale images in tagged image file format (TIFF). Digital Images were analyzed by using the Image-Pro-Plus image analysis software (IPP; Media Cybernetics, Silver Spring, MD). The staining intensity was assessed by a macro module developed for the IPP program in our laboratory to quantify light microscopic immunohistochemical staining (Paizs et al., 2009).

Briefly, after the specification of the region of interest (I) and a control region (C; for internal reference) in each section, the program calculates the logarithm of the ratio of the transmitted light intensities at these regions [−ln{intensity(I)/intensity(C)}], which is, according to the attenuation law (Bouguer-Lambert-Beer law), proportional to the difference between the concentrations of the light-absorbing material (immunohistochemical staining) at areas I and C. These values, representing the background-corrected staining intensities, were pooled, to form four groups according to the strains (B6/SJL and PV +/+) and motor nerve nuclei (III and XII). Eight fields were analyzed in each group, and the corresponding average values were compared by one-way ANOVA with Duncan post hoc comparison (StatSoft, Statistica, Tulsa, OK).

Parvalbumin-positive motor neurons in nerve nuclei III and XII were identified according to their shape, size, and distribution. The size distribution of the PV-positive cellular profiles was determined by using the appropriate

built-in function of the IPP program, and then frequency histograms were constructed in each group that were compared with those of motor neurons in the corresponding nuclei available in the literature (Eberhorn et al., 2006; Schwarz et al., 2009).

Specimen preparation for electron microscopic detection of calcium

Mice anesthetized irreversibly with methoxyflurane were perfused transcardially, first with 90 mM potassium oxalate (Sigma; pH adjusted to 7.4 with KOH) and then with 3% glutaraldehyde (Polysciences, Eppelheim, Germany) containing 90 mM potassium oxalate (pH 7.4) (Borgers et al., 1977, 1981). Tissue blocks containing the nuclei of either cranial nerve III or XII were dissected and fixed overnight in the same fixative (4°C). Specimens were rinsed in 7.5% sucrose in 90 mM potassium oxalate (pH 7.4), and then postfixed for 2 hours (4°C) in 2% potassium pyroantimonate (Merck) and 1% osmic acid (Sigma), adjusted to pH 7.4 with acetic acid (Molar). Following postfixation, specimens were rinsed in distilled water (pH adjusted to 10 with KOH) for 10 minutes, dehydrated in graded series of ethanol, processed through propylene oxide (Sigma), and embedded in plastic (Durcupan ACM, Fluka). Blocks were polymerized for 2 days at 56°C.

Semithin (0.3-μm) sections were cut from the blocks on an Ultracut UCT ultramicrotome (Leica), etched (Maxwell, 1978), stained (Richardson et al., 1960), and screened under the light microscope (Olympus Vanox-T) to identify the borders of nuclei III and XII. After trimming of the blocks, 50-nm ultrathin sections were obtained, mounted on formvar-coated single-hole copper grids, contrasted with uranyl acetate and lead citrate (Reynolds, 1963), and analyzed under the electron microscope (Zeiss CEM 902). The oxalate-pyroantimonate procedure applied for the demonstration of calcium at the ultrastructural level resulted in electron-dense deposits (EDDs) due to the precipitation of tissue calcium by the fixative, which was easily recognized by conventional transmission electron microscopy.

Specificity control of the histochemical reaction for calcium

The specificity of the fixation procedure for calcium was checked by electron spectroscopic imaging (Bauer, 1988; Reimer et al., 1988). For such analysis, 15–25-nm sections were prepared, mounted on uncoated 700-mesh copper grids, and, without contrasting, examined under the electron microscope in spectroscopic imaging mode at $\Delta e = 250$ eV. During the analysis, the accelerating voltage was set to 80 kV; 90-μm objective and a 650-μm spectrometer entrance apertures were used, with the slit width adjusted to 8–10 eV. By using the attached image analysis system (MTI-66 DAGE high-sensitivity camera; IBAS 2.0 image analysis program, Kontron, Munich, Germany), two-dimensional spectroscopic analysis was carried out at 20,000× instrumental magnification by recording element-specific and background images at energy loss values of the absorption edge of calcium (355 eV) and below (310 eV). To produce low-noise images for calculations, 500–600 video images were averaged for each energy loss value. The analytical image displaying the net calcium distribution was obtained by subtracting the background image from the "edge" image. The nonsignificant signal below the (mean + 2.5 × s.d.) level was deleted in the analytical image, and then, for easier comparison of the co-distribution of the EDDs with the true calcium, the significant calcium signal was false-colored according to the significance level in the [mean + 2.5 × s.d.] to [mean + 6 × s.d.] interval.

This final image, representing the distribution of the precipitated calcium in the tissue, was compared visually with micrographs obtained by structural imaging of the same area, displaying the arrangement of the EDDs. To match the resolution of the structural image to the digital analytical images (512 × 512 pixel), fine structural images were obtained in the spectroscopic mode of the analyzer as well, tuned to the carbon absorption edge (250 eV), which resulted in good-quality structural images of the sections (Körtje and Körtje, 1992). Such images, resembling "darkfield" images, were then inverted for easier comparison.

Semiquantitative evaluation of the intracellular amount of EDDs

Ultrathin sections prepared from the motor nuclei were screened under the electron microscope at low magnification (3,000×) to identify motor neurons, which were selected randomly for measurements. One region from each cell body, also selected at random, was photographed at a magnification of 12,000×, until 12–15 samples had been collected from both the operated and the nonoperated side of each nucleus. The negatives were printed at 2.7× enlargement. The amounts of calcium in the tissue compartments were determined by measuring the volume of the EDDs, and were expressed as volume-to-volume ratios (volume fractions) with respect to a selected reference volume. Three types of reference spaces were selected: either the whole perikaryal volume, or the mitochondrial, or the extramitochondrial compartments of the perikaryal space. For brevity, the latter was called the cytoplasmic volume. The three-dimensional parameters, the relative perikaryal, mitochondrial, and cytoplasmic volumes occupied by the

EDDs were determined on two-dimensional electron microscopic prints with a point counting technique (Mayhew, 1992).

After random superimposition of a tessellation of sampling points on the prints, grid points overlying either the EDDs [$P_{EDD(cyt)}$, or $P_{EDD(mit)}$] or the corresponding reference area [$P_{(cyt)}$, or $P_{(mit)}$] were counted. The scores obtained on individual micrographs for both compartments were pooled according to the operated and nonoperated sides of the examined nucleus of each animal, and the corresponding ratios expressing the "histochemical concentration of calcium" in the mitochondrial and cytoplasmic compartments were calculated for both sides [$\Sigma P_{EDD(cyt)}/\Sigma P_{(cyt)}$ and $\Sigma P_{EDD(mit)}/\Sigma P_{(mit)}$]. Finally, the corresponding values obtained on the operated side were divided by those obtained on the nonoperated side to express the changes (fold increase) induced by the axotomy in the mitochondrial and cytoplasmic calcium contents for each animal.

The fold increases in calcium in the hypoglossal and oculomotor nuclei of the PV+/+ animals and in the hypoglossal nucleus of the B6/SJL mice were statistically compared on postoperative days 1, 4, 7, 14, and 21 (two-way ANOVA with Duncan post hoc comparison; StatSoft Statistica). The differences were accepted as significant at $P < 0.05$.

To produce mounted sets of figures for the illustration of the results, electron micrographs and light microscopic images were selected and processed digitally with the Photoshop program (Adobe Systems, San Jose, CA, version 8.0). Electron microscopic negatives were scanned with a transillumination scanner (HP ScanJet 7400c) at 300 dpi resolution as grayscale images, inverted, and imported to the Photoshop program. Light microscopic images were directly transferred to the Photoshop program at the original resolution of the CCD camera (1,600 × 1,200 pixel). Images were cropped, resized, and mounted to produce tables of figures at the final size. Shading corrections (contrast/brightness and gamma corrections) were applied to compensate for the occasional slight differences in the appearance of the individual pictures to harmonize the overall appearance of all the figures.

RESULTS

Although the PV+/+ mouse line #14 used in the present study was bred to homozygosity, from time to time the integrity of the colony was confirmed with polymerase chain reaction (PCR), by using tail samples from the animals (Fig. 1).

For characterization of the distribution of calcium precipitated during fixation, the specificity of the method was checked periodically in the present study by two-dimensional analytical electron microscopy. These measurements proved that the pattern of EDDs visible in conventional transmission mode of the microscope can be identified with the distribution of calcium in the tissue (Fig. 2). Qualitatively, a gradual elevation of the intracellular calcium content in the axotomized hypoglossal motor neurons of the B6/SJL mice was seen with increasing postoperative time relative to the nonoperated side, with a tendency to return to the control level by postoperative day 21 (Fig. 3). In the hypoglossal neurons of the PV+/+ animals, however, except for a slight increase in the mitochondrial calcium content on postoperative day 1, the calcium content was observed not to be elevated relative to the control side on any postoperative day (Fig. 4). In the oculomotor neurons of the PV+/+ mice, similarly as in the hypoglossal neurons in these animals, no calcium increase was detected in the injured neurons as compared with the intact cells at any time point after the surgery (Fig. 5).

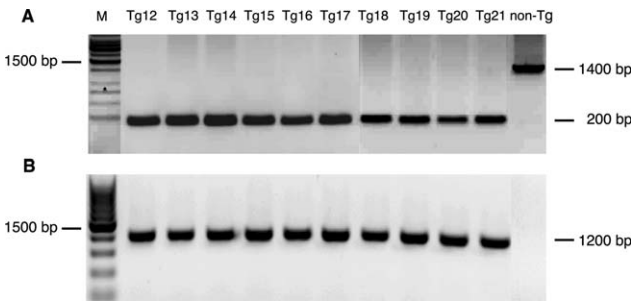

Figure 1. PCR-based genotyping of CamKII-parvalbumin transgenic mice. Transgenic litters from a homozygous cross between mice #4031x#4034, #4045 of line parv 14-4 (#12-21) were tailed-clipped, and DNA from tail biopsies was purified and subjected to 30 rounds of PCR with two different primer pairs as detailed in Materials and Methods. **A**: Primers resulting in a transgene-specific 200-bp and 1,400-bp (endogenous CamKII gene) bands were used. This band is missing in the lanes of transgenic DNA because of highly preferential amplification of the transgene. **B**: Primer pair B was used, resulting in a 1,200-bp, transgene-specific band. All mice from this cross (Tg12-Tg21) were positive for the transgene.

In both motor nuclei, the volume fraction of the EDDs, characterizing the distribution of calcium in the tissue, was expressed quantitatively. The results are presented graphically in Figure 6. The visual evaluation of the charts depicting the temporal changes in the total (Fig. 6A), mitochondrial (Fig. 6B), and cytoplasmic calcium (Fig. 6C) was consistent with the qualitative findings on the electron microscopic prints, suggesting that the calcium level in the hypoglossal neurons of the B6/SJL animals gradually increased after axotomy, whereas in the PV+/+ animals there was no significant increase in calcium in either the oculomotor or the hypoglossal motor neurons at any time point. According to the raw data, the calcium increase in the mitochondria of the motor neurons of the

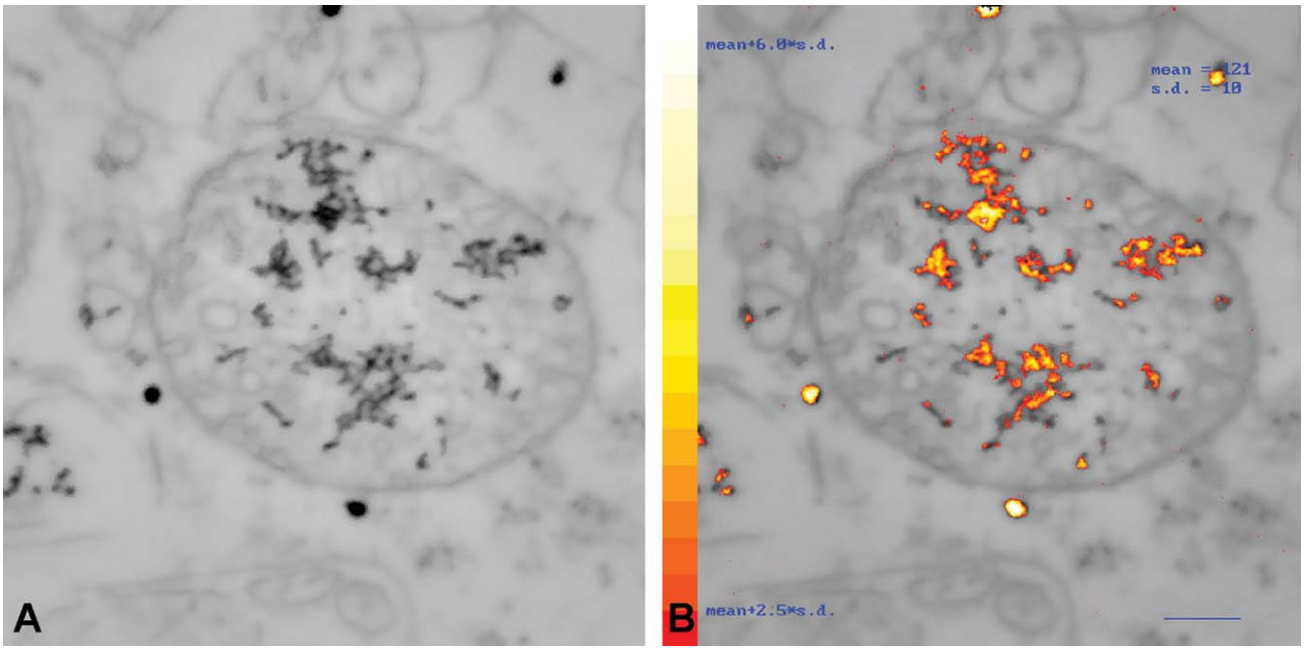

Figure 2. Electron spectroscopic imaging (ESI) of electron-dense deposits (EDDs), products of the histochemical reaction applied to visualize tissue calcium. **A**: Fine structural image of a typical intramitochondrial cluster of EDDs. The picture was obtained by inverting an ESI image made at the carbon absorption edge (250 eV). **B**: The same area was also analyzed by ESI set to produce the net distribution of calcium at the significance level of <background + 2.5 s.d.>. This significant calcium signal was false-colored from red to white (left) that corresponded to the range of significance from <mean + 2.5 s.d.> to <mean + 6 s.d.>, and then superimposed on the structural image. The comparison of A with B demonstrates a good correlation of the EDDs with the tissue calcium. Scale bar = 0.2 μm in B (applies to A,B).

B6/SJL mice commenced earlier (day 1, Fig. 6B) and lasted longer (day 14, Fig. 6B) than in the cytoplasmic compartment (day 4 and day 7, Fig. 6B), a temporal difference that was not, however, significant ($P = 0.55$).

Statistically, the time dependences of the calcium levels in the two nuclei in the PV+/+ strain did not differ, regardless of whether the total calcium ($P = 0.21$) or the cytoplasmic ($P = 0.43$) and mitochondrial ($P = 0.20$) calcium levels separately were compared (two-way ANOVA). However, the postoperative calcium increase in the motor neurons from the B6/SJL mice was significantly different from the corresponding situation in the PV+/+ animals ($P = 0.001$, two-way ANOVA). The subsequent multiple comparison procedure revealed that this difference could be attributed to an approximately 1.5-fold increase in the total calcium in the hypoglossal neurons of the B6/SJL animals on day 7 ($P = 0.009$) and day 14 ($P = 0.002$) after the operation. The separate analysis of the mitochondrial and cytoplasmic calcium levels revealed similar significant differences after injury on postoperative days 7 ($P = 0.018$) and 14 ($P = 0.016$), and postoperative days 4 ($P = 0.018$) and 7 ($P = 0.0005$), respectively.

The PV contents in the hypoglossal and oculomotor nuclei were visualized by means of light microscopic immunocytochemistry. Whereas numerous cellular profiles with positive staining were observed in the hypoglossal nucleus of PV+/+ animals (Fig. 7A), only background staining was seen in the same nucleus from the B6/SJL mice (Fig. 7B). The oculomotor nuclei from both strains contained stained cells and displayed strong PV staining in the neuropil (Fig. 7C, D). The intensity of the staining was expressed quantitatively on an arbitrary scale in each motor nucleus by determining the average net (background-corrected) amount of the chromophore (DAB). Compared with the control hypoglossal nucleus, a significant, 1.6-fold increase of immunostaining was detected in nucleus XII of the PV+/+ mice (Table 1). Similar comparison of the oculomotor nuclei did not yield a significant difference (Table 1).

The increased intensity of PV immunostaining in the hypoglossal nucleus of PV+/+ animals was attributed to the presence of PV-positive cellular profiles, which were missing in the nerve XII nucleus of B6/SJL mice. A frequency histogram of the profile diameter of the stained cells was constructed (Fig. 8A), which showed a range of 15–33 μm and a mean value of 21.8 ± 3.8 μm (mean ± s.d.) of the profile diameters. These numbers coincided well with the corresponding data available in the literature characterizing hypoglossal motor neurons (range: 11–34 μm; mean ± s.e.m.: 22.7 ± 0.68 μm) (Schwarz et al., 2009). Similar histograms have been constructed from the stained profiles visible in the oculomotor nuclei

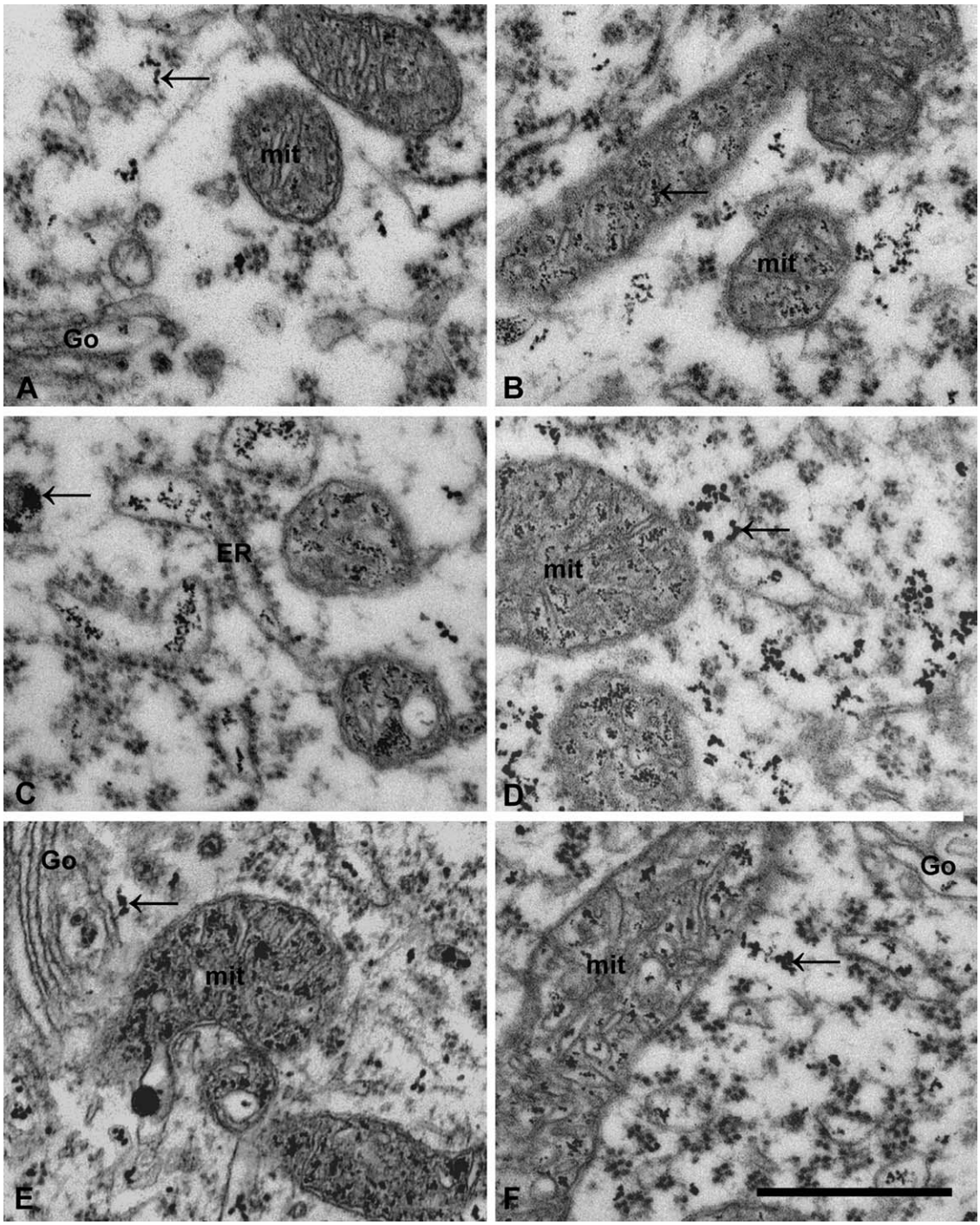

Figure 3. A–E: Calcium distribution in motor neurons from the hypoglossal nucleus of B6/SJL animals. Arrows indicate electron-dense deposits reflecting the distribution of calcium. Motor neurons in cytoplasmic and mitochondrial locations from the nonoperated side (A) contain few deposits. The number of deposits gradually increases at postoperative day 1 (B) to days 4 (C), 7 (D), and 14 (E) and is lower on day 21 (F). ER, rough endoplasmic reticulum; Go, Golgi apparatus; mit, mitochondrion. Scale bar = 1 μm in F (applies to A–F).

of both strains (Fig. 8B,C), which showed somewhat smaller mean diameter values (PV+/+: 15.7 ± 2.1 μm; B6/SJL: 16.4 ± 2.8 μm; mean ± s.d.), but were in agreement with the corresponding values from the literature describing oculomotor neurons (18.0 ± 3.3 μm; mean ± s.d.) (Eberhorn et al., 2006).

DISCUSSION

Neuroprotective role of CaBPs

CaBPs within the cells are also located at critical positions: in the vicinity of plasmalemmal calcium pumps and channels, around the mitochondria and endoplasmic reticulum, organelles known to play key roles in Ca^{2+}

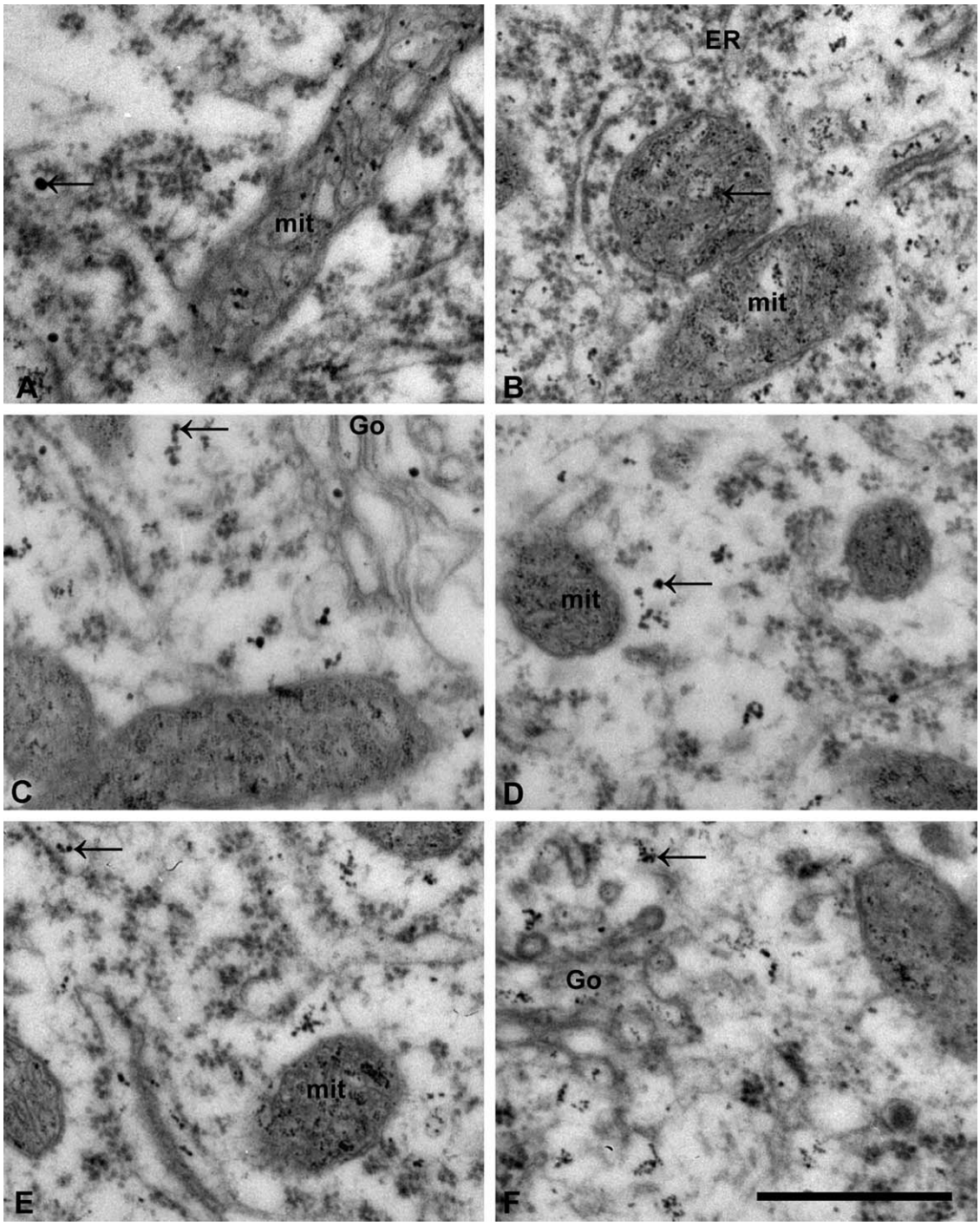

Figure 4. **A–F**: Calcium distribution in motor neurons from the hypoglossal nucleus of PV+/+ animals. Arrows indicate the reaction product of the histochemical procedure reflecting the distribution of the intracellular calcium. A small number of deposits can be seen in neurons from the nonoperated side (A) that, mainly within the mitochondria, were increased slightly on postoperative day 1 (B). At the subsequent time points, on postoperative days 4 (C), 7 (D), 14 (E), and 21 (F), the numbers of deposits are comparable with the control. ER, rough endoplasmic reticulum; Go, Golgi apparatus; mit, mitochondrion. Scale bar = 1 μm in F (applies to A–F).

signaling and buffering (Brini, 2003). Thus, these proteins may slow down the diffusion of calcium ions away from the influx regions, or facilitate their recycling into internal stores, and thereby reduce the amplitude of calcium concentration changes in the cytosol (Vanselow and Keller, 2000; von Lewinski and Keller, 2005; Müller et al., 2007). Because an elevated calcium level (Berridge et al., 1998; Arundine and Tymianski, 2003) and calcium-dependent mechanisms (Artal-Sanz and Tavernarakis, 2005) have often been implicated in acute injuries of the nervous

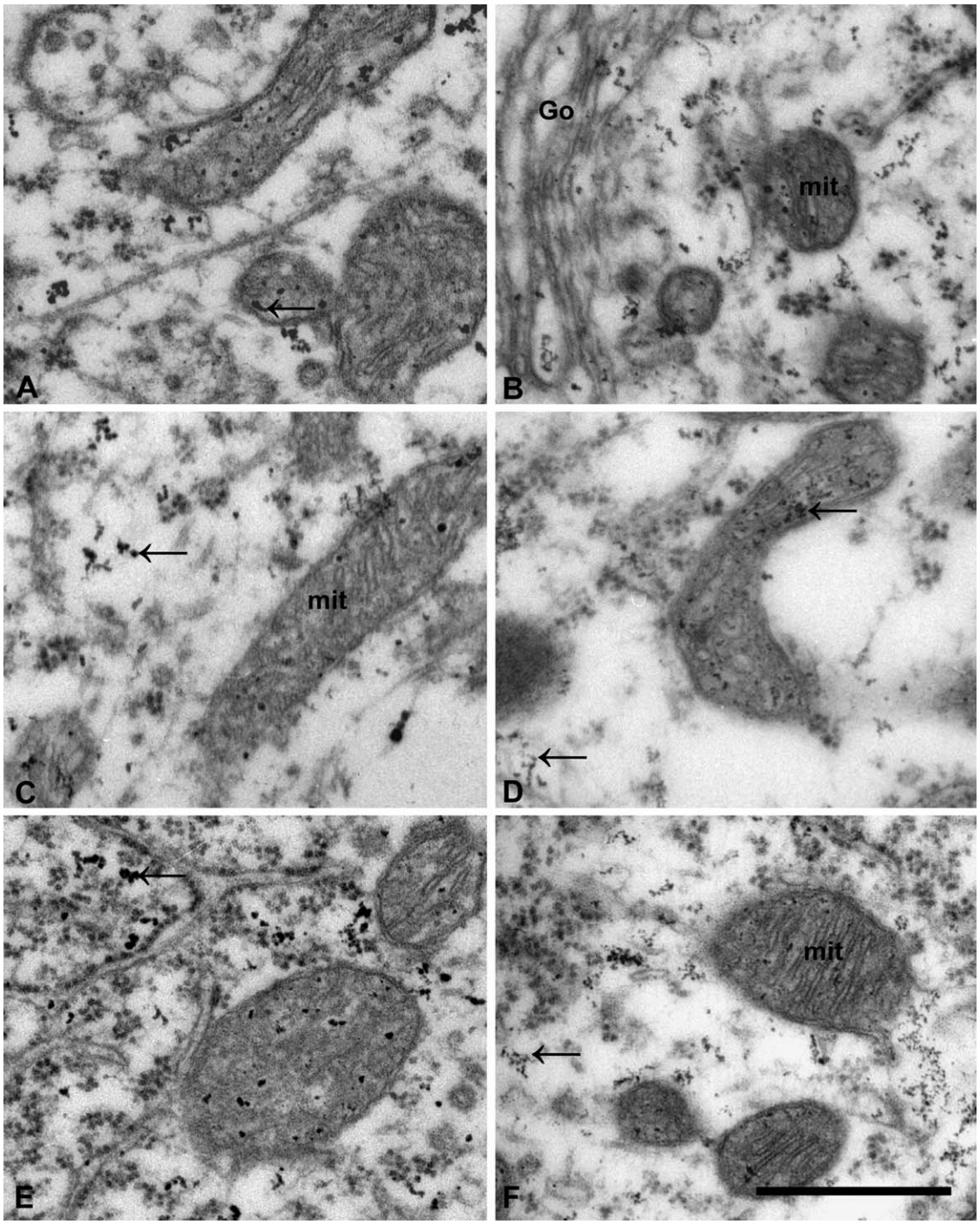

Figure 5. A–F: Calcium distribution in motor neurons from the oculomotor nucleus of PV+/+ animals. Arrows indicate the electron-dense deposits that reflect the distribution of the intracellular calcium. A low number of deposits can be seen in the control condition (A), this pattern remaining practically the same on postoperative days 1 (B), 4 (C), 7 (D), 14 (E), and 21 (F). Go, Golgi apparatus; mit, mitochondrion. Scale bar = 1 μm in F (applies to A–F).

system (Choi, 1995; Lipton, 1999; Raghupathi, 2004; Sullivan et al., 2005) or in neurodegenerative disorders (Mattson, 2007), as exemplified by Huntington's disease (Bezprozvanny and Hayden, 2004), Alzheimer's disease (Mattson and Chan, 2003), and ALS (Appel et al., 2001), it is a reasonable assumption that a larger buffering capacity of the intracellular calcium may confer a higher resistance against injury on the neurons via stabilization of the calcium homeostasis.

The concept that CaBPs may exert a general neuroprotective effect was proposed on the basis of data acquired from a wide range of in vitro (Mattson et al., 1991;

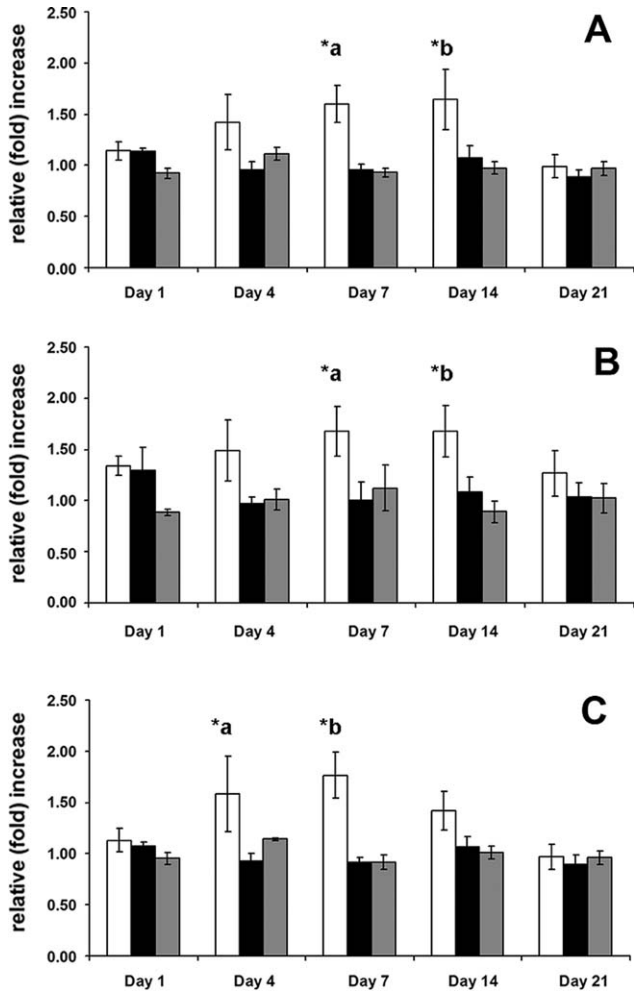

Figure 6. **A–C**: Quantification of the number of electron-dense deposits in the total perikaryal volume (A), in the mitochondrial compartment (B), and in the cytoplasm (C) of the hypoglossal motor neurons of B6/SJL (white bars) and PV+/+ mice (black bars) and of the oculomotor neurons of PV+/+ animals (gray bars). Data are expressed as the fold increases in the volume density of the deposits relative to the nonoperated side on days 1, 4, 7, 14, and 21 postoperatively. The data characterizing the two types of nuclei of the PV+/+ strain (black and gray bars) did not differ when either the total calcium ($P = 0.21$), or separately the cytoplasmic ($P = 0.43$) and mitochondrial ($P = 0.20$) calcium levels were compared (two-way ANOVA). The postoperative calcium level increase in the motor neurons from the B6/SJL mice was significantly different from that for the PV+/+ animals ($P = 0.001$, two-way ANOVA). Multiple comparison (Duncan post-hoc test) revealed that the difference between the strains could be attributed to an approximately 1.5-fold increase in the total calcium in the hypoglossal neurons of the B6/SJL animals on days 7 (*a: $P = 0.009$) and 14 (*b: $P = 0.002$) after the operation. The separate analysis of the mitochondrial and cytoplasmic calcium levels revealed similar significant differences after injury on postoperative days 7 (*a: $P = 0.018$) and 14 (*b: $P = 0.016$), and postoperative days 4 (*a: $P = 0.018$) and 7 (*b: $P = 0.0005$), respectively.

Clementi et al., 1996; McMahon et al., 1998) and in vivo experiments (Rami et al., 1992; Tortosa and Ferrer, 1993; Beck et al., 1994; Vig et al., 1998). The idea has received additional support from a variety of clinical observations, e.g., the age-dependent loss of CB from the cholinergic neurons of the basal forebrain in humans displayed a similar pattern to that of the loss of these cells in Alzheimer's disease (Geula et al., 2003), whereas in Huntington's disease those striatal neuronal groups that contained high levels of CB proved to have a decreased vulnerability (Mitchell and Griffiths, 2003). In Parkinson's disease, the CB-positive dopaminergic neurons in the substantia nigra are relatively spared (Yamada et al., 1990). Finally, in ALS, the most susceptible motor neurons are comparatively deficient in CB and/or PV (Ince et al., 1993; Alexianu et al., 1994), which leads to the concise statement that "PV is a marker of ALS-resistant motor neurons" (Elliott and Snider, 1995).

However, not all studies lend support to the protective role of the CaBPs during injury. The reports range from documentation of the inability of a high CaBP content to confer resistance on the (Purkinje) cells in the cerebellum (Slemmer et al., 2005), through the lack of a correlation between the CB and/or PV content and the neuronal vulnerability in the hippocampus (Freund et al., 1990), to the finding that PV actually enhances N-methyl-D-aspartate (NMDA)-mediated toxicity (Hartley et al., 1996), or to the notion that not an excess, but rather a deficiency in CB might be protective (Klapstein et al., 1998). The diversity of these results, however, might be attributed to the fact that the actual impact of the CaBPs on survival is affected by the developmental state of the neuron (Lema Tomé et al., 2006, 2008), shaped by the local cellular environment, and influenced by the neuronal network properties of the injured cells. In an effort to eliminate such perturbations of the results, in the present study, we decided to assay the changes in calcium level after injury in motor neurons with an artificially elevated PV content, and to compare the results obtained from the same population of neurons with a naturally low PV content in wild-type animals.

Lesion induced by axotomy

Axonal transection is an experimental method for the study of neuronal responses to injury leading to degeneration, or resulting in plastic changes and recovery (Price et al., 1992; Koliatsos and Price, 1996). The lesion of motor axons induces retrograde changes in neurons (Lieberman, 1971), some of which resemble those seen in ALS (Price et al., 1994). Factors known to influence the outcome of axotomy-induced injury are the type of lesion (crush, cut, target deprivation, or avulsion), the location of the trauma relative to the perikaryon, differences in species, type of the motor neurons, and age of the animals (Snider et al., 1992; Koliatsos and Price, 1996).

For example, approximately 70% of adult hypoglossal motor neurons survive target deprivation in rats, but only

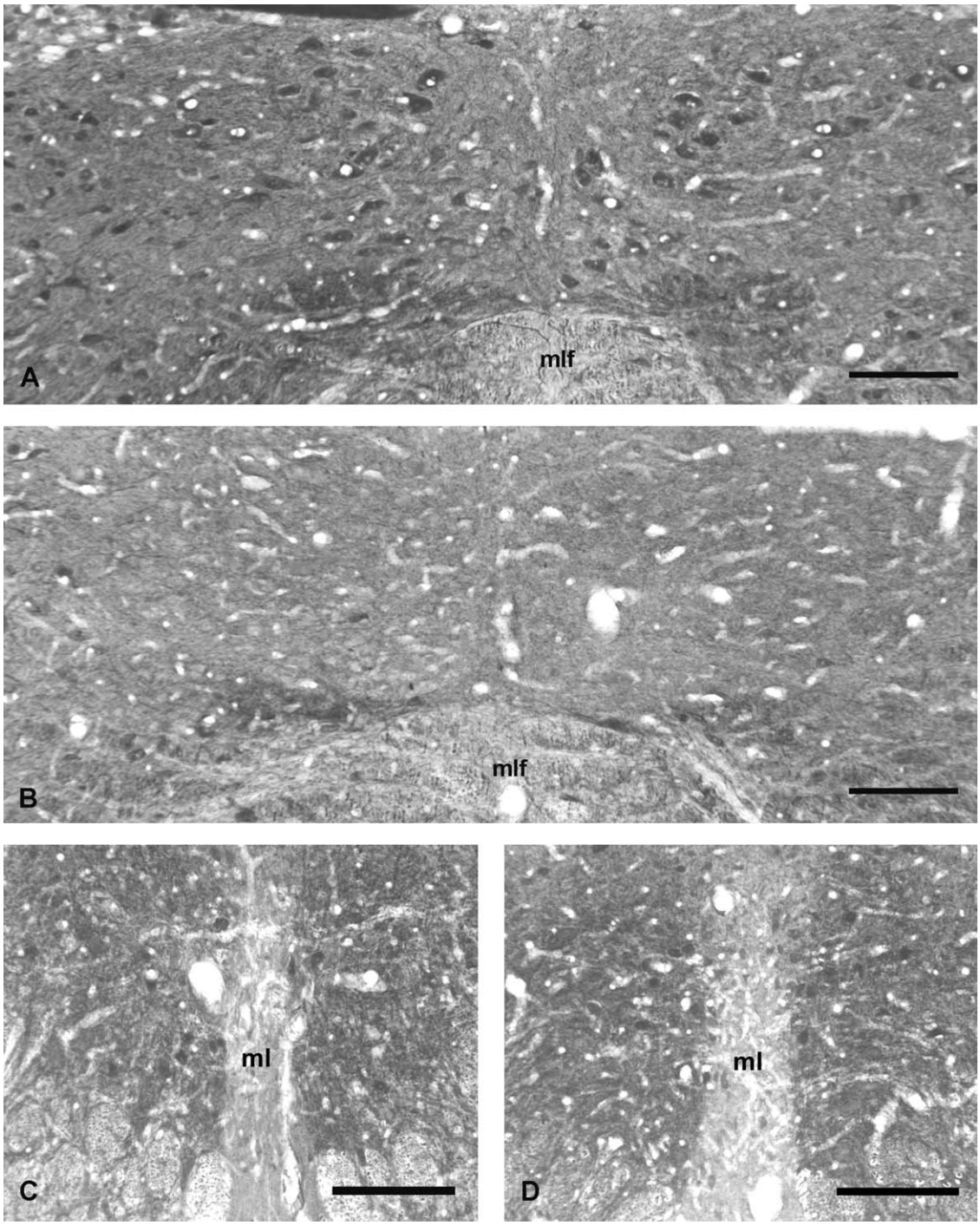

Figure 7. **A–D**: Parvalbumin staining of the hypoglossal (A,B) and oculomotor nuclei (C,D) of PV+/+ (A,C) and B6/SJL (B,D) mice. In the hypoglossal nucleus of the PV+/+ animals, numerous stained cellular profiles are visible, which, according to their size, shape, and distribution, can be considered as motor neurons (A). In the hypoglossal nucleus of the B6/SJL mice only background staining can be seen (B). The neuropil staining and some stained cellular profiles at the ventromedial and lateral border of the hypoglossal nucleus in both figures may belong to the nucleus of Roller and the intercalated nucleus of medulla, respectively. The parvalbumin staining patterns of the oculomotor nuclei of the PV+/+ (C) and B6/SJL (D) mice are similar: in the heavily stained neuropil, stained cellular profiles are present. mlf, medial longitudinal fasciculus; ml, midline. Scale bar = 100 μm in A–D.

40% survive if the surgery is made during the first postnatal week (Snider and Thanedar, 1989). In the spinal cord of newborn animals, whereas avulsion or crush of the sciatic nerve produces a 73–80% loss of lumbar motor neurons (Schmalbruch, 1984; Koliatsos and Price, 1996; Dekkers et al., 2004), axotomy of the same nerve

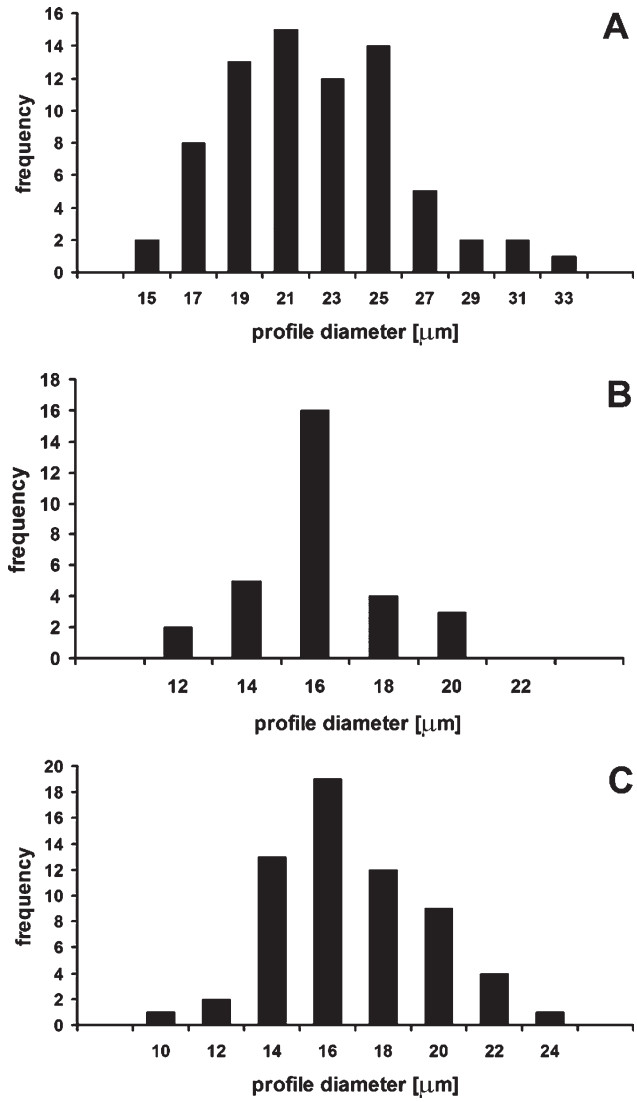

Figure 8. A–C: Size distribution of the parvalbumin-positive cellular profiles in the hypoglossal nucleus of PV+/+ mice (A) and in the oculomotor nucleus of PV+/+ (B) and B6/SJL (C) animals. The ranges and the mean values of the distribution (PV+/+ hypoglossal nucleus: 21.8 ± 3.8 μm; PV+/+ oculomotor nucleus: 15.7 ± 2.1 μm; B6/SJL oculomotor nucleus: 16.4 ± 2.8 μm; mean ± s.d.) coincided well with corresponding data from the literature characterizing populations of motor neurons in these nuclei. According to Schwarz and co-workers (2009), the mean profile diameter of hypoglossal motor neurons is 22.7 ± 0.68 μm (mean ± s.e.m.), and the mean profile diameter of oculomotor neurons, according to Eberhorn and co-workers (2006), is 18.0 ± 3.3 μm. Similar histograms from the hypoglossal nucleus of B6/SJL animals could not be prepared, because only background staining was present.

induces the complete loss of motor neurons (Schmalbruch, 1984). In contrast, sciatic nerve cut in adult animals generates no visible loss of motor neurons (Schmalbruch, 1984). It seems to be a general rule, however, that motor neurons become less vulnerable to axotomy by the time the animals have attained the age of 1 month: whereas the majority of motor neurons in adults can survive target deprivation for prolonged periods, in postnatal animals the proportion of the surviving population is merely 25–35%, or less (Koliatsos and Price, 1996).

In view of the fact that the majority of motor neurons in newborn animals do not survive injury to their axons, this model appears to be sufficiently attractive and sensitive to assay the effect of PV upregulation on the altered vulnerability of these cells. Indeed, in a recent publication, although the calcium level changes were not monitored, the higher PV level was documented to have a positive effect on the survival of neonatal spinal motor neurons after a sciatic nerve crush (Dekkers et al., 2004). However, in that experiment no re-establishment of the motor functions was observed, which might be attributed to the surviving population persisting in some altered form (Martin et al., 1998), as interference with the developmental regulation of CaBP expression during the early postnatal phase may have adverse effects (Clowry et al., 1997). In the present experiments, therefore, we performed the surgical interventions in animals 12 weeks of age, when the adult response was already present.

Calcium level changes induced by axotomy

The lesion of the hypoglossal nerve of the B6/SJL animals was followed by a transient increase in the intracellular calcium in the corresponding motor neurons, with a peak increase of approximately 1.5-fold around days 7–14 (Fig. 6A). In the same hypoglossal motor neurons of the PV+/+ animals, apart from a slight, insignificant increase in the mitochondrial calcium on day 1 after surgery, no increase was detected relative to the calcium level in the motor neurons on the nonoperated side at any time point postoperatively (Fig. 6A–C). Likewise, no calcium increase was seen in the motor neurons of the oculomotor nuclei of the PV+/+ mice after axotomy, and no significant difference could be discerned statistically between the two examined motor nuclei of the PV+/+ animals. Thus, as concerns the intracellular calcium increase after injury, the PV upregulation in these animals lends resistance of "oculomotor type" to the hypoglossal motor neurons.

Demonstration of tissue calcium by electron microscopy

The empirical approach used to gain information on the fine structural distribution of calcium is based on a cytochemical reaction to precipitate and visualize calcium as electron-dense deposits at the electron microscope. Such techniques, based on either the oxalate-pyroantimonate- (Borgers et al., 1977, 1981), the bichromate-

TABLE 1.

Intensity and Significance of Parvalbumin Staining in the Oculomotor and Hypoglossal Nuclei of PV+/+ Transgenic and B6/SJL Control Mice[1]

	-ln(intensity(I)/ intensity(C)) x 10^{-3}		*P*-value for significance			
	Mean	S.D.	Hypoglossus B6/SJL	Hypoglossus PV+/+	Oculomotor B6/SJL	Oculomotor PV+/+
Hypoglossus B6/SJL	90.8	29.1		0.02	0.003	0.001
Hypoglossus PV+/+	142.4	44.7	0.02		0.37	0.19
Oculomotor B6/SJL	173.1	49.5	0.003	0.37		0.60
Oculomotor PV+/+	168.1	62.3	0.001	0.19	0.60	

[1]The background-corrected intensity of the staining, due to the light absorption of the DAB chromophore, is proportional to the logarithm of the ratio of the transmitted light intensity measured at the region of interest (I) and at a control region (C) in the same section. Although the nominal values representing the staining intensity in the oculomotor nuclei in both strains are higher than the corresponding numbers in the hypoglossal nucleus of the PV+/+ stain, this difference is statistically not significant. However, the staining intensity in the hypoglossal nucleus of PV+/+ mice is significantly increased compared with the staining intensity measured in the control hypoglossus. In multiple comparisons, the only significant difference is the lower staining in the hypoglossal nucleus of B6/SJL mice, compared with the other groups (ANOVA with Duncan post hoc comparison).

(Probst, 1986), or the phosphate-chromium(III)-trisoxalate precipitation methods (Buchs et al., 1994), probably reveal a fraction of mobile, or loosely bound calcium (Buchs et al., 1994). In this study, a glutaraldehyde fixative containing oxalate anions was employed to conserve the distribution of calcium and preserve the structure for electron microscopy (Borgers et al., 1977, 1981). Tissue calcium precipitated by the primary fixative was transformed during postfixation to EDDs, which are visible in the transmission electron microscope.

Accordingly, the calcium distribution can be analyzed by conventional electron microscopy, without the customary need for time-consuming analytical microscopy, and the results can be simultaneously related to the morphological parameters. The method for quantification of the distribution of calcium, based on identification of the pattern of EDDs with that of calcium, was confirmed in earlier experiments, and proved useful for following slowly evolving function-dependent changes in the intracellular calcium in a variety of experimental paradigms (Somosy et al., 1993; Siklós and Kuhnt, 1994; Kittel et al., 1996; Siklós et al., 1997, 1998).

Relevance of CaBPs in ALS

The suggestion that CaBPs may protect motor neurons in ALS was based on the parallelism observed between the relatively spared motor functions in patients, such as the eye movement and voluntary sphincter functions (Bergmann et al., 1995), and the elevated CaBP contents of the corresponding motor neurons (Ince et al., 1993; Alexianu et al., 1994; Elliott and Snider, 1995). These clinical and pathological data led to the potential of CaBPs to rescue motor neurons being extensively studied in vitro in experiments mimicking stress conditions known to contribute to their degeneration during ALS, such as immune-mediated (Ho et al., 1996), excitotoxicity-induced (Van Den Bosch et al., 2002), and oxidative injury (Roy et al., 1998). Although cultured cells do not possess the cellular milieu that is present in the nervous tissue, which is known to affect the degree of the lesion, in these experiments the protective role of the CaBPs was verified directly.

Ex vivo arrangements (either acute or organotypic slices, or whole mount neuromuscular preparations) integrate at least some of the natural environment of the motor neurons, with the consequence that the outcome of such experiments can be translated more reliably to protective strategies, or to conclusions relevant to the pathomechanism of the disease. The results of electrophysiology experiments on tissue slices containing either the oculomotor (Vanselow and Keller, 2000) or the hypoglossal nucleus (Lips and Keller, 1998; Ladewig et al., 2003) or spinal motor neurons (Palecek et al., 1999) have provided further support for the idea that a higher calcium buffer capacity, manifested by a higher CaBP content, affords resistance against calcium-mediated injury in the motor neurons (von Lewinski and Keller, 2005). These data accorded with the results of miniature endplate potential measurements on whole mount neuromuscular preparations made from muscles containing vulnerable and resistant types of synapses (Mosier et al., 2000). The drawback of these experiments, however, is the fact that they do not sample motor neurons from the same location and, thus the results do not reflect the effects of the CaBPs alone, but may be influenced by the environmental differences.

The most widely used model of ALS suitable for in vivo research is a variety of transgenic mice developed on the basis of mutations of the enzyme SOD1 detected in a

subpopulation of ALS patients (Deng et al., 1993; Rosen et al., 1993; Gurney et al., 1994). By using transgenic animals based on the G93A mutation of SOD1, we earlier demonstrated not only that changes in the intracellular calcium level paralleled the degeneration of the motor neurons, but also that the survival of the motor neurons was associated with higher levels of CB and/or PV (Siklós et al., 1998). Because those experiments still involved the comparison of different motor neurons, (spinal versus oculomotor neurons), it was decided to develop a mouse line with an elevated PV content, suitable for measuring the protective effect of CaBPs in the same neuronal population in vivo (Beers et al., 2001). When PV+/+ transgenic mice were bred to the mutant SOD1 animals, a significantly increased preservation of the spinal motor neurons and a delayed onset of the disease was noted as compared with the mice containing only the SOD1 transgene.

Although the survival of the double transgenic mice was also considerably improved, the animals could not be ultimately rescued. The lack of success in preventing the death of mutant SOD1 animals by the upregulation of PV in the motor neurons could be a consequence either of the CaBPs acting solely as calcium buffers, which could be saturated if the stress signal endures (Siklós and Appel, 2005), or of the effect of the neighboring cells contributing to the damage (Boillée et al., 2006; Julien, 2007; Obál et al., 2001). To test directly whether an elevated PV level attenuates the calcium increases in the motor neurons, in the present study, PV+/+ mice were subjected to axotomy, which is accepted as a standard model for the induction of an acute sublethal injury in adult-type neurons (Koliatsos and Price, 1996). As expected, a nonsignificant calcium level increase was demonstrated in the hypoglossal motor neurons of PV+/+ mice, which was similar to that measured in the oculomotor neurons.

On the basis of this concept, the maximum goal would be a delay of the injury of the vulnerable motor neurons and a provision of a neuroprotection similar to that present in the relatively resistant motor neurons (Bergmann et al., 1995). The modest protective effect of the PV upregulation in the PV × SOD1 motor neurons was unexpected. Because an increased intracellular calcium level appears to be a key factor in the coupling of different pathways to cell destruction in models of ALS (Appel et al., 2001), the failure to prevent motor neuron death completely in the animals could be a consequence of failing to address all the cellular processes, or critical molecular steps of the destructive processes (Moisse and Strong, 2006; Cozzolino et al., 2008; Rothstein, 2009). This clearly warrants further studies in PV+/+ animals after the induction of similar lesions in order to assess the contributions of nonmotor neuronal compartments to survival or degeneration.

LITERATURE CITED

Alexianu ME, Ho B-K, Mohamed AH, La Bella V, Smith RG, Appel SH. 1994. The role of calcium-binding proteins in selective motoneuron vulnerability in amyotrophic lateral sclerosis. Ann Neurol 36:846–858.

Appel SH, Siklós L, Engelhardt JI, Mosier DR. 2001. Calcium: the Darth Vader of ALS. ALS Mot Neuron Disord 2(suppl 1):s47–s54.

Artal-Sanz M, Tavernarakis N. 2005. Proteolytic mechanisms in necrotic cell death and neurodegeneration. FEBS Lett 579:3287–3296.

Arundine M, Tymianski M. 2003. Molecular mechanisms of calcium-dependent neurodegeneration in excitotoxy. Cell Calcium 34:325–337.

Bauer R. 1988. Electron spectroscopic imaging: an advanced technique for imaging and analysis in transmission electron microscopy. Methods Microbiol 20:113–146.

Beck KD, Hefti F, Widmer HR. 1994. Deafferentation removes calretinin immunopositive terminals, but does not induce degeneration of calbindinD-28k and parvalbumin expressing neurons in the hippocampus of adult rats. J Neurosci Res 39:298–304.

Beers DR, Ho B-K, Siklós L, Alexianu ME, Mosier DR, Mohamed AH, Otsuka Y, Kozovska M, McAlhany RE, Smith RG, Appel SH. 2001. Parvalbumin overexpression alters immune-mediated increases in intracellular calcium, and delays disease onset in a transgenic model of familial amyotrophic lateral sclerosis. J Neurochem 79:499–509.

Bendotti C, Carri MT. 2009. Amyotrophic lateral sclerosis: mechanisms and countermeasures. Antiox Redox Sign 11: 1519–1522.

Bergmann M, Volpel M, Kuchelmeister K. 1995. Onuf's nucleus is frequently involved in motor neuron disease/ amyotrophic lateral sclerosis. J Neurol Sci 129:141–146.

Berridge MJ, Bootman MD, Lipp P. 1998. Calcium—a life and death signal. Nature 395:645–648.

Bezprozvanny I Hayden MR. 2004. Deranged neuronal calcium signaling and Huntington disease. Biochem Biophys Res Commun 322:1310–1317.

Boillée S, Vande Velde C, Cleveland DW. 2006. ALS: a disease of motor neurons and their nonneuronal neighbors. Neuron 52:39–59.

Borgers M, De Brabander DM, Van Reempts DJ, Awouters F, Jacob WA. 1977. Intranuclear microtubules in lung mast cells of guinea pigs in anaphylactic shock. Lab Invest 37: 1–8.

Borgers M, Thoné F, van Neuten JM. 1981. The subcellular distribution of calcium and the effects of calcium-antagonists as evaluted with a combined oxalate- pyroantimonate technique. Acta Histochem S 24:327–332.

Brini M. 2003. Ca^{2+} signalling in mitochondria: mechanism and role in physiology and pathology. Cell Calcium 34: 399–405.

Buchs P-A, Stoppini L, Párducz A, Siklós L, Muller D. 1994. A new cytochemical method for the ultrastructural localization of calcium in the central nervous system. J Neurosci Methods 54:83–93.

Celio MR. 1990. Calbindin D_{28K} and parvalbumin in the rat nervous system. Neuroscience 35:375–475.

Choi DW. 1995. Calcium: still center-stage in hypoxic-ischemic neuronal death. Trends Neurosci 18:58–60.

Clementi E, Racchetti G, Melino G, Meldolesi J. 1996. Cytosolic Ca^{2+} buffering, a cell property that in some neurons markedly decreases during aging, has a protective effect against NMDA/nitric oxide-induced excitotoxicity. Life Sci 59:389–397.

Clowry GJ, Fallah Z, Arnott G. 1997. Delemopmental expression of parvalbumin by rat lower cervical spinal cord

neurones and the effect of early lesions to the motor cortex. Dev Brain Res 102:197–208.

Cozzolino M, Ferri A, Carri MT. 2008. Amyotrophic lateral sclerosis: from current developments in the laboratory to clinical applications. Antiox Redox Sign 10:405–443.

Dekkers J, Bayley P, Dick JRT, Schwaller B, Berchtold MW, Greensmith L. 2004. Over-expression of parvalbumin in transgenic mice rescues motoneurons from injury-induced cell death. Neuroscience 123:459–466.

Deng H-X, Hentati A, Tainer JA, Iqbal Z, Cayabyab A, Hung W-Y, Getzoff ED, Hu P, Herzfeldt B, Roos RP, Warner C, Deng G, Soriano E, Smyth C, Parge HE, Ahmed A, Roses AE, Hallewell RA, Pericak-Vance MA, Siddique T. 1993. Amyotrophic lateral sclerosis and structural defects in Cu,Zn superoxide dismutase. Science 261:1047–1051.

Eberhorn AC, Büttner-Ennever JA, Horn AKE. 2006. Identification of motoneurons supplying multiply- or singly-innervated extraocular muscle fibers in the rat. Neurosci 137: 891–903.

Elliott JL Snider WD. 1995. Parvalbumin is a marker of ALS-resistant motor neurons. NeuroReport 6:449–452.

Freund TF, Buzsáki G, Leon A, Baimbridge KG, Somogyi P. 1990. Relationship of neuronal vulnerability and calcium binding protein immunoreactivity in ischemia. Exp Brain Res 83:55–66.

Geula C, Bu J, Nagykery N, Scinto LFM, Chan J, Joseph J, Parker R, Wu C-K. 2003. Loss of calbindin-D_{28K} from aging human cholinergic basal forebrain: relation to neuronal loss. J Comp Neurol 455:249–259.

Gurney ME, Pu H, Chiu AY, Dal Canto MC, Polchow CY, Alexander DD, Caliendo J, Hentati A, Kwon YW, Deng H-X, Chen W, Zhai P, Sufit RL, Siddique T. 1994. Motor neuron degeneration in mice that express a human Cu,Zn superoxide dismutase mutation. Science 264:1772–1775.

Hartley DM, Neve RL, Bryan J, Ullrey DB, Bak S-Y, Lang P, Geller AI. 1996. Expression of the calcium-binding protein, parvalbumin, in cultured cortical neurons using a HSV-1 vector system enhances NMDA neurotoxicity. Mol Brain Res 40:285–296.

Ho B-K, Alexianu ME, Colom LV, Mohamed AH, Serrano F, Appel SH. 1996. Expression of calbindin-D_{28K} in motoneuron hybrid cells after retroviral infection with calbindin-D_{28K} cDNA prevents amyotrophic lateral sclerosis IgG-mediated cytotoxicity. Proc Natl Acad Sci U S A 93: 6796–6801.

Ince P, Stout N, Shaw P, Slade J, Hunziker CW, Baimbridge KG. 1993. Parvalbumin and calbindin D_{28K} in human motor system and in motor neuron disease. Neuropathol Appl Neurobiol 19:291–299.

Julien J-P. 2007. ALS: astrocytes move in as deadly neighbors. Nat Neurosci 10:535–537.

Kittel A, Siklós L, Thuróczy G, Somosy Z. 1996. Qualitative enzyme histochemistry and microanalysis reveals changes in ultrastructural distribution of calcium and calcium-activated ATPases after microwave irradiation of the medial habenula. Acta Neuropathol 92:362–368.

Klapstein GJ, Vietla S, Lieberman DN, Gray PA, Airaksinen MS, Thoenen H, Meyer M, Mody I. 1998. Calbindin-D_{28k} fails to protect hippocampal neurons against ischemia in spite of its cytoplasmic calcium buffering properties: evidence from calbindin-D28k knockout mice. Neuroscience 85:361–373.

Koliatsos VE, Price DL. 1996. Axotomy as an experimental model of neuronal injury and cell death. Brain Pathol 6: 447–465.

Körtje K-H, Körtje D. 1992. The application of electron spectroscopic imaging for quantification of the area fractions of calcium-containing precipitates in nervous tissue. J Microsc 166:343–358.

Ladewig T, Kloppenburg P, Lalley PM, Zipfel WR, Webb WW, Keller BU. 2003. Spatial profiles of store-dependent calcium release in motoneurones of the nucleus hypoglossus from newborn mouse. J Physiol 547:775–787.

Lema Tomé CM, Bauer C, Nottingham C, Smith C, Blackstone K, Brown L, Hlavaty C, Nelson C, Daker R, Sola R, Miller R, Bryan R, Turner CP. 2006. MK801-induced caspase-3 in the postnatal brain: inverse relationship with calcium binding proteins. Neuroscience 141:1351–1363.

Lema Tomé CM, Miller R, Bauer C, Smith C, Blackstone K, Leigh A, Busch J, Turner CP. 2008. Decline in age-dependent, MK801-induced injury coincides with developmental switch in parvalbumin expression: somatosensory and motor cortex. Dev Psychobiol 50:665–679.

Lieberman AR. The axon reaction: a review of the principal features of perikaryal responses to axon injury. Int Rev Neurobiol 14:49–124.

Lips MB, Keller BU. 1998. Endogenous calcium buffering in motoneurones of the nucleus hypoglossus from mouse. J Physiol 511:105–117.

Lipton P. 1999. Ischemic cell death in brain neurons. Physiol Rev 79:1431–1568.

Martin LJ, Al-Abdulla NA, Brambrink AM, Kirsch JR, Sieber FE, Portera-Cailliau C. 1998. Neurodegeneration in excitotoxicity, global cerebral ischemia, and target deprivation: a perspective on the contributions of apoptosis and necrosis. Brain Res Bull 46:281–309.

Mattson MP. 1998. Free radicals, calcium, and the synaptic plasticity—cell death continuum: emerging roles of the transcription factor NFκB. Int Rev Neurobiol 42:103–168.

Mattson MP. 2007. Calcium and neurodegeneration. Aging Cell 6:337–350.

Mattson MP, Chan SL. 2003. Neuronal and glial calcium signaling in Alzheimer's disease. Cell Calcium 34:385–397.

Mattson MP, Rychlik B, Chu C, Christakos S. 1991. Evidence for calcium-reducing and excito-protective roles for the calcium-binding protein calbindin-D_{28k} in cultured hippocampal neurons. Neuron 6:41–51.

Maxwell MH. 1978. Short technical note: two rapid and simple methods used for the removal of resins from 1.0 μm thick epoxy sections. J Microsc 112:253–255.

Mayhew TM. 1992. A review of recent advances in stereology for quantifying neural structure. J Neurocytol 21:313–328.

McMahon A, Wong BS, Iacopino AM, Ng MC, Chi S, German DC. 1998. Calbindin-D_{28k} buffers intracellular calcium and promotes resistance to degeneration in PC12 cells. Mol Brain Res 54:56–63.

Mitchell IJ Griffiths MR. 2003. The differential susceptibility of specific neuronal populations: insights from Huntington's disease. IUBMB Life 55:293–298.

Moisse K Strong MJ. 2006. Innate immunity in amyotrophic lateral sclerosis. Biochim Biophys Acta 1762:1083–1093.

Mosier DR, Siklós L, Appel SH. 2000. Resistance of extraocular motoneuron terminals to effects of amyotrophic lateral sclerosis sera. Neurology 54:252–255.

Müller M, Felmy F, Schwaller B, Schneggenburger R. 2007. Parvalbumin is a mobile presynaptic Ca^{2+} buffer in the calyx of held that accelerates the decay of Ca^{2+} and short-term facilitation. J Neurosci 27:2261–2271.

Obál I, Soós J, Jakab K, Siklós L, Engelhardt JI. 2001. Recruitment of activated microglia cells in the spinal cord of mice by ALS IgG. NeuroReport 12:2449–2452.

Obál I, Engelhardt JI, Siklós L. 2006. Axotomy induces contrasting changes in calcium and calcium-binding proteins in oculomotor and hypoglossal nuclei of Balb/c mice. J Comp Neurol 499:147–32.

Paizs M, Engelhardt JI, Siklós L. 2009. Quantitative assessment of relative changes of imunohistochemical staining

by light microscopy in specified anatomical regions. J Microsc 234:103–112.
Palecek J, Lips MB, Keller BU. 1999. Calcium dynamics and buffering in motoneurons of the mouse spinal cord. J Physiol 520:485–502.
Price DL, Martin LJ, Clatterbuck RE, Koliatsos VE, Sisodia SS, Walker LC, Cork LC. 1992. Neuronal degeneration in human diseases and animal models. J Neurobiol 23: 1277–1294.
Price DL, Cleveland DW, Koliatsos VE. 1994. Motor neuron disease and animal models. Neurobiol Dis 1:3–11.
Probst W. 1986. Ultrastructural localization of calcium in the CNS of vertebrates. Histochemistry 85:231–239.
Raghupathi R. 2004. Cell death mechanisms following traumatic brain injury. Brain Pathol 14:215–222.
Rami A, Rabié A, Thomasset M, Krieglstein J. 1992. Calbindin-D_{28k} and ischemic damage of pyramidal cells in rat hippocampus. J Neurosci Res 31:89–95.
Reimer L, Fromm I, Rennekamp R. 1988. Operation modes of electron spectroscopic imaging and electron energy-loss spectroscopy in a transmission electron microscope. Ultramicroscopy 24:339–354.
Reynolds ES. 1963. The use of lead citrate at high pH as an electron-opaque stain in electron microscopy. J Cell Biol 17:208–212.
Richardson KC, Jarett L, Finke EH. 1960. Embedding in epoxy resins for ultrathin sectioning in electron microscopy. Stain Technol 35:313–323.
Rosen DR, Siddique T, Patterson D, Figlewich DA, Sapp P, Hentati A, Donaldson D, Goto J, O'Regan JP, Deng HX, Rahmani Z, Krizus A, McKenna-Yasek D, Cayabyab A, Gaston SM, Berger R, Tanzi RE, Halperin JJ, Herzfeldt B, Van den Berg R, Hung WY, Bird T, Deng G, Mulder DW, Smyth C, Laing NG, Soriano E, Pericak-Vance MA, Haines J, Rouleau GA, Gusella JS, Horvitz HR, Brown RHJ. 1993. Mutations in Cu/Zn superoxide dismutase gene are associated with familial amyotrophic lateral sclerosis. Nature 362:59–62.
Rothstein JD. 2009. Current hypotheses for the underlying biology of amyotrophic lateral sclerosis. Ann Neurol 65: S3–S9.
Rowland LP Shneider NA. 2001. Amyotrophic lateral sclerosis. N Engl J Med 344:1688–1700.
Roy J, Minotti S, Dong L, Figlewicz DA, Durham HD. 1998. Glutamate potentiates the toxicity of mutant Cu/Zn-superoxide dismutase in motor neurons by postsynaptic calcium-dependent mechanisms. J Neurosci 18:9673–9684.
Schmalbruch H. 1984. Motoneuron death after nerve section in newborn rats. J Comp Neurol 224:252–258.
Schwarz EC, Thompson JM, Connor NP, Behan M. 2009. The effect of aging on hypoglossal motoneurons in rats. Dysphagia 24:40–48.
Siklós L Appel SH. 2005. Calcium binding proteins in selective vulnerability of motor neurons. In Beal MF, Lang A, Ludolph A, editors. Neurodegenerative diseases. Cambridge: Cambridge University Press. p 65–79.
Siklós, L Kuhnt U. 1994. Calcium accumulation by dendritic mitochondria declines along the apical dendrites of pyramidal neurons in area CA1 of guinea pig hippocampal slices. Neurosci Lett 173:131–134.
Siklós L, Engelhardt J, Harati Y, Smith RG, Joó F, Appel SH. 1996. Ultrastructural evidence for altered calcium in motor nerve terminals in amyotrophic lateral sclerosis. Ann Neurol 39:203–216.
Siklós L, Kuhnt U, Párducz A, Szerdahelyi P. 1997. Intracellular calcium accompanies changes in total tissue Na^+, K^+, and water during the first two hours of in vitro incubation of hippocampal slices. Neuroscience 79:1013–1022.
Siklós L, Engelhardt J, Alexianu ME, Gurney ME, Siddique T, Appel SH. 1998. Intracellular calcium parallels motoneuron degeneration in SOD-1 mutant mice. J Neuropathol Exp Neurol 57:571–587.
Slemmer JE, De Zeeuw CI, Weber JT. 2005. Don't get too excited: mechanisms of glutamate-mediated Purkinje cell death. Prog Brain Res 148:367–390.
Snider WD, Thanedar S. 1989. Target dependence of hypoglossal motor neurons during development and in maturity. J Comp Neurol 279:489–498.
Snider WD, Elliott JL, Yan Q. 1992. Axotomy-induced neuronal death during development. J Neurobiol 23:1231–1246.
Somosy Z, Kovács J, Siklós L, Köteles GJ. 1993. Morphological and histochemical changes in intercellular junctional complexes in epithelial cells of mouse small intestine upon X-irradiation: changes of ruthenium red permeability and calcium content. Scanning Microsc 7:961–971.
Sullivan PG, Rabchevsky AG, Waldmeier PC, Springer JE. 2005. Mitochondrial permeability transition in CNS trauma: cause or effect of neuronal cell death? J Neurosci Res 79:231–239.
Tortosa A Ferrer I. 1993. Parvalbumin immunoreactivity in the hippocampus of the gerbil after transient forebrain ischaemia: a qualitative and quantitative sequential study. Neuroscience 55:33–43.
Van Den Bosch L, Schwaller B, Vleminckx V, Meiers B, Stork S, Ruehlicke T, Van Houtte E, Klaassen H, Celio MR, Missiaen L, Robberecht W, Berchtold MW. 2002. Protective effect of parvalbumin on excitotoxic motor neuron death. Exp Neurol 174:150–161.
Vanselow BK Keller BU. 2000. Calcium dynamics and buffering in oculomotor neurons from mouse that are particularly resistant during amyotrophic lateral sclerosis (ALS)-related motoneurone disease. J Physiol 525:433–445.
Vig PJS, Subramony SH, Burright EN, Fratkin JD, McDaniel DO, Desaiah D, Qin Z. 1998. Reduced immuoreactivity to calcium-binding proteins in Purkinje cells precedes onset of ataxia in spinocerebellar ataxia-1 transgenic mice. Neurology 50:106–113.
von Lewinski F, Keller BU. 2005. Ca^{2+}, mitochondria and selective motoneuron vulnerability: implications for ALS. Trends Neurosci 28:494–500.
Yamada T, McGeer PL, Baimbridge KG, McGeer EG. 1990. Relative sparing in Parkinson's disease of substantia nigra dopamine neurons containing calbindin-D_{28k}. Brain Res 526: 303–307.